CARRIER-PHASE DIFFERENTIAL GPS FOR AUTOMATIC CONTROL OF LAND VEHICLES

A DISSERTATION

SUBMITTED TO THE DEPARTMENT OF AERONAUTICS AND ASTRONAUTICS

AND THE COMMITTEE ON GRADUATE STUDIES

OF STANFORD UNIVERSITY

IN PARTIAL FULFILLMENT OF THE REQUIREMENTS

FOR THE DEGREE OF

DOCTOR OF PHILOSOPHY

Michael Lee O'Connor

December 1997

I certify that I have read this thesis and that in my opinion it is fully adequate, in scope and quality, as a dissertation for the degree of Doctor of Philosophy

Professor Bradford W. Parkinson
(Principal Adviser)

I certify that I have read this thesis and that in my opinion it is fully adequate, in scope and quality, as a dissertation for the degree of Doctor of Philosophy

Professor J. David Powell

I certify that I have read this thesis and that in my opinion it is fully adequate, in scope and quality, as a dissertation for the degree of Doctor of Philosophy

Professor Stephen M. Rock

Approved for the University Committee on Graduate Studies:

Abstract

Real-time centimeter-level navigation has countless potential applications in land vehicles, including precise topographic field mapping, runway snowplowing in bad weather, and land mine detection and avoidance. Perhaps the most obvious and immediate need for accurate, robust land vehicle sensing is in the guidance and control of agricultural vehicles.

Accurate guidance and automatic control of farm vehicles offers many potential advantages; however, previous attempts to automate these vehicles have been unsuccessful due to sensor limitations. With the recent development of real-time carrier-phase differential GPS (CDGPS), a single inexpensive GPS receiver can measure a vehicle's position to within a few centimeters and orientation to fractions of a degree. This ability to provide accurate real-time measurements of multiple vehicle states makes CDGPS ideal for automatic control of vehicles.

This work describes the theoretical and experimental work behind the first successfully demonstrated automatic control system for land vehicles based on CDGPS. An extension of pseudolite-based CDGPS initialization methods was explored for land vehicles and demonstrated experimentally. Original land vehicle dynamic models were developed and identified using this innovative sensor. After initial automatic control testing using a

Yamaha Fleetmaster golf cart, a centimeter-level, fully autonomous row guidance capability was demonstrated on a John Deere 7800 farm tractor.

To my mother and father, with gratitude.

Acknowledgments

I owe a special thanks to my advisor, Professor Bradford W. Parkinson, not only for his keen technical direction, but also for providing the continual inspiration and the academic freedom that has allowed this project to flourish. His guidance in generating the research and support for this project has been an invaluable aspect of my education.

I also owe a debt of gratitude to Professor J. David Powell. His discerning comments at lab meetings and in personal conversations have helped to provide focus throughout the course of this research. I am also indebted to Professor Powell for his feedback in preparing this dissertation.

The opportunity to take and instruct courses with Professor Stephen M. Rock has been one of my most rewarding academic experiences. His contagious enthusiasm and dynamic teaching style are truly inspirational. I feel very fortunate to have had Professor Rock on my dissertation reading committee, and I am thankful to him for his thoughtful feedback.

I wish to express my gratitude to some of my former and current colleagues. I was extremely fortunate to have had generous assistance from Thomas Bell, David Lawrence, Clark Cohen, Boris Pervan, and Stewart Cobb. The original research presented in this work is largely dependent on the work of these individuals. Andrew Barrows, Jock

Christie, Sam Pullen, Harris Teague, and Konstantin Gromov have also been a great source of assistance and support

None of this work would have been possible without the generous support provided by Deere and Company. I owe a special thanks to Robert Mayfield and Wayne Smith for their vision, their investment of time and resources into this project, and especially for their willingness to share ideas that have been essential for the success of this project. The close collaboration with these individuals has helped guide this project toward a platform that exists not only in the laboratory, but also on a genuine farm tractor.

A special thanks also goes out to Trimble Navigation, Ltd., for graciously donating the GPS receivers used in this project, and to IntegriNautics Corporation for providing the vehicle positioning software and ground-based pseudolite hardware.

My biggest debt is owed to my parents, Richard and Ellen, and to my sister Michelle, for their unwavering emotional support and love. Without their support I could never have made it to where I am today. Finally, I am thankful to my future wife Gail, for sitting through my *entire* thesis defense and for having the patience to put up with me through the conclusion of this research.

Contents

List of Tables

List of Figures

Chapter 1

Introduction

In recent years, a profound change has occurred in the field of vehicle navigation. The driving force behind this change is the recent emergence of the Global Position System (GPS). Initially developed by the United States government for military use, this satellite navigation system is now used by millions of civil users in countless applications on land, over water, in the air, and in space.

With the ever-increasing consumer demand for GPS-based products, commercial receiver prices are rapidly falling while accuracy and reliability continue to improve. These factors, combined with recent advances in GPS technology, make satellite receivers an affordable, extremely accurate sensor for navigation, guidance, system identification, and automatic vehicle control. This thesis explores the use of emerging high-performance GPS technologies for the automatic control of land vehicles.

1.1 The Global Positioning System

Many references describing the details of GPS are available[1,2,3,4]. This section outlines the three basic levels of GPS available to civil users: (1) stand-alone GPS, (2) code-phase

differential GPS (DGPS), and (3) carrier-phase differential GPS (CDGPS). This third method, CDGPS, is the positioning method used for the research in this work.

1.1.1 Stand-Alone GPS Navigation

The conventional method for computing a stand-alone GPS position fix requires a user to measure and apply "pseudoranges" from satellites. Each GPS satellite transmits a different, known pseudo-random "noise" bit sequence (PRN code) on an L-band carrier. The pseudorange (ρ) is based on the time required for the PRN code to travel from the satellite to the user (See Figure 1). The simple pseudorange equation for a single satellite j is:

$$\rho_j = c\left(t_{AU,j} - t_{TS,j}\right) \tag{1.1}$$

where c is the speed of light in a vacuum, $t_{AU,j}$ is the true time of signal arrival at the user, and $t_{TS,j}$ is the true time of signal transmission from the satellite.

Unfortunately, time of transmission and time of arrival measurements are never known exactly, and atmospheric effects can cause significant signal delays. A pseudorange equation that takes these effects into account is:

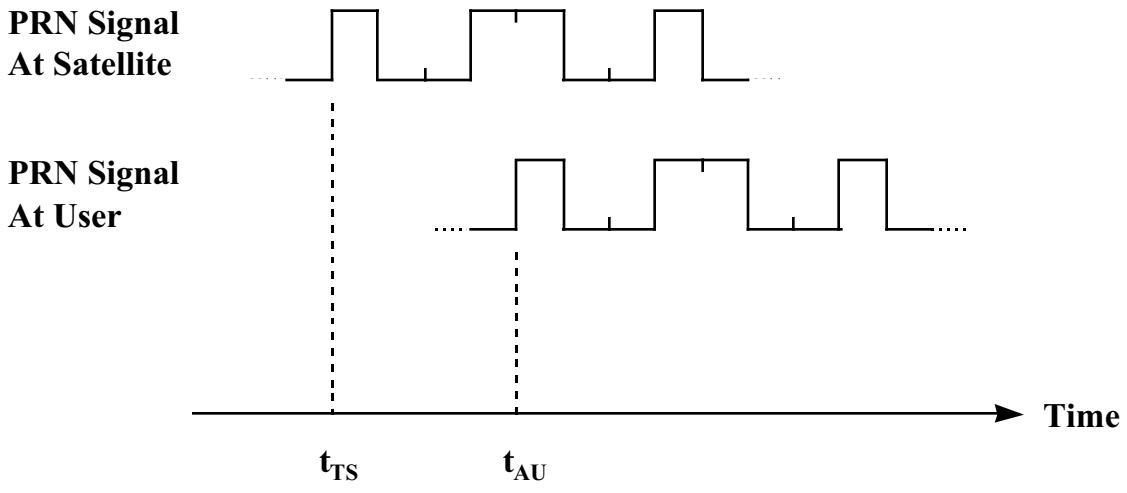

Figure 1 - Pseudorange Measurement

$$\frac{\rho_j}{c} = \left(t_{A,j} + \tau\right) - \left(t_{T,j} + B_j\right) + I_j + T_j + \varepsilon_j \qquad (1.2)$$

where $t_{A,j}$ is the measured time of signal arrival at the user, τ is the user clock bias, $t_{T,j}$ is the expected time of signal transmission from satellite j, B_j is the satellite clock bias (intentional and unintentional), I_j and T_j are the signal delays due to ionosphere and troposphere respectively, and ε_j is a term encompassing all other error sources including internal receiver noise, spacecraft ephemeris errors, and external signal reflections known as multipath.

Due to the use of inexpensive clocks in user receivers, the user clock bias (τ) is usually large and varies rapidly, so it must be computed explicitly by the user. For this reason, four (not three) GPS satellites are needed to solve for the user's position. Four pseudorange measurement equations are needed to solve for the four unknowns at each time period – three degrees of freedom in position, and one user clock bias.

In contrast to most user clocks, highly accurate atomic clocks in GPS satellites could provide a very small satellite clock bias (B_j); however, the Department of Defense intentionally adds a random, slowly varying error to the time of transmission of the civilian signal. This intentional signal degradation, referred to as Selective Availability (SA), strongly dominates the navigation error for a stand-alone GPS user, producing 1-σ errors on the order of 30 meters.

Many people believe that economics and common sense shall soon prevail, and Selective Availability will be turned off by the U.S. government[5]. When this occurs, there will be a dramatic improvement in the accuracy attainable by stand-alone GPS users. The primary error source from Equation 1.2 will change from the satellite clock error (B_j) to the ionosphere error (I_j) and receiver noise (ε_j). Since civil users have access to the PRN code on only one frequency transmitted by GPS satellites, they cannot easily measure the

effects of the ionosphere. The basic horizontal accuracy available to a stand-alone user without SA would be approximately 10 meters[1].

1.1.2 Code-Phase Differential GPS

One method employed by civil users to improve upon GPS navigation accuracy is code-phase differential GPS. The theory behind this technique is that a receiver in a fixed, known location (i.e. a reference station) may take pseudorange measurements for each satellite in view, subtract the measured pseudorange from the expected pseudorange, and transmit the pseudorange corrections. Nearby users may then apply these corrections to their own computations, significantly reducing the effects of satellite clock bias (including SA), spacecraft ephemeris errors, and atmospheric errors.

In practice, the accuracy available using a DGPS system is, at best, around one to two meters. Special techniques such as carrier smoothing[6] and narrow correlator design[7] help reduce this error, but fundamental limits exist in a receiver's ability to track the PRN code. These limits are due to receiver noise (especially multipath), spatial decorrelation of the atmosphere, and temporal decorrelation of SA.

One disadvantage of DGPS systems is the complexity and cost associated with maintaining a reference station. In the United States and other nations, governments are providing some DGPS coverage at no cost to civil users; however, this coverage is not geographically complete. The U.S. Federal Aviation Administration is currently developing a Wide-Area DGPS (WADGPS) system which is similar to DGPS but is based on more advanced PRN code processing[8]. This WADGPS system is expected to cover the entire continental United States, providing 1-2 meter horizontal accuracy by the year 2001[9].

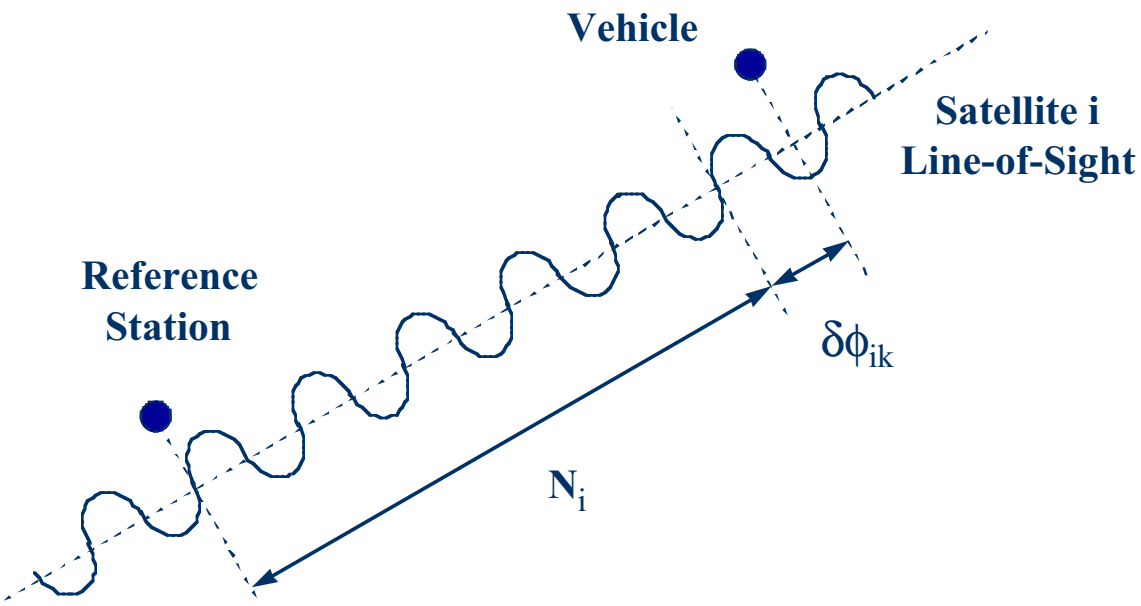

Figure 2 - Differential Carrier-Phase Measurement

1.1.3 Carrier-Phase Differential GPS

The highest level of accuracy currently possible using GPS is carrier-phase differential GPS. While there are several varieties of CDGPS positioning algorithms, they are all fundamentally very similar. Instead of positioning with pseudorange measurements, CDGPS systems use the raw GPS L-band carrier signals for positioning. Unlike PRN code measurements, which are only accurate to the meter level, carrier-phase measurements are accurate to fractions of a centimeter once the integer number of wavelengths between the vehicle and reference station has been determined.

Figure 2 illustrates a differential carrier-phase measurement for one satellite. The equation describing this measurement for satellite i at epoch k is:

$$\delta\phi_{ik} = -e_{ik}^{i}\delta\mathbf{x}_k + \tau_k + N_i + \nu_{ik} \tag{1.3}$$

where $\delta\varphi_{ik}$ is the fractional differential carrier-phase measurement, e_{ik}^{i} is the line-of-sight unit vector to satellite i, $\delta\mathbf{x}_k$ is the position of the vehicle relative to the reference

station, τ_k is the clock bias difference between the vehicle and reference station, N_i is the whole number of carrier-phase wavelengths between the reference station and user, and ν_{ik} is the carrier-phase measurement random noise. Upon initialization of a CDGPS system, the number of integer carrier cycles (N_i) cannot be immediately determined. Reliable resolution of this integer cycle ambiguity is the biggest difficulty in using CDGPS.

1.1.4 Basic CDGPS Initialization Techniques

The first basic CDGPS integer cycle ambiguity resolution technique developed for survey applications is still widely used today. A reference antenna is held at a fixed, known location while a second antenna is held at a fixed, unknown location. Collecting data while satellites move slowly overhead provides the observability needed to resolve the integer cycle ambiguities. The location of the second antenna can then be found to the sub-centimeter level. The mathematics required to perform a survey are often done in post-processing. *This integer cycle ambiguity resolution method provides an accurate and extremely reliable solution after approximately 15 to 90 minutes of data collection.*

The second basic technique for CDGPS initialization is often referred to as On-The-Fly (OTF) Kinematic processing[10]. This method takes advantage of the fact that the cycle ambiguity for each satellite is an integer value. A variety of integer candidates are substituted into the carrier equations for a single epoch. The solution providing the lowest mean-squared measurement residual is often, *but not always*, the correct solution. One variation of this technique uses the military L2 carrier signal and "wide-laning" methods to reduce the number of integer possibilities. Another variation tracks a set of low-residual integer possibilities for multiple epochs allowing satellite motion to sort out the correct solution. In general, *this integer cycle ambiguity resolution method can work very quickly (within a few minutes), but the underlying principle behind guessing integer values based on measurement residuals is prone to false solutions*. Also, since a measurement

Table 1 - Comparison of GPS Techniques

	Horizontal Accuracy (1-σ)	Relative Integrity Level	Range of Coverage	Ground System Cost	Cost per Vehicle	Relative Complexity to User
Stand-Alone GPS	20-30m	Med.	worldwide	-	<$1k	Low
Stand-Alone GPS, no SA	8-12m	Med.	worldwide	-	<$1k	Low
WADGPS	1-2m	High	continental	-	$3k	Med.
DGPS	1-2m	Med.	100-500 km	$5k	$3k	High
OTF CDGPS	2-4 cm	Low	10-15 km	$10k	$10k-20k	High
Pseudolite CDGPS	2-4 cm	High	10-15 km	$10k	$10k-20k	High

residual is needed to compare solutions, a minimum of 5 satellites is needed to initialize a CDGPS system using this type of algorithm.

A third CDGPS initialization technique combines the reliability of the survey method with real-time operation and resolution speeds comparable to integer search methods. Changing geometry between the vehicle and a fixed GPS pseudo-satellite transmitter (pseudolite) provides near-survey quality solutions in a matter of seconds[11]. A more detailed description of this method is found in Chapter 4. *This method shows great promise because it resolves integer cycles quickly and extremely reliably*.

1.1.5 Summary of GPS Techniques

A summary of the civil user accuracy, integrity, coverage range, and approximate cost for real-time GPS-based navigation techniques are shown in Table 1. *Please note that all values and costs are approximate, based on 1997 technology.* While accuracies are not expected to change much, costs will continue to fall across the board. As a result, the key issues for most users will become accuracy and integrity.

1.2 GPS for Vehicle Automatic Control

The combination of low-cost, high-accuracy GPS technology with modern inexpensive and powerful processors will provide unprecedented capabilities. The most exciting of these capabilities lies in the potential for sophisticated control systems for autonomous vehicles.

1.2.1 Previous Demonstrations of GPS for Vehicle Control

GPS has previously been demonstrated for the automatic control of various vehicles. Most of these have used CDGPS technology, including the automatic landing of a Boeing 737[12], the completely automatic flight of a small, unpiloted airplane[13], a fully autonomous small, unpiloted helicopter[14], an indoor simulated space station[15], and a free flying robot[16].

1.2.2 Previous Land Vehicle Control Work

Automatic control of land vehicles is not a new idea, but previous attempts have been limited by high cost and complexity[17,18] or dependence on vision systems[19,20]. DGPS techniques have been used for driver-assisted guidance[21] as well as automatic control of a land vehicle[22], but as expected, only meter-level performance was attainable.

1.2.3 The Future of CDGPS for Vehicle Control

The first widespread use of CDGPS for vehicle automatic control is likely to occur in farm equipment. Agricultural fields typically have good sky visibility, making them highly suitable for GPS. Also, the rewards to be gained through precision farming are enormous[23]. Today, a large market for GPS data collection systems in land vehicles is the farming industry. Meter-level DGPS techniques are used for field mapping and yield

monitoring[24,25], and the use of CDGPS for field topographic mapping has been explored[26].

Real-time centimeter-level positioning using CDGPS has countless applications in other land vehicles as well. Automobiles, snowplows on airport taxiways, and construction equipment are just a few of the other vehicles that could benefit from a reliable, accurate sensor producing high-bandwidth position measurements for automatic control. Robot vehicles using this technology may someday be used to clear minefields, clean up toxic waste, apply hazardous pesticides, tirelessly harvest crops, and transport disabled persons.

1.3 Motivation for Centimeter-Level Farm Vehicle Guidance

Since the advent of the plow, farming has been a driving force in our civilization. By historical standards, modernized farms are incredibly efficient. Most of this improved efficiency can be directly attributed to the invention and refinement of the tractor, which was "more fundamentally revolutionary than any machine that preceded it" in farming[27]. While the number of American farm workers has fluctuated between 1 and 10 million in that past two centuries, the percentage of the labor force in this country employed by agriculture has continually declined – from 80% in 1810 to 1.8% in 1980[28]. Geographical regions today which have not made the transition to modern farming techniques occupy up to 70% of their labor force in agriculture.[29]

Despite today's relatively heightened farming efficiency, there are many areas where improvements are possible even today. One invention that could bring about such improvements is a robotic farm vehicle. Farmers are not likely to embrace such a system without financial motivation. A GPS guided farm vehicle could save time, effort, and money for farmers by improving vehicle capabilities, reducing overall waste, and simplifying vehicle design.

1.3.1 Improved Vehicle Capabilities

The most obvious benefit of automatic farm vehicle steering is driver workload reduction. This capability will improve driver morale and reduce fatigue, allowing an operator to work longer hours without sacrificing performance or safety. Taking the concept one step further, a fully robotic farm vehicle would require even less human attention, and possibly allow one person to operate multiple vehicles simultaneously.

Other capabilities added through CDGPS-based navigation, guidance, and control include flawless operation during darkness, dust, and heavy fog, as well as prolonged operations at high speeds without losing accuracy. An photo of dust obstruction on a field in the Southwestern United States is shown in Figure 3. During time-critical periods such as planting and harvesting, these improvements in vehicle efficiency translate directly into higher profits for farmers.

Figure 3 - Dust Visual Interference

Two more farming techniques that would be enabled through a CDGPS-based guidance system are tape irrigation and "Zamboni" row skip patterns. Tape irrigation is a process providing water, fertilizer, and chemicals directly to the roots of row crops through plastic underground tubes. While this method greatly improves the quality of crops and reduces water usage, without centimeter level navigation, planting seeds over the subterranean tapes without frequently damaging them with the vehicle implement is very difficult.

Zamboni row skip patterns are a new concept designed to minimize the time required to turn a farm vehicle around at the end of a row. By skipping rows between consecutive passes, a vehicle may never need to back up or even slow down to acquire the next row. This can be accomplished by repeating the row pattern shown in Figure 4. Clearly an

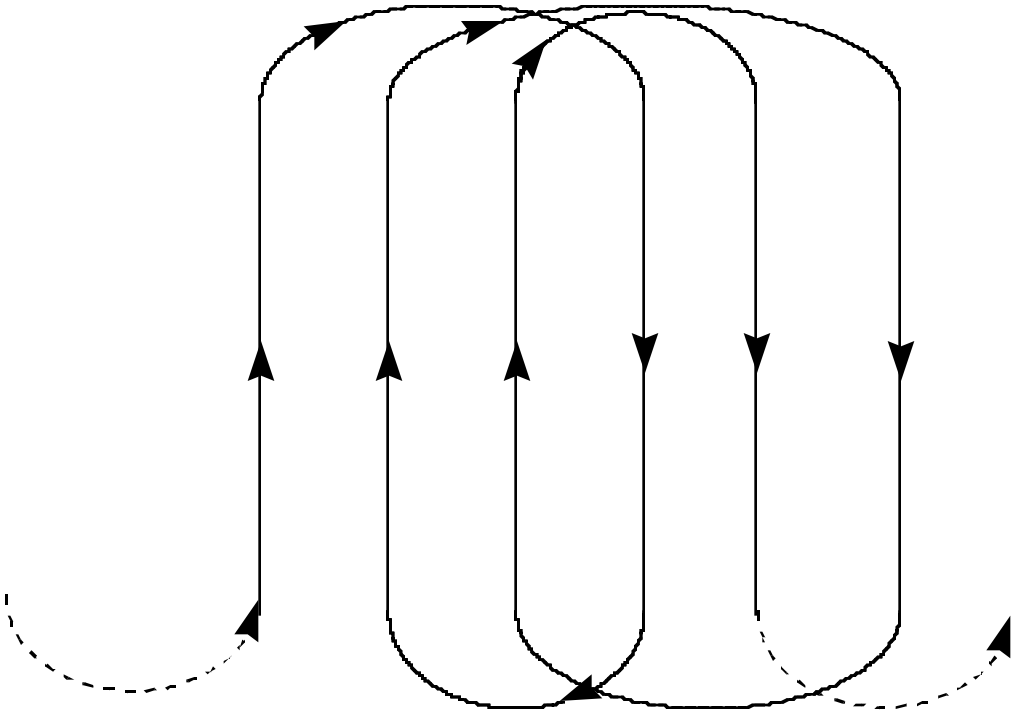

Figure 4 - "Zamboni" Row Skip Pattern

accurate navigation system is required to follow such a complicated path with sufficient accuracy to eliminate overlap between rows.

1.3.2 Reduced Waste

Even without taking advantage of the *special* capabilities enabled by accurate farm vehicle guidance, significant savings are possible. Research shows that during normal daytime operation, drivers following straight rows overlap previous rows by 8% to 10% of implement width[23] (See Figure 5). This directly corresponds to 8-10% waste in materials such as seed, fertilizer, and herbicides, as well as an equivalent increase in operator effort. In addition, field areas which fall in the overlap regions may produce less crop as a result of double chemical application. For large implements, which may exceed 20 meters in width, vehicle guidance to the centimeter level could reduce the overlap by two orders of magnitude. One study showed that, since farmers tend to work on such small financial

Figure 5 - Farm Vehicle Row Overlap

margins, a typical Canadian wheat farmer with 2000 acres could increase profits by over 50% if skips and overlaps between rows could be eliminated[23].

Wasted water and chemicals mean more than increased cost. In the heavily farmed regions of the Southwestern United States, the majority of the water used for irrigation comes from underground aquifers. Some sources believe the source of this water is not replenishable, and care must be taken for this water supply to last[30]. In addition to

wasted water, the overuse of herbicides and pesticides increases driver exposure to these hazardous chemicals and has harmful environmental side effects.

1.3.3 Simplified Vehicle Design

The use of GPS for farm vehicle guidance will obviate some of the equipment used on farm vehicles today. One standard piece of hardware is a doppler radar which is used to measure true ground speed. This information is used with a wheel speed sensor to compute the longitudinal wheel slip of the rear tires. CDGPS offers the potential to eliminate this radar while providing even more accurate ground speed measurements.

A piece of equipment that often accompanies wide tractor implements is a set of row marker arms. These devices hydraulically extend half the width of the implement to mark

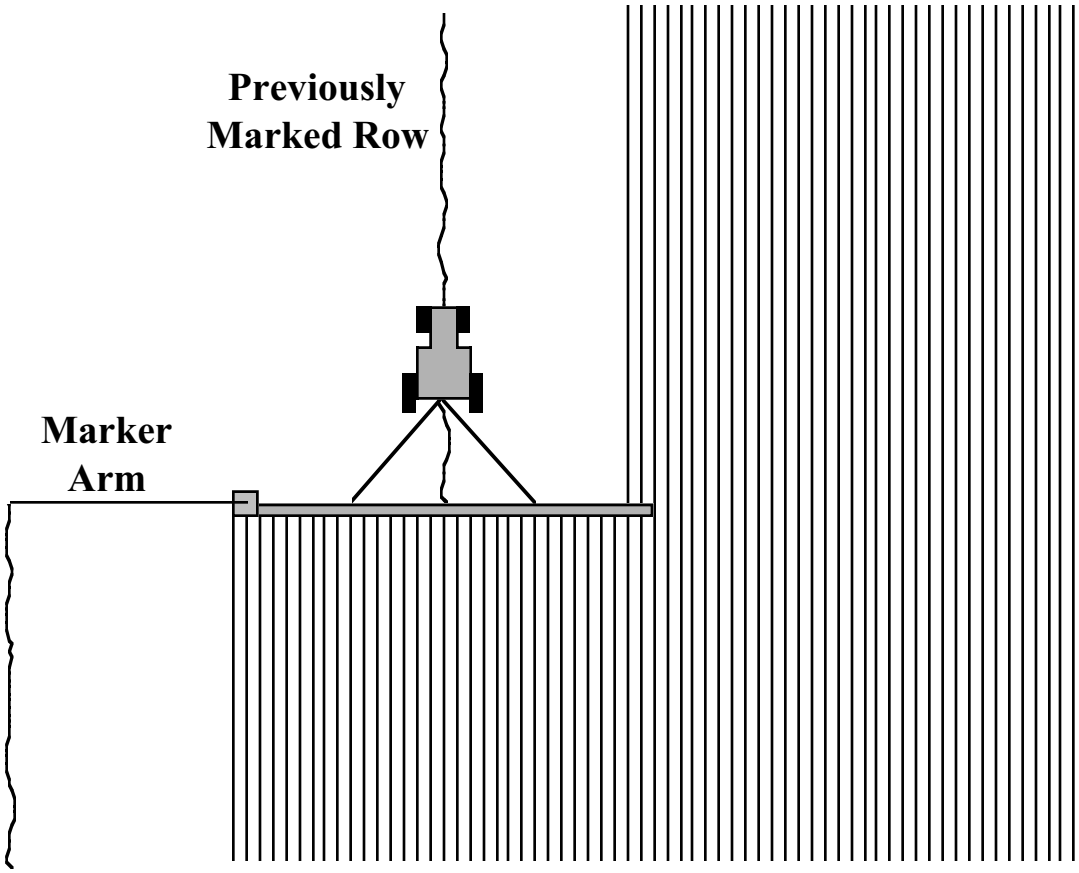

Figure 6 - Row Marker Arm Concept

a line in the soil for the farmer to follow on his or her next pass over the field (See Figure 6). The motivation for such hardware is that an operator can drive more accurately when following a line ahead of the vehicle instead of one several meters to the side. Due to their length, these arms tend to be very fragile and quite expensive (up to $5000 each). CDGPS guidance would replace these marker arms, thus eliminating this cost.

In the long term, as fully autonomous farm vehicles become available, these vehicles could be produced at much lower cost. Much of the cost in producing a large modern farm vehicle goes toward human factors. Cabs with large windows, air conditioning, radios, and seats with complex suspension systems are standard equipment – all designed to make a human driver more comfortable during long hours in the field. A huge cost advantage would be to eliminate the need for these amenities. The chassis, engine, and transmission of an autonomous farm vehicle could be completely redesigned to lower the center of gravity and allow operation on steeper terrain. Also, without the need for operator visibility, an implement could be added to the front of farm vehicles, allowing them to perform two tasks at once.

1.4 Objectives

The objective of this work is to study the feasibility of applying a new technology (CDGPS) to the automatic control of land vehicles. This study was designed with two primary goals in mind: (1) To develop a general, flexible framework for a land vehicle navigation, guidance, and automatic control system; and (2) to provide and demonstrate a potentially cost-effective solution for a specific class of commercial land vehicles.

The first goal was met through a general approach to CDGPS initialization, land vehicle dynamic modeling, and automatic control system design. The second goal was accomplished by experimentally demonstrating a successful navigation, guidance, and automatic control system on a large farm tractor.

1.5 Synopsis and Organization

This thesis is comprised of nine chapters beginning with this introduction as Chapter 1. Chapter 2 describes the Automatic Farming System concept in detail. Some key technical issues are discussed, along with an outline for possible product development over the next few years.

The following five chapters describe the work culminating in the first demonstration of an automatic farm tractor steering system using carrier-phase differential GPS. Chapter 3 describes the navigation and control system hardware used for the land vehicle experiments in this work. The theory and application of CDGPS initialization using a single pseudolite is detailed in Chapter 4. Chapter 5 describes a set of land vehicle models that are feasible for automatic control purposes, and Chapter 6 discusses the selection and identification of the most appropriate model. Chapter 7 shows experimental results from closed-loop automatic control of a golf cart and a large farm tractor, comparing the latter results to those obtained by an expert human driver on the same tractor.

The final two chapters establish possible future experimentation on the tractor. Chapter 8 describes a set of computer simulations based on various untested sensor combinations. The accuracies shown in these simulations suggest possible variations in the experimental setup described in Chapter 3. Conclusions are drawn in Chapter 9, along with recommendations for future work in this area.

1.6 Contributions

The fundamental new achievement of this research is the first ever design, fabrication, demonstration, and evaluation of a system to automatically control a farm vehicle to accuracies better than a human driver. In the course of achieving this goal, the following research contributions were made:

- Land vehicle CDGPS initialization using a single pseudolite was designed, simulated, and experimentally demonstrated for the first time[31].

- An original set of state-space models were developed for automatic control of land vehicles that accurately characterized vehicle motion and enabled control synthesis.

- An experimental method was developed and implemented for the linearization of highly nonlinear steering sensors and actuators.

- A relatively general technique to experimentally characterize the lateral dynamics of a farm tractor using optimal parameter identification was developed and demonstrated.

- Critical land vehicle automatic control issues were discovered through golf cart experimentation, including the need for a real-time antenna lever-arm correction and nonlinear control regimes[32]. These general issues and solutions apply to many classes of land vehicles

- Created and demonstrated accurate control algorithms for the general case of a maneuvering land vehicle. These included automatic line acquisition, U-turns, and centimeter-level line following[33].

- Using GPS instrumentation, the tractor driving accuracy of an expert human operator was experimentally measured as a benchmark for this and future automatic control system experiments.

- Simulations were performed to explore the use of new sensor combinations for land vehicle automatic control.

Chapter 2

Automatic Farming System Concept

Prior to beginning development of a novel system, careful consideration is needed to identify the most relevant unsolved technical research issues. In the case of a potential commercial product, the prioritization of these research issues will depend on the most likely course of product development. While the primary goal of this thesis is to demonstrate the technical feasibility of automatic land vehicle control using GPS, this chapter serves to outline the likely steps leading to the development of an Automatic Farming System.

The introduction of CDGPS-based farm vehicle equipment into the commercial marketplace will be an evolving process. Like current DGPS farming systems, initial CDGPS products will simply provide the user with navigation information. As farmers and farm equipment manufacturers gain experience and trust in CDGPS technology, products based on this technology will perform increasingly advanced functions. The evolution of CDGPS in farm vehicles will probably take place in four basic steps:

- Navigation Data Collection - The collection of high precision navigation data for use in real-time or post-processing

- Driver-Assisted Guidance - Enhanced real-time vehicle operation using a graphical video display
- Automatic Row Guidance - Automatic vehicle steering along straight rows with manual turns
- Automatic Farming - Fully automated field operations with one person supervising multiple vehicles

2.1 Navigation Data Collection

The first step toward an automatic farm vehicle controller is the introduction of a basic, highly accurate navigation unit. This first-generation CDGPS system will provide vehicle position and orientation data in real-time at unprecedented accuracies. This information could be used by the vehicle operator to vary the application of materials to the field. The navigation data could also be combined with vehicle status information and sent to a fixed location, such as a farmer's office, as part of a Farm Productivity Monitoring System.

2.1.1 Hardware Description

The basic Navigation Data Collection hardware consists of a vehicle navigation unit and a ground reference station connected by a two-way radio link (see Figure 7). Pseudolites may optionally be used to assist system initialization and provide additional GPS-like ranging signals. The vehicle navigation unit will be a single piece of hardware which may be mounted to new or existing farm vehicles. This pre-fabricated unit will contain GPS equipment, radio link transceivers, and processing hardware, with a general real-time input-output capability. The reference station will be comprised of GPS equipment, radio link hardware, an inexpensive processor, and an optional Farm Productivity Monitoring System software package .

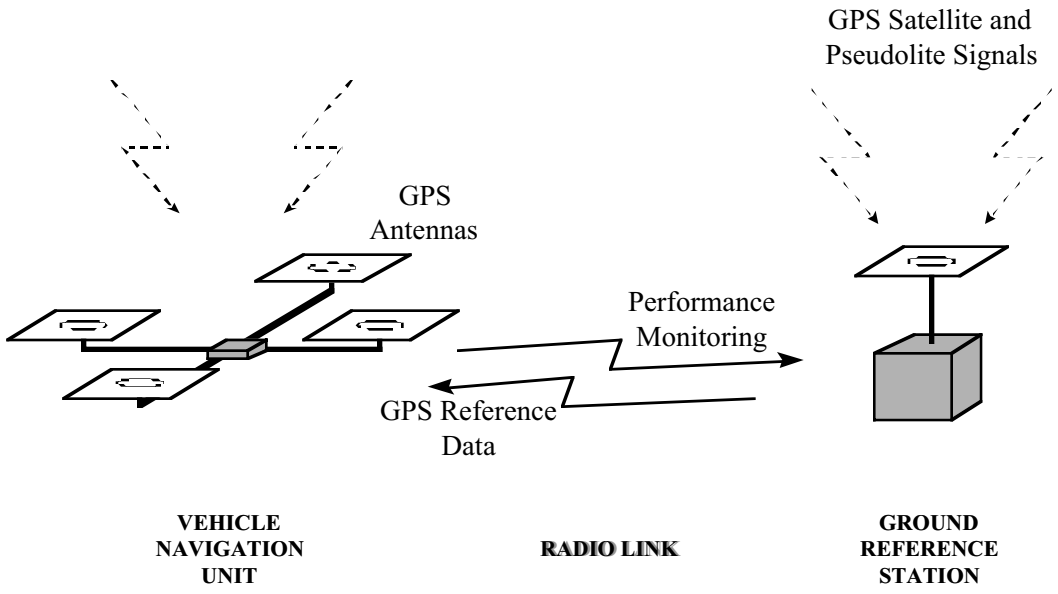

Figure 7 - CDGPS Navigation System

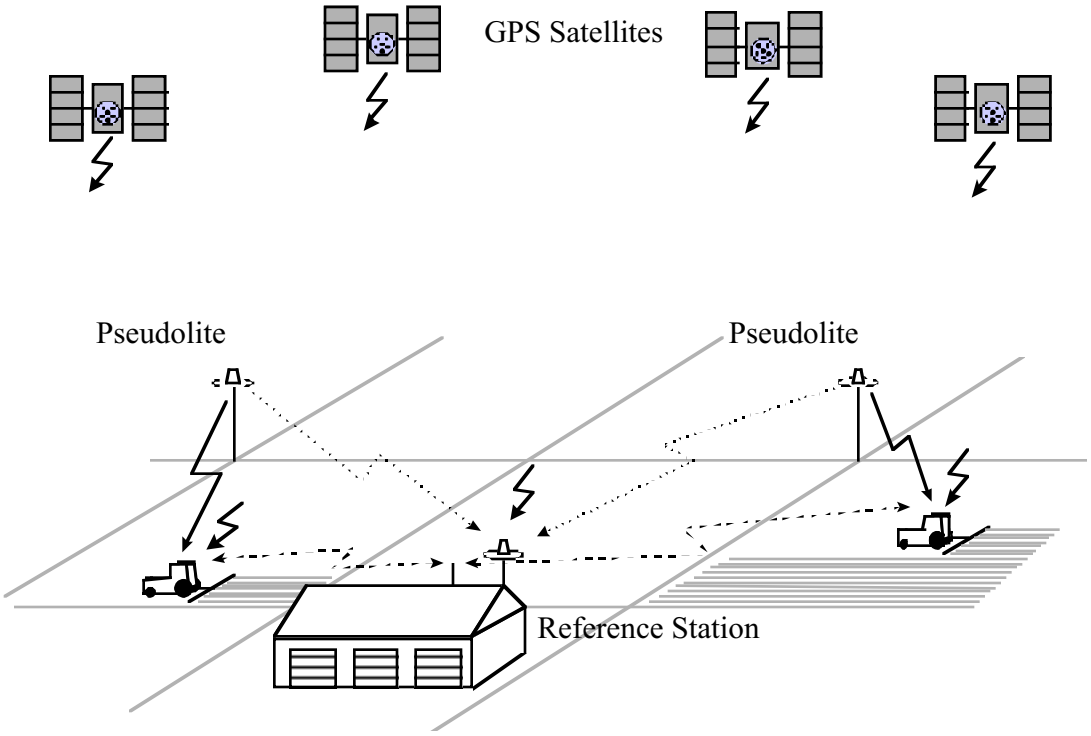

Figure 8 - Complete Navigation Data Collection System

In practice, each participating vehicle will need a separate navigation unit, while a single ground reference station will be sufficient to track and provide corrections for multiple vehicles in a 100 square-mile area. One vision for the complete Navigation Data Collection system is shown in Figure 8. GPS signals are received at the ground reference station and at each participating vehicle (dark solid arrows). A radio link transfers information between the vehicles and the reference station (dashed arrows). Pseudolites may optionally be used to improve CDGPS integrity (robustness) and availability (the percentage of time in which GPS coverage is sufficient for positioning). Signals from the pseudolites will be received by participating vehicles (thin solid arrows) and, prior to the refinement of synchrolites[11], by the reference station as well (dotted arrows). The development of synchrolites, which are an autonomous form of pseudolites, will completely eliminate the need for a connection between the pseudolite and the reference station. Synchrolites may even eliminate the need for a reference station altogether[11].

The biggest question surrounding this navigation system concept is the need for pseudolites. Each additional unit adds to the cost of the navigation system; however, these devices may be used to reliably initialize CDGPS positioning (see Chapter 4) and provide additional ranging sources to augment the GPS satellites in view. The availability of CDGPS in land vehicles is terrain dependent. Cliffs and trees may block satellites, while steep slopes orient the vehicle's GPS antennas away from portions of the sky. Because farms are so varied, no specific configuration will work in all cases. The final Navigation Data Collection unit must be versatile enough to operate with zero or multiple pseudolites. Fortunately, this does not present any unsolved technical constraints on the existing pseudolite-based CDGPS system.

2.1.2 Benefits

The primary advantage to developing a Navigation Data Collection unit lies in its potential as a foundation for future guidance and control systems; however, use of the

navigation unit alone does provide benefits for both the farm equipment manufacturer and the farmer.

The first farm vehicle manufacturer to provide a fully supported CDGPS navigation system will receive the following benefits:

- Begin to familiarize customers with CDGPS technology and its potential for high reliability with high accuracy
- Establish itself as a leader in high-tech agriculture
- Help assess the need for pseudolites in realistic farm settings
- Generate volumes of real-world sensor data for development of future CDGPS-based navigation and guidance systems
- Allow refinement of CDGPS products based on customer feedback

For farmers, a CDGPS navigation sensor complete with a Farm Productivity Monitoring System will give the following advantages over current code-based meter-level DGPS systems:

- More accurate monitoring of crop yield, soil moisture content, and weeds
- Topographic field maps accurate to the centimeter level
- Accurate tracking of vehicle and driver performance in real-time, including speed and row overlap
- Quick recognition and response to vehicles that break down in the field
- The ability to manage vehicle and implement resources from a central location based on up-to-date information about their location and progress.

2.1.3 Cost

Farmers are involved in a highly competitive and efficient industry. Before purchasing a piece of farm equipment, most farmers must be convinced that the product will pay for itself within 18 months. The cost of the basic Navigation Data Collection unit will be

relatively high, especially considering the research and development costs of the navigation unit. This high initial cost may prevent the data collection unit from becoming immediately profitable as a stand-alone production system.

If this navigation system were in production today, the unit retail cost would be about $10,000 for a reference station with one pseudolite and a reliable RF data communication system, and about $10,000 for each navigation unit. For comparison, the price of a medium size tractor is around $100,000. The cost of the GPS system will continue to fall in the future due to the declining cost of solid-state components and the widespread commercialization of GPS.

2.2 Driver-Assisted Guidance

The most immediate follow-on to high precision Navigation Data Collection is to allow the real-time navigation system to feed a Driver-Assisted Guidance display. Such a display will have three basic capabilities: (1) provide "at a glance" situational awareness to the user, including vehicle status, field boundaries, above-ground obstacles, and known underground objects such as irrigation tapes; (2) visually display a reference path for the driver to follow, eliminating the need for devices such as marker arms; and (3) generate a low-level steering reference for the driver to follow for improved accuracy.

When using the display, the driver will have the option to operate as usual, occasionally checking the display to monitor status, or to use the display as the sole source of guidance in the case of fog, dust, darkness, and high-accuracy applications such as tape irrigation. The user interface must display vehicle status (especially a "use / don't use" navigation system integrity indicator), along with sensor information such as position, heading, wheel angle, and implement angle. Much research has been performed to generate a useful graphical display for general aviation aircraft pilots[34], but more research and testing is needed to create a display that is useful for land vehicles. The difficult challenge

is to create a display that provides useful information and is still simple enough for anyone to use.

2.2.1 Hardware Description

The additional hardware needed to provide video display capability consists of video interface electronics (e.g. an inexpensive VGA computer card), a cable, and a flat, sunlight-readable display. The image could be generated by the same processor used inside the Data Collection Unit with some software modifications.

2.2.2 Additional Benefits

The jump from centimeter-level data collection to driver-in-the-loop guidance will provide tremendous advantages for farmers. The two most dramatic effects of the system will be a significant reduction in implement overlap without the need for marker arms, and the ability to plant and harvest during low visibility. These effects will translate directly into increased profits for farmers. In addition, tape irrigation, which has been pursued by farmers for years, will finally become a financially viable farming method. "Zamboni" row skip patterns will become feasible, and in row crop operations, flag markers will no longer be needed to line up straight rows.

The widespread use of this guidance system will deepen farmers' trust in CDGPS technology while supplying the farm equipment manufacturer with the abundance of real-world data needed to develop automatic guidance products.

2.2.3 Additional System Cost

The Driver-Assisted Guidance system is identical to the Navigation Data Collection unit with some new software and an improved user interface. The retail cost of these additions in a production system would be approximately $3000 today, and this figure is sure to decline with the heated research currently underway in the flat panel display industry. In

farming, a system that will pay for itself in 18 months or less is considered commercially viable. This centimeter-level Driver-Assisted Guidance display will easily fulfill this requirement. Once a few farmers use the display to recoup much of the system cost in one rainy or nighttime session that would have otherwise been impossible to perform, all farmers will want this system.

2.3 Automatic Row Guidance

The next step in product development after Driver-Assisted Guidance will be to automate the tedious task of vehicle steering along straight rows. In the proposed Automatic Row Guidance system, the driver will have the option to manually operate the farm vehicle, using the graphical display for awareness and guidance, or to flip a switch and supervise as the vehicle automatically steers to the end of the current row.

2.3.1 Hardware Description

The hardware requirement for Automatic Row Guidance capability will be identical to the Driver-Assisted Guidance system with an added steering actuator, steering sensor, and automatic steering switch. The difficult challenge in creating this system is to design easy-to-use software which can perform the automatic control task safely, reliably, accurately, and in a wide range of circumstances.

2.3.2 Additional Benefits

The semi-autonomous Automatic Row Guidance system carries with it the same benefits as the Driver-Assisted Guidance system with some added features. For one, an automatic steering system will follow rows more accurately, at higher speeds, and for longer periods of time than a human driver is capable of doing. Also, stringent tasks such as row crop operations in low visibility will be performed with significantly less effort on the part of the driver. Without the tedious task of fine steering, drivers will be able to pay more

attention to the surroundings, watching for obstacles and noting factors such as crop yield, crop damage, and weed growth in different areas.

2.3.3 Additional Cost

The additional cost for Automatic Row Guidance is very small relative to advantages gained. Steering sensors and actuators are currently available as off-the-shelf parts which would add approximately $2000 to the retail system cost, including installation. Liability protection and the added one-time costs of software development, political acceptance, and government certification may be significant, but the rewards will make up for these drawbacks. Interviews with farmers clearly indicate that the value of an Automatic Row Guidance system will far outweigh the projected cost[35,36,37].

2.4 Automatic Farming

The far-reaching goal of these product development steps will be an Automatic Farming system, in which several fully-autonomous farm vehicles are maintained and managed remotely by a handful of centralized operators. The safety and liability issues surrounding such a system are daunting, but the potential rewards are enormous.

2.4.1 Hardware Description

The jump from semi-autonomous Automatic Row Guidance to Automatic Farming will require minimal hardware changes. The critical tasks of commanding the transmission gear, engine speed, and implement hydraulics are electronically straightforward in most modern farm vehicles. The primary hardware additions will probably involve robustness and safety. Without the presence of a human operator, an autonomous vehicle will need new external sensing devices to ensure the safety of the vehicle and anything within its vicinity. Some devices which may be necessary include touch sensitive bumper devices and a forward-looking sonar or radar type of device.

2.4.2 Additional Benefits

The are many advantages to farm operation with an Automatic Farming system. The most obvious benefit is the possible reduction of manpower required to operate a farm. Not only does this reduce the cost of farm operation and the level of tedious labor, but it also removes humans from dangers such as pesticide exposure and farm vehicle accidents. Agriculture is a relatively hazardous occupation, with 6.7 work fatalities per 100,000 employees in 1989[38]. The effects of vibration, noise, dust, and stress on farm equipment operators can also be health threatening.

The removal of drivers from farm vehicle operations will allow improvements in vehicle design. By eliminating the amenities such as air conditioning, radio, and possibly even the cab, vehicle cost could be greatly reduced. Also, with human ride comfort and vision requirements eliminated, the entire engine and chassis of farm vehicle could be redesigned with a lower center of gravity for better efficiency.

Finally, with successful autonomous farm vehicle control, high level robotic functions such as field path planning with curved paths and contours would become possible.

2.4.3 Additional Cost

The additional cost to develop an Automatic Farming system will be dominated by the requirements for safety equipment, certification, and liability protection. The additional retail system cost will probably be around $5000.

2.5 System Summary

Table 2 summarizes the benefits and costs associated with each step toward Automatic Farming.

Table 2 - Summary of Automatic Farming System Development

	Navigation Data Collection	Driver-Assisted Guidance	Automatic Row Guidance	Automatic Farming
Approximate System Cost Today	$10K	$13K	$15K	$20K
Better Management of Seed, Fertilizer, Pesticide	Yes	Yes	Yes	Yes
Farm Productivity Monitoring System	Yes	Yes	Yes	Yes
Reduced Overlap Between Rows	No	Yes	Yes	Yes
Eliminate Delays Due to Visibility	No	Yes	Yes	Yes
Allow Precision Applications	No	Some	Yes	Yes
Alleviate Farmer Workload	No	No	Yes	Yes
Allow Farmer Multi-Tasking	No	No	No	Yes
Human Removed From Pesticide Application	No	No	No	Yes
Vehicle Design to Reduce Cost	No	No	No	Yes
Design for Improved Vehicle Efficiency	No	No	No	Yes

Chapter 3

Vehicle Navigation Hardware

The first major challenge in demonstrating a useful land vehicle automatic control system is to generate an accurate, reliable navigation signal at a reasonable cost. This chapter describes the prototype navigation system used on the land vehicles described in this work. Figure 9 shows the basic hardware configuration of the CDGPS reference station and Figure 10 diagrams the vehicle navigation system hardware.

Initial land vehicle testing was performed on the Yamaha Fleetmaster golf cart shown in Figure 11. The remainder of the experimental research described in this thesis was

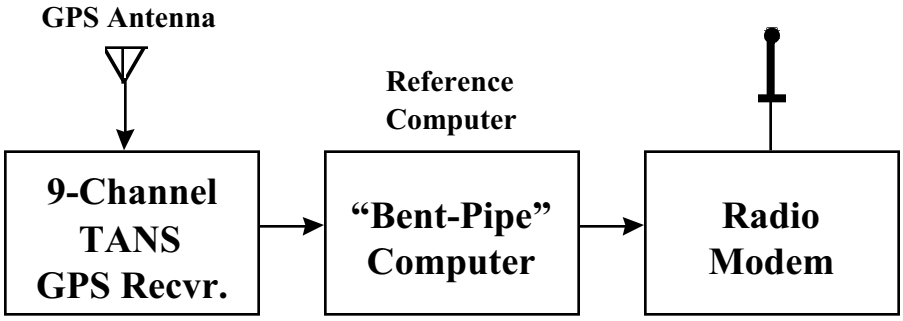

Figure 9 - CDGPS Reference Station Diagram

performed on the John Deere 7800 farm tractor shown in Figure 12.

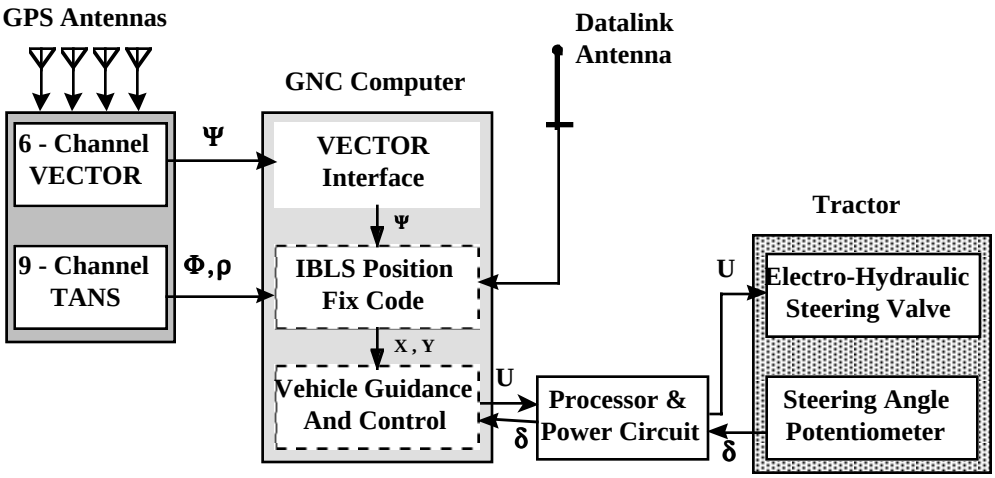

Figure 10 - Vehicle Positioning System Diagram

Figure 11 - Experimental Golf Cart

Figure 12 - Experimental Farm Tractor

3.1 Navigation Electronics

The heart of the land vehicle testing system used for this research was the Integrity Beacon Landing System (IBLS). This pseudolite-based CDGPS system has been the subject of much research over the past several years, including three engineering doctoral dissertations[39,40,41]. This system was invented by Clark Cohen and associates at Stanford University, and is currently under product development at IntegriNautics Corporation. The system used for land vehicle experimentation was comprised of a CDGPS ground reference station, vehicle navigation electronics, and a basic user interface.

3.1.1 CDGPS Reference Station

A CDGPS reference station provides participating vehicles with raw, synchronous carrier-phase measurements taken from a GPS antenna at a known fixed location. Such a

Figure 13 - CDGPS Reference Station

reference station requires a GPS antenna, a GPS receiver, a radio modem transmitter, and a power source. These are all solid-state, off-the-shelf components which could easily be packaged together to form a small, inexpensive, low-power unit.

The ground reference station used for experimentation in this work included a Trimble survey-quality GPS antenna and a 9-channel Trimble TANS GPS receiver. An Intel-based computer was used to initialize the receiver and serially transmit raw carrier-phase measurements through a Pacific Crest RFM96 radio modem at 4800 bits per second. The system was powered using a marine deep cycle 12 volt battery with a 110 volt power inverter. A Trimble 4000SSi receiver and TrimTalk radio modem were also included in the reference station for use as a secondary CDGPS reference, *however, this additional hardware was not utilized by the vehicle navigation and control system*. A photo of the reference station hardware situated in its environmentally robust housing is shown in Figure 13.

3.1.2 Vehicle Electronics

A CDGPS navigation system computes vehicle position by comparing carrier-phase measurements taken on the vehicle with measurements taken at the ground reference station. The vehicle navigation system requires a GPS antenna, a GPS receiver, a radio link receiver, a processing computer, and a power source. In addition, if the point of control interest on the vehicle is not the location of the positioning antenna, a sensor is needed to provide vehicle attitude measurements to account for the lever-arm correction. These are all solid state, off the shelf components which could be easily packaged together to form a small, low power, low cost unit.

Each vehicle positioning system used for experimentation in this work contained four Trimble TANS GPS antennas, a Trimble TANS 9-channel GPS receiver, a 6-channel Trimble TANS Vector attitude receiver, an Intel 90 MHz Pentium-based Industrial Computer Source computer, a Pacific Crest RDDR96 Radio Modem, and a 110 volt power inverter utilizing the vehicle electrical source A Trimble 7400MSi receiver and

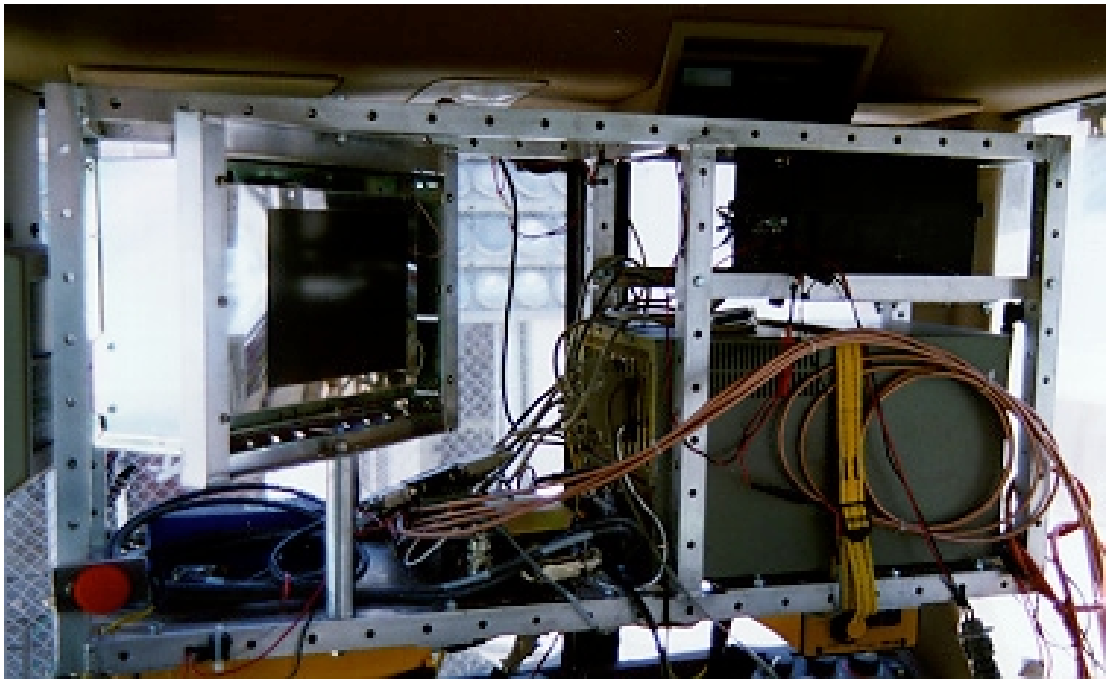

Figure 14 - Vehicle Positioning System Photo

TrimTalk radio modem were also included on the vehicle navigation system rack for use as a secondary CDGPS reference, however, *this additional hardware was not utilized by the vehicle navigation and control system*. A photo of the vehicle navigation system inside the tractor is shown in Figure 14.

3.1.3 Navigation System User Interface

For control system applications, navigation data must be collected in a synchronous manner with minimal latency. For this reason, the LYNX real-time operating system was chosen for the vehicle computer. Separate applications were written to process attitude measurements, generate position fixes, and execute control system logic. The user was able to track program status using a sunlight-readable monochrome monitor.

3.2 Non-GPS Sensor Hardware

The golf cart and tractor navigation systems both included steering measurements from a simple potentiometer. This was the only sensor signal used by the vehicle controller that was not provided by satellite navigation. The steering sensing and actuation is described in detail in Chapter 6. The navigation system and its relationship to the automatic control hardware is diagrammed in Figure 10.

Measurements of hitch load, rear wheel speed, and velocity were also available on the tractor through existing hardware. The hitch load and rear wheel speed were sampled and recorded by the controls computer, but *were not utilized by the controller*. The doppler radar velocity measurement was not read by the controls computer.

3.3 Pseudolite Hardware

The pseudolite used for experimentation in this work transmitted a steady GPS-like signal at 1575.42 MHz (the standard L1 GPS carrier frequency). Since it is currently not part of

the GPS constellation, PRN code 32 was chosen for the pseudolite. A standard Trimble patch antenna with no pre-amplifier was used to transmit the pseudolite signal.

Chapter 4

Pseudolite Use in Land Vehicles

Most CDGPS systems currently available are initialized using integer search techniques, which have fundamental integrity limitations. A second technique created for ultra-reliable precision aircraft landing uses two or more GPS pseudolites for CDGPS initialization. In an effort to reduce the cost and complexity of the complete land vehicle navigation system, a single pseudolite may be sufficient to reliably initialize the CDGPS position of a land vehicle. As part of this research, the use of a single pseudolite for CDGPS initialization was explored in simulation and demonstrated experimentally on a farm tractor.

Three aspects of this problem were explored: the relationship between vehicle path geometry and navigation system accuracy, the mathematics of incorporating a ground constraint into the carrier-phase equations, and the benefits and difficulties of using a dipole antenna to transmit the GPS signal to standard patch antennas.

4.1 Motivation for Pseudolites

Ground-based GPS pseudolite transmitters are a useful tool for vehicle navigation. By providing additional ranging signals, pseudolites are able to improve GPS system availability and integrity[39,42]. This is especially important when obstructions or excessive vehicle attitude motion may result in the loss of GPS satellite signals.

As an added benefit, pseudolites can be used for reliable initialization of CDGPS positioning systems. The biggest difficulty in achieving centimeter-level GPS position accuracy is the initialization procedure. During initialization, the integer number of carrier cycles between a vehicle and reference station are resolved or estimated for all commonly visible satellites. Most CDGPS systems on the market use a search technique for initialization. These systems require at least five GPS signals in view, and they often rely on the noisy L2 signal which carries an encrypted PRN code that is unreadable by civilian users.

4.2 Pseudolite Theory

Integer search techniques typically use measurement residuals to find the correct integers, a technique prone to false solutions. The resulting loss of system integrity could be costly or even dangerous in many high accuracy GPS applications. These initialization problems can be solved by taking advantage of a quickly changing line-of-sight vector between a moving vehicle and a pseudolite. Pseudolites were first used for this purpose by Cohen and associates in the Integrity Beacon Landing System (IBLS)[11]. By flying between two or more pseudolites, this aircraft navigation system is able to *explicitly solve for* (without guessing) an estimate of vehicle position and the expected 3-dimensional covariance of this estimate.

The nonlinear equation for a differential carrier-phase measurement of pseudolite J at epoch K is[39]:

$$\phi_{jk} = \left| p_j - x_k \right| + \tau_k + N_j + \nu_{jk} \quad , \tag{4.1}$$

where ϕ_{jk} is the raw single difference carrier-phase measurement, p_j is the position of pseudolite j, x_k is the vehicle antenna position, τ_k is the clock bias between receiver and reference station, N_j is the cycle ambiguity for pseudolite j, and ν_{jk} is the measurement noise (assumed Gaussian with standard deviation σ_ϕ).

This equation may be linearized about an estimate of vehicle position and combined with the satellite differential carrier-phase equations. If we begin with an estimate of vehicle position ($\bar{x}_k$), we can use Equation 4.1 to generate an expected value for the differential carrier-phase measurement ($\bar{\phi}_{jk}$). Defining $\delta x_k \equiv x_k - \bar{x}_k$ and $\delta\phi_k \equiv \phi_k - \bar{\phi}_k$, the linearized carrier-phase measurement equations for m satellites and n pseudolites at epoch k may be written as follows[39]:

$$\delta\phi_{1k} = -e_{1k}^T \delta x_k + \tau'_k + \nu_{1k} \quad , \tag{4.2}$$

$$\delta\phi_{ik} = -e_{ik}^T \delta x_k + \tau'_k + N'_i + \nu_{ik} \quad i = 2 \ldots m \quad , \tag{4.3}$$

$$\delta\phi_{jk} = -\hat{e}_{jk}^T \delta x_k + \tau'_k + N'_j + \nu_{jk} \quad j = 1 \ldots n \quad , \tag{4.4}$$

where e_{ik} is the line-of-sight unit vector to satellite i, $\hat{e}_{jk}$ is the estimated line-of-sight unit vector to pseudolite j, τ'_k is the differential clock bias plus the cycle ambiguity for satellite 1, and N'_i is the difference in cycle ambiguity between satellite i and satellite 1.

For a single epoch, there are more equations ($m + n$) than unknowns ($n + n + 3$), so there is no explicit solution for this set of equations. If a wide range of integer cycle ambiguity candidates are substituted into these equations, the set producing the lowest mean-square residual is often *but not always* the correct integer solution.

As additional epochs of data are collected, the integer cycle ambiguities do not change. Each new epoch of data produces $m+n$ more equations and only four more unknowns (δx_k and τ'_k). It first appears that if the number of combined pseudolites and satellites in view exceeds four, the vehicle trajectory and integer cycle ambiguities can be explicitly solved (not guessed) in three epochs or less.

In practice, the accuracy of the solution depends upon the accuracy of the differential carrier-phase measurements and the satellite and pseudolite line-of-sight motion relative to the vehicle. While most modern receivers provide relatively low levels of *random* carrier-phase measurement noise, small *bias errors*, especially due to multipath, may lead to a large bias in the final position estimate. Since multipath errors are a function of instantaneous satellite geometry and the location of nearby signal reflecting objects, the effect of this class of errors may be significantly mitigated through vehicle motion during a pseudolite pass.

Even in the case of relatively small, zero-mean carrier-phase measurement noise, if there is little change in the line-of-sight unit vectors during data collection, the solution is only weakly observable and the resulting position and integer estimate covariances will be large. This problem can be overcome by moving the vehicle in the vicinity of one or more

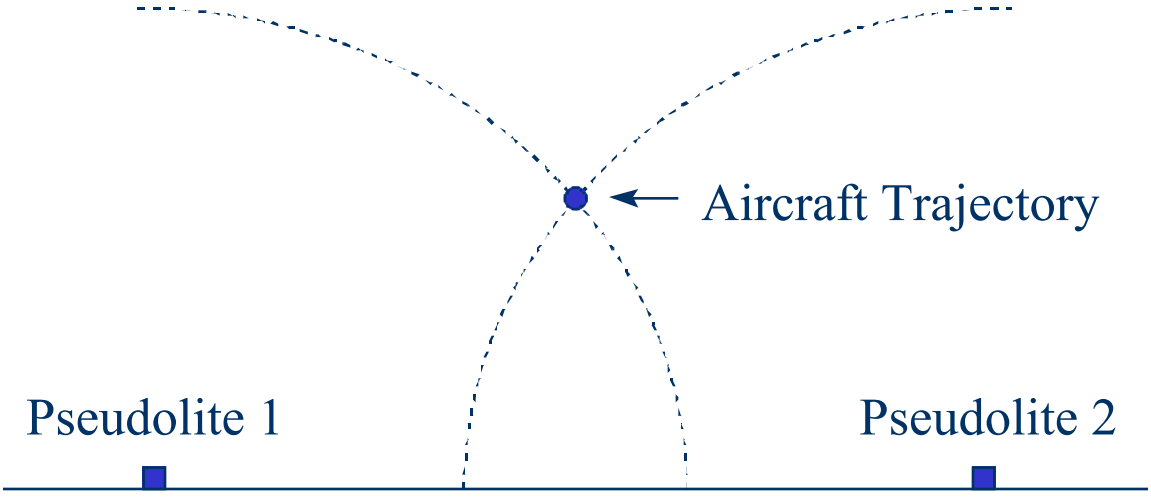

Figure 15 - Along Track View of Straight Aircraft Trajectory

pseudolites, causing rapid changes in the line-of-sight unit vectors to these transmitters. With adequate pseudolite pass geometry, a batch process may be used to produce a solution with very small position and integer estimate covariances.

For a straight vehicle trajectory, it can be shown from Equation 4.1 that each pseudolite provides an accurate measurement of along-track and radial position, but no information about cross-track position[39]. In the IBLS system, this problem is solved by placing two pseudolites on opposite sides of the approach path. These pseudolites complement each other to produce a highly accurate and robust 3-D navigation solution (Figure 15). Because an aircraft on final approach must fly straight for safety reasons, a minimum of two pseudolites are needed in aircraft landing system applications.

Unlike airplanes on final approach, most land vehicles using GPS have the freedom to execute a curved trajectory near a pseudolite. The theory and experiments presented below were founded on the idea that, with an appropriate ground trajectory, it is possible to initialize a CDGPS system using a single pseudolite that is outside the plane of motion of the vehicle positioning antenna.

4.3 Mathematical Ground Constraint

A second navigation advantage land vehicles have over aircraft is two-dimensional motion. Since land vehicles are constrained to move on the ground, this information could be used to improve the accuracy, integrity, and nonlinear convergence properties of the pseudolite solution.

4.3.1 Accuracy Improvement

Some noise is created on the vertical motion of a land vehicle due to ground disturbances such as tire compression, bumps, and vehicle roll and pitch motion. For this reason, it is usually not realistic to impose a hard equality constraint on the vehicle position in

Equations 4.2 - 4.4. If the ground near the pseudolite is fairly well modeled as a planar surface, the noise may be modeled as Gaussian white noise. The following equation for a soft ground constraint can then be added at each epoch, improving the accuracy of the final position solution:

$$z = -e_{ground}^{T} x_k + \mu_k \tag{4.5}$$

where z is the ground plane distance from the reference antenna, e_{ground} is the ground unit normal vector (pointing up), and μ_k is the ground noise with assumed Gaussian standard deviation σ_z.

In practice, z, e_{ground} and σ_z can be found empirically by driving in the vicinity of the pseudolite while collecting accurate position fixes. If the ground measurement standard deviation (σ_z) is very small compared to the carrier standard deviation (σ_ϕ), the solution obtained using Equation 4.5 in the batch process mathematically approaches the solution obtained using a hard equality ground constraint.

4.3.2 Integrity Improvement

By applying symmetry to Equation 4.1, it can be shown that two identical linear trajectories equidistant above and below a pair of pseudolites will yield the same carrier-phase measurements (Figure 15). It can also be shown mathematically that two identical planar trajectories an equal distance above and below a single pseudolite will yield identical pseudolite carrier-phase measurements (Figure 16). The false "mirror" solution represents a second minimum for the nonlinear convergence of the batch algorithm.

Even when the trajectory is not perfectly planar, a false local minimum often exists in the nonlinear convergence equations. A ground constraint or some other logic must be added to ensure that the algorithm converges on the correct solution. For example, if the pseudolite is on a pole and the vehicle is on the ground, the vertical position of the vehicle may be mathematically constrained to lie below the pseudolite.

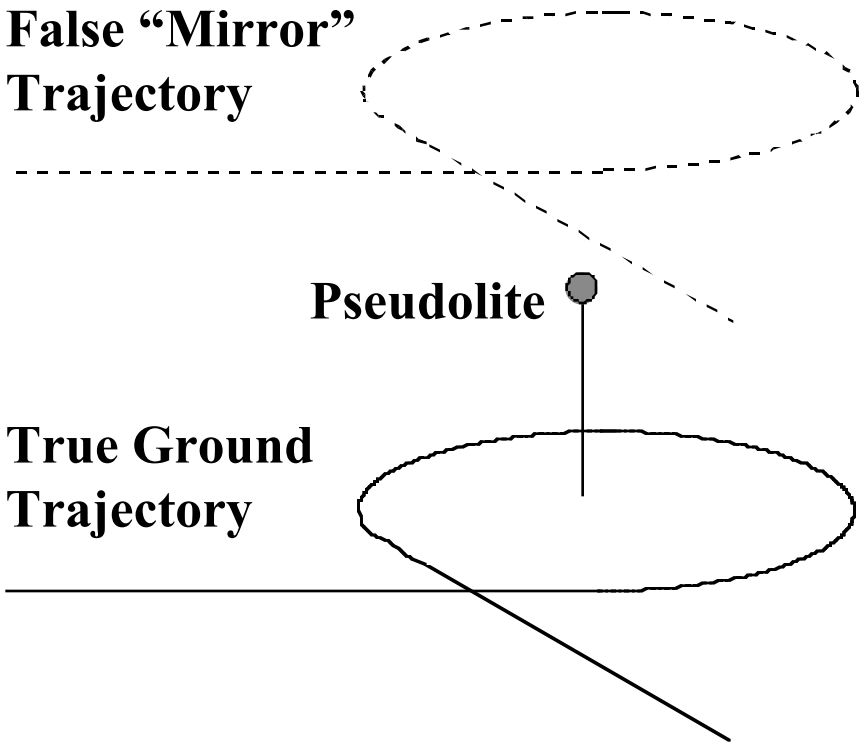

Figure 16 - Mirror Solution for Planar Trajectory

4.4 Simulation

To verify the feasibility of CDGPS initialization in a land vehicle using a single pseudolite, simulations were run for three possible bubble pass trajectories: (1) full 360° motion around the pseudolite, (2) 270° motion around the pseudolite, and (3) 180° motion around the pseudolite (Figure 17). These paths were chosen to be fairly simple while still including large line-of-sight geometry changes to the pseudolite. The minimum approach distance to the pseudolite was 4 meters, and the altitude of the pseudolite was 2.25 meters.

The limits on motion around the pseudolite reflect possible real-world constraints such as physical obstructions or directional antenna patterns. For example, a pseudolite placed over the corner of a building would limit vehicle motion to 270°, while a patch antenna angled to face the ground would limit pseudolite reception to one side of the pseudolite.

Monte-carlo simulations were performed to determine the CDGPS position accuracy after a pseudolite pass. For each trajectory, 500 passes were performed. The ground constraint equation (4.5) was not used, and each pass incorporated a new satellite geometry based on a recent satellite almanac and a 10° elevation mask. The simulations used Gaussian white carrier-phase measurement noise with a 1 centimeter standard deviation. The statistics of the results are shown in Table 3. The convergence properties

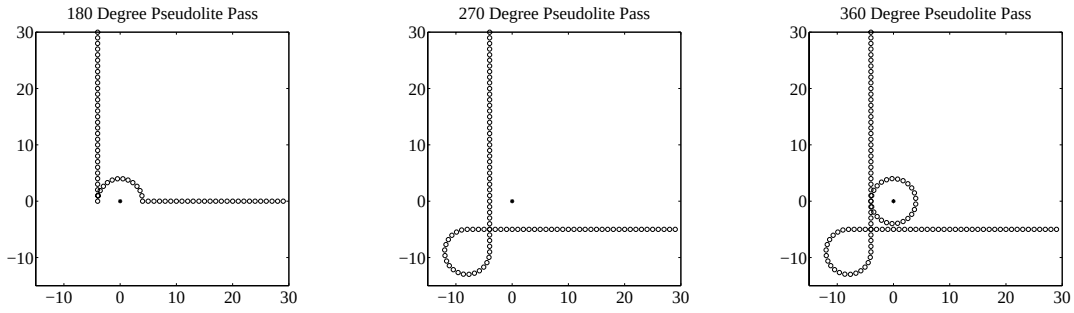

Figure 17 - Simulated Pseudolite Pass Trajectories

Table 3 - Monte-Carlo Simulation Results for Pseudolite Solution Accuracy

	360° Path	270° Path	180° Path
East (1-σ)	0.84 cm	0.86 cm	1.24 cm
North (1-σ)	1.12 cm	1.14 cm	1.77 cm
Up (1-σ)	2.49 cm	3.30 cm	3.47 cm

of the nonlinear algorithm were not explored in these simulations.

The simulations show that centimeter-level accuracies are achievable by following these simple trajectories. As expected, the best performance is achieved by the 360° path. Constraining vehicle motion to 270° slightly degrades the vertical accuracy of the final solution but has little effect on the horizontal accuracy. The 180° path suffers an added degradation in horizontal performance, but the total horizontal error is still better that an inch (2.16 centimeters 1-σ).

These accuracies can be improved even further by incorporating the ground constraint equation (4.5) into the algorithm. Figure 18 shows the simulated error standard deviation for the 180° path as a function of ground noise. As expected, when the ground noise approaches zero, the vertical error of the solution also approaches zero. An interesting result is that improving the vertical solution also improves the horizontal solution. As the ground noise approaches zero, the East and North errors are reduced by approximately 30%.

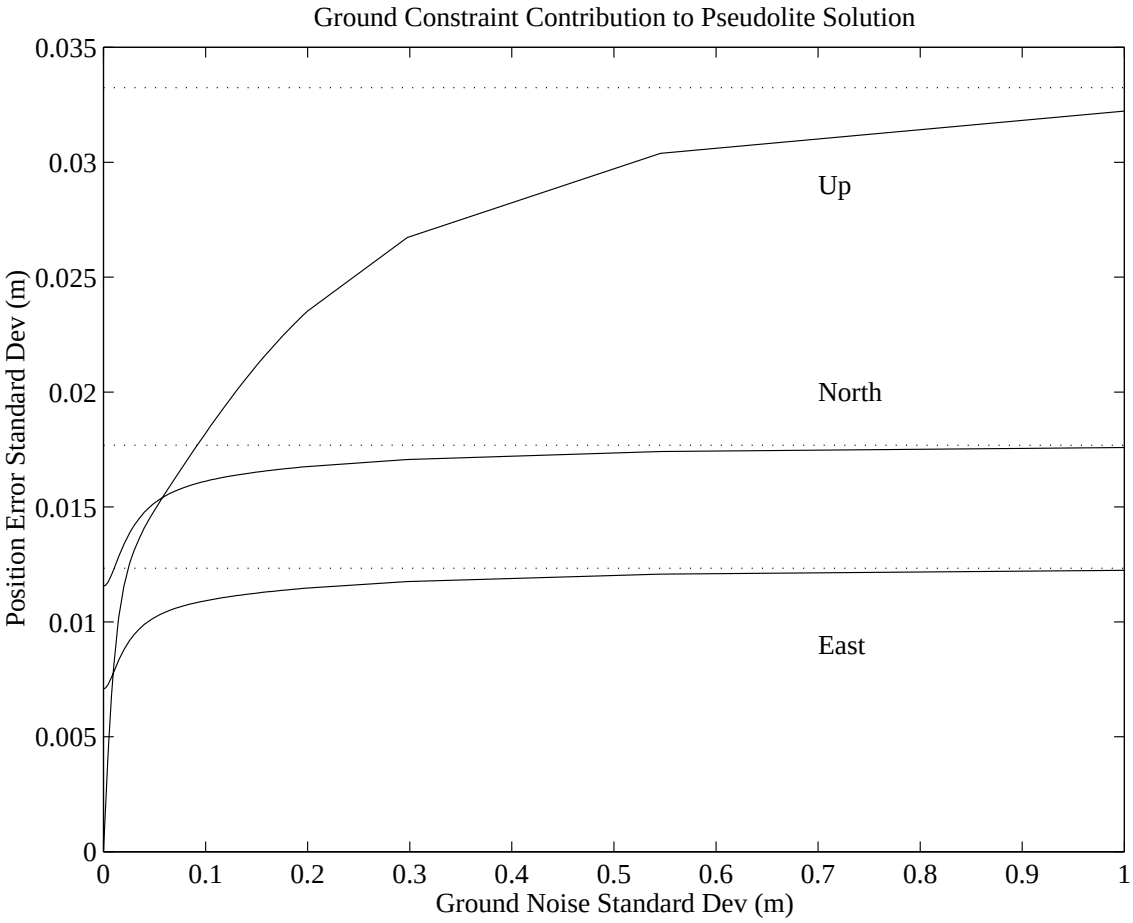

Figure 18 - Effect of Ground Constraint on Pseudolite Pass Accuracy

4.5 Experimental Setup

For hardware compatibility reasons, a standard patch antenna with no pre-amplifier was used as the pseudolite transmit antenna in these experiments. The pseudolite antenna was located atop a tall aluminum pole and had line-of-sight to the reference station and test field. The antenna location was surveyed using a pair of Trimble 4000SSE receivers. After surveying, the antenna was angled 45 degrees toward the ground so the pseudolite signal could be received by the tractor. Early attempts to survey the pseudolite position with the antenna angled toward the ground were unsuccessful. It is believed the problems were caused by ground multipath.

4.6 Real-Time Testing

The primary goal of vehicle testing was to demonstrate the real-time accuracy and convergence capability of the pseudolite algorithm with just one pseudolite. For the simplicity of early experimentation, the ground constraint equation was not implemented in the real-time system during these tests.

Since the pseudolite used a patch antenna, a slight modification to the 180° pass described above was used during testing. Figure 19 sketches the basic trajectory. The minimum and maximum ranges, often referred to as the near and far pseudolite bubbles, result from the pseudolite power level received by the vehicle. When the vehicle is within the near bubble, the pseudolite signal is so strong that it overpowers the GPS signals from satellites, effectively jamming the receiver. When the vehicle is outside the far bubble, the range causes the pseudolite signal to fall below the level required for carrier tracking. A

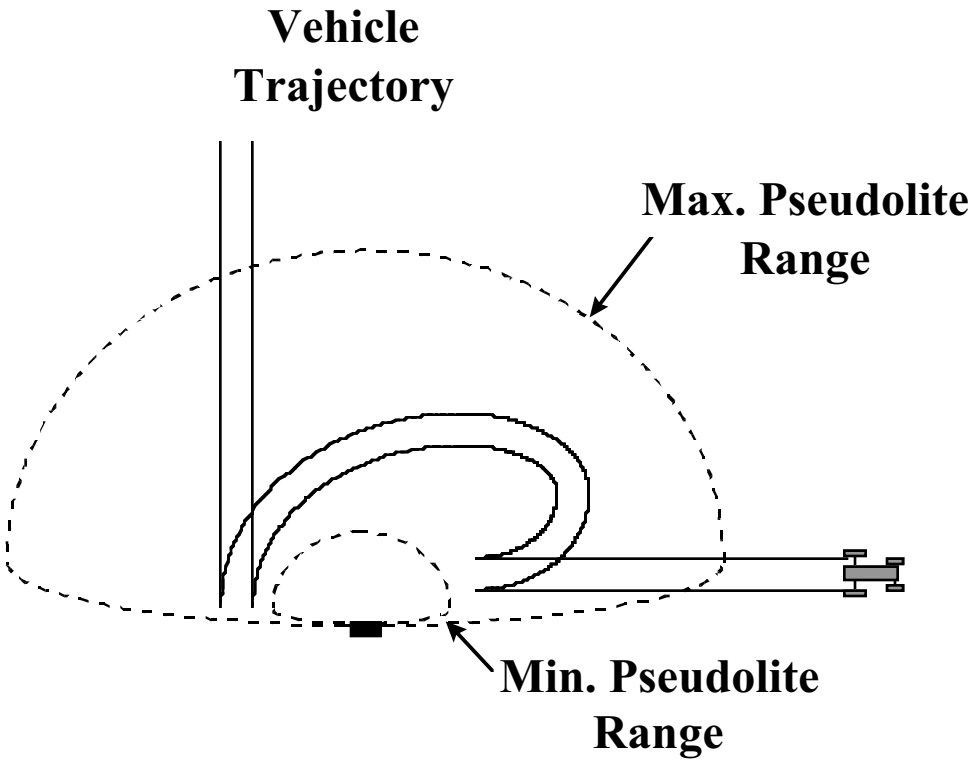

Figure 19 - Experimental Pseudolite Pass – Top View

solution to this "near-far" problem using a pulsing pseudolite has been demonstrated experimentally at Stanford University[41].

Of the 30 initial experiments, only twelve resulted in a successful mathematical solution in real-time. An important fact to note is that all eighteen unsuccessful trials recognized the false solution or the inability to reach a solution, *so there was no breach in system integrity*. It is expected that all eighteen failures were caused by receiver jamming (traveling within the near bubble), insufficient bubble pass geometry (due to leaving the far bubble prematurely), or converging to the mirror solution (since no ground constraint logic was used). These hypotheses could be confirmed by repeating these tests with a logical ground constraint and a pulsing pseudolite.

After each successful pseudolite pass, the tractor was manually driven over a repeatable ground track after leaving the pseudolite signal area to verify the solution accuracy. The results from twelve successful pseudolite passes are shown in Figure 20. A sharp improvement in position accuracy is clearly seen as the tractor leaves the pseudolite signal region and the batch algorithm is executed. The high precision and repeatability are evident from the low noise around the repeated track. On the repeated track, the overall horizontal noise, *including driver error and path deviations*, had better than a five centimeter standard deviation.

The ground constraint equation (4.5) and mirror solution logic were not implemented in the real-time software during testing. As a result, it was found in post-processing that the algorithm converged on the incorrect mirror solution for five pseudolite passes. When the unsuccessful passes were processed while constraining the vehicle position below the pseudolite, all converged to the correct solution.

Experimentally, it was found that vehicle motion during a bubble pass was not perfectly planar. Therefore, the mirror solution represents a local minimum in the vehicle position solution space, not a global minimum. Even if a ground constraint is not used, it may be

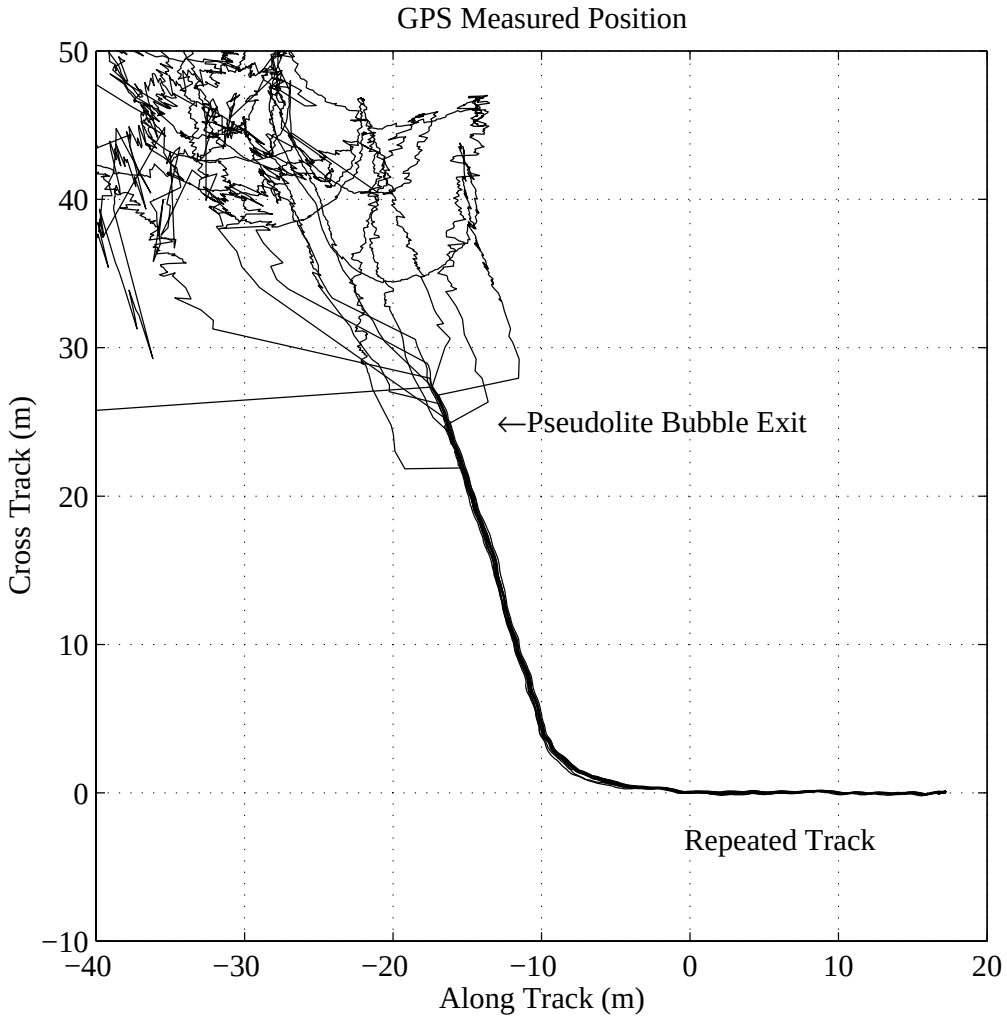

Figure 20 - GPS Measurements for Successful Pseudolite Passes

possible to identify a mirror solution by its larger than expected integrity-check residual. For all five cases examined in post-processing, the residual for the correct solution was better than the residual for the mirror solution.

4.7 Pseudolite Antenna Considerations

According to simulations presented earlier in this work, a transmit antenna which could be received on the ground in all directions would allow 270° and 360° pseudolite passes, which would greatly improve the accuracy and integrity of this system. A simple dipole

or half-dipole antenna would meet this requirement at low cost and reduced complexity. The vertical polarization of a dipole or half-dipole antenna would also serve to reduce ground multipath of the pseudolite signal[43].

Two major potential problems exist when using a simple pseudolite antenna, both of which are due to the fundamental differences in phase characteristics between a patch and a dipole.

4.7.1 Dipole Survey Issues

The first problem arises in surveying the location of the pseudolite. Data processing in existing survey equipment assumes two circularly polarized antennas are used in the survey. If a vertically polarized antenna was surveyed relative to a patch antenna, phase corrections would have to be applied within the survey software.

A basic method of examining circular electromagnetic polarization corrections for CDGPS has been developed and tested[44]. Applying these methods to a vertically polarized antenna receiving a circularly polarized wave is straightforward. It can be shown that GPS satellite rotation about its boresight increases the carrier-phase measured at a patch and a dipole antenna equally. It can also be shown that satellite elevation motion has no phase effect for either receive antenna, so long as the elevation does not perfectly coincide with the null of the dipole at 90°. A phase difference between the antennas is seen, however, when the GPS satellite moves in azimuth. By symmetry, a vertically polarized antenna will see no phase difference with satellite azimuth motion, however, a patch antenna will see a phase angle difference equal to the azimuth angle change (Figure 21).

One solution to this problem is to modify the standard survey software to make this phase correction. This would be a straightforward change since the azimuth angle to a GPS satellite is well known after receiver initialization. A second solution would be to perform a pseudolite pass with the vehicle position already known to high accuracy. By

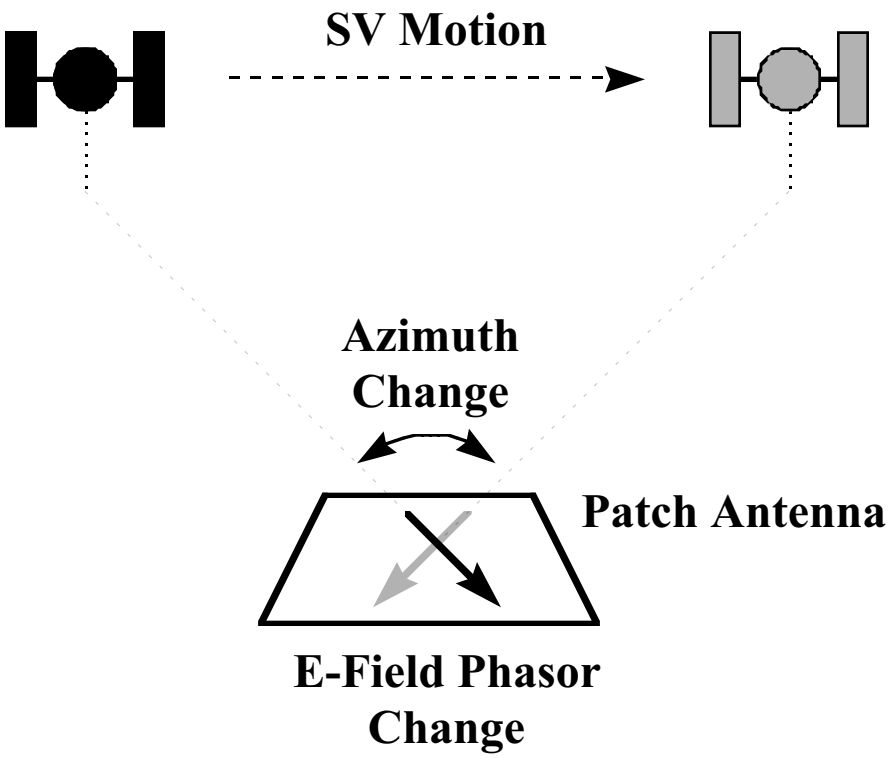

Figure 21 - Patch Phase Difference Due to Satellite Azimuth Motion

rewriting Equation 4.1 and combining with Equations 4.2 and 4.3, the pseudolite pass algorithm may be easily modified to solve for the position of the pseudolite. Instead of Equation 4.4, the following linearized equation would be used:

$$\delta\phi_{jk} = +\hat{e}^{\iota}_{jk}\delta p_j + \tau'_k + N'_j + \nu_{jk} \quad j = 1...n \tag{4.6}$$

where $^{op}_{j}$ is the linearized deviation in position for pseudolite J .

4.7.2 Dipole Transmission Issues

The second potential problem with using a dipole pseudolite antenna arises when receiving the vertically polarized signal through a patch antenna. It can be shown that rotating a vehicle receive antenna about its boresight has the same phase effect whether the pseudolite signal is of circular or linear polarization. It can also be shown that moving

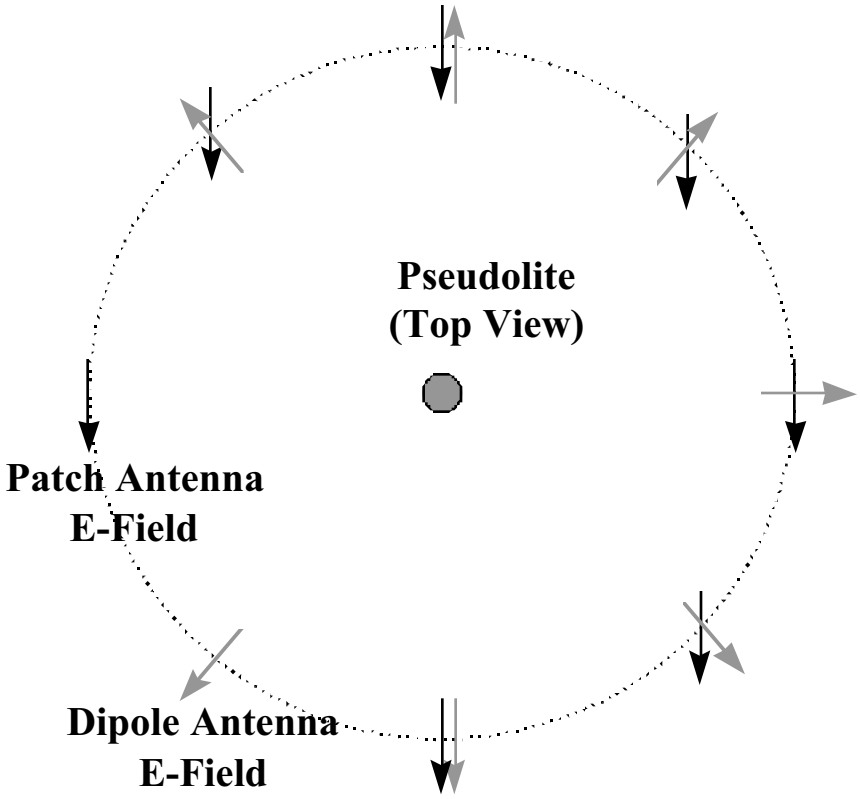

Figure 22 - Instantaneous Horizontal E-Field Below a Pseudolite

the receive antenna radially away from the pseudolite will have the same effect regardless of which transmit antenna is used. However, moving the receive antenna tangentially around a pseudolite with a dipole antenna will produce an increase in phase that is not present with a pseudolite using a patch antenna (Figure 22). This difference is equal to the change in azimuth angle around the pseudolite.

This second problem is readily solved by adding a phase correction term to Equations 4.1 and 4.4 which increases as the vehicle moves around the pseudolite. The pseudolite carrier-phase measurement equation becomes

$$\phi_{jk} = \left| p_j - x_k \right| + \tau_k + \beta_{jk} + N_j + \nu_{jk} \tag{4.7}$$

where β_{jk} is defined as the azimuth angle from the pseudolite to the vehicle. This angle is tracked in the vehicle positioning software, and continues to increase in increments of 2π as the vehicle moves in circles around the pseudolite.

Chapter 5

Land Vehicle Dynamics

Before land vehicle automatic control is possible, a simple yet accurate mathematical model of vehicle dynamics is required. Unfortunately most of the land vehicle models found in the literature were established for manufacturing design, driving simulations, or ride handling studies and are too complex for controller design[45,46]. For control system experiments, previously published models by Wong[47] and Ellis[48] are often used, but these make very specific assumptions about land vehicle dynamics, and in particular about lateral tire slip. This chapter serves to introduce a new set of land vehicle lateral dynamic models for use in the automatic control of land vehicles.

While a complex mathematical model that is applicable for *any* land vehicle is desirable, a model identification process which could potentially be automated for post-processing or possibly even real-time operation is also a goal. As models become more complicated, the procedures to identify model parameters from experimental data becomes less effective. A set of models is desired which vary in complexity to facilitate this engineering trade-off.

The procedure for model selection and identification using experimental data is described in Chapter 6.

5.1 Land Vehicle Model Assumptions

Countless mathematical models can be used to describe the motion of a land vehicle. Each of these models is based on a certain set of assumptions. The engineering challenge in designing a control system is to choose the simplest model whose assumptions are sufficiently valid to allow accurate, robust, and/or adaptive control system design.

5.1.1 Linear Assumption

No physical system is truly linear; however, most control systems are designed about a fixed operating point and are based on linear assumptions. While nonlinear modeling and automatic control offer the potential for elegant solutions and more accurate control over a wider range of conditions, these models are difficult to experimentally characterize and are often highly susceptible to modeling errors. Also, since linearization is often perfectly sufficient to provide satisfactory performance in the range of interest, the linear assumption is often made in control system design.

5.1.2 Time Invariance Assumption

A second common assumption in system modeling for automatic control system design is the assumption of time invariance. Even though the dynamics of most physical systems change with time, this change often occurs very slowly and the details of this variation are usually not known in advance. As a result, most control systems assume a time invariant plant.

Land vehicle dynamics are subject to relatively rapid change due to variations in load, driving surface, tire inflation, and other parameters. Unless the variation in these parameters is known in advance, a time-invariant *form* for the plant model can be

assumed. With an appropriate model in place, one way to account for time variation of parameters is to identify these parameters in real-time and adjust the control system accordingly.

5.1.3 Bicycle Model Assumption

Figure 23 shows some of the definitions, sign conventions, and nomenclature used throughout this work. The wheelbase (L), front wheel angles (δ_L and δ_R), heading (Ψ), and lateral position (y) are shown. Note that the center of the rear axle is defined as the vehicle reference point for consistency between various land vehicles, even in the presence of added vehicle components such as a towed trailer or hitched implement. A

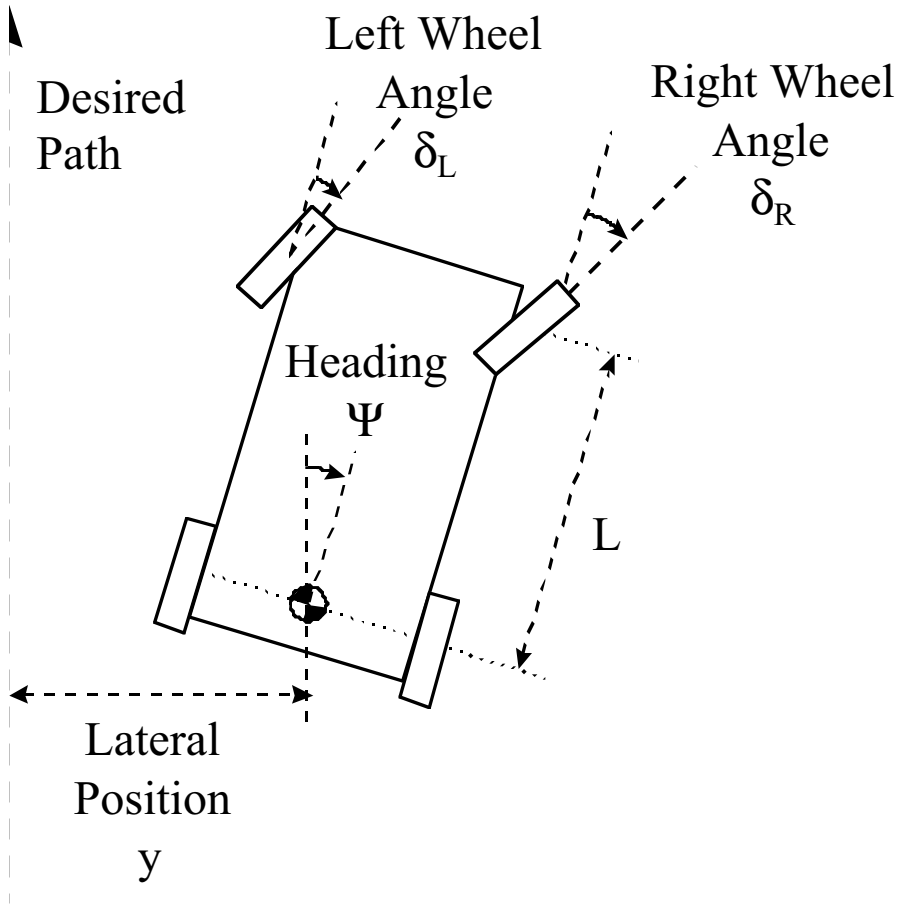

Figure 23 - Land Vehicle State Definitions

lever-arm correction is needed within the automatic control system when the point of control interest is located at a position other than the reference point.

During turns, the two front wheels of most land vehicles create different angles relative to the vehicle body. The first simplifying assumption often made for land vehicles is the "bicycle model" assumption[47]. This simplification combines the effects of the two front wheels and treats them as a single wheel with an "effective" wheel angle (δ). The definition of this effective wheel angle is somewhat arbitrary, though it will be shown that carefully defining this variable can simplify the control design process. The bicycle model also combines the two rear wheels and treats them as a single wheel. In most land vehicle control applications, a linear and time invariant (LTI) model based on these assumptions is used.

5.2 LTI Bicycle Model Special Cases

Most previous work in the automatic control of land vehicles has assumed a simple model derived by Ellis[22,49] or a parameterized force based model described by Wong[50,51,52,53]. These models are described below.

5.2.1 Ellis Bicycle Model

The simplest vehicle model adequate to describe land vehicle lateral dynamics with a commanded wheel angle rate is based on the bicycle model assumptions, as well as the assumption of no lateral tire slip, no steering actuator dynamics, and constant rear wheel forward velocity (V_x). These approximations tend to hold well for vehicles driving on hard, flat surfaces at slow speeds, but they break down for fast-moving vehicles or vehicles on a loose or slippery surface.

Since zero lateral tire slip is assumed, the perpendicular component of front wheels velocity (V_{yf}) is found by the following equation (see Figure 24):

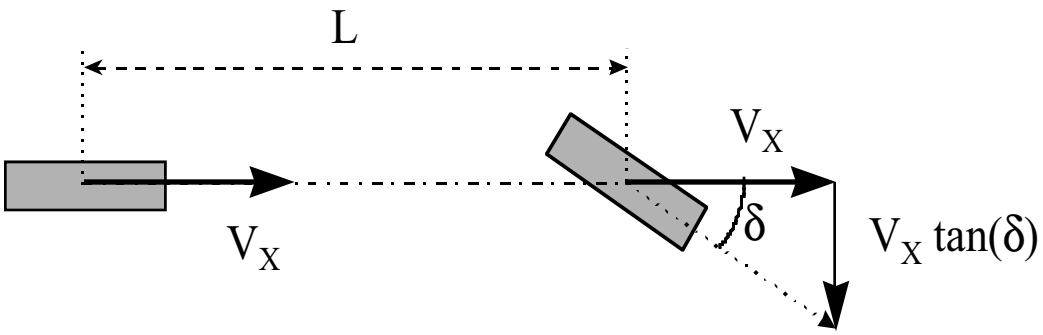

Figure 24 - Simple Vehicle Model Derivation

$$V_{yf} = V_x \tan(\delta) \quad . \tag{5.1}$$

Since the rear wheel is laterally constrained as well, the heading rate may be found by dividing this velocity by the wheel base length (L),

$$\dot{\Psi} = \frac{V_{yf}}{L} = \frac{V_x}{L}\tan(\delta) \quad . \tag{5.2}$$

In an *earth-fixed coordinate frame*, the motion of the reference point, which is located at the center of the rear axle, may be found by the following non-linear equations:

$$\dot{x} = V_x \cos(\Psi) \quad , \tag{5.3}$$

$$\dot{y} = V_x \sin(\Psi) \quad , \tag{5.4}$$

where x is the along-path position of the vehicle, and y is the lateral position deviation of the vehicle. Note that the position variables x and y are defined in earth-fixed coordinates, while the velocity V_x is defined in the body frame.

If we assume the vehicle is following a nominal straight line, Ψ and δ are small, and higher order terms are negligible, Equations 5.2 - 5.4 can be decoupled, linearized, and formulated in the standard state-space form. If we also assume the input command to the system is a front wheel angle rate, the noise-free lateral equations of motion become:

$$\begin{bmatrix} \dot{y} \\ \dot{\Psi} \\ \dot{\delta} \end{bmatrix} = \begin{bmatrix} 0 & V_x & 0 \\ 0 & 0 & \frac{V_x}{L} \\ 0 & 0 & 0 \end{bmatrix} \begin{bmatrix} y \\ \Psi \\ \delta \end{bmatrix} + \begin{bmatrix} 0 \\ 0 \\ 1 \end{bmatrix} u \quad . \tag{5.5}$$

There are three roots to the characteristic equation of this model, all of which lie at the origin in the s-plane. The open-loop transfer function from the control input to the lateral position output is simply a triple integrator with no zeros:

$$\frac{Y(s)}{U(s)} = \frac{\left(\frac{V_x^2}{L}\right)}{s^3} \quad . \tag{5.6}$$

5.2.2 Wong Bicycle Model

The Wong model is the method typically used to account for the effects of lateral tire slip in land vehicles. A generic free body diagram showing velocities and forces on a bicycle land vehicle model are shown in Figure 25. Because V_x and V_y are defined in the rotating vehicle coordinate frame, care must be taken to generate the following equations of motion for the system:

$$m\left(\dot{V}_x - V_y \Omega_z\right) = F_{xr} + F_{xf} \cos\delta - F_{yf} \sin\delta \quad , \tag{5.7}$$

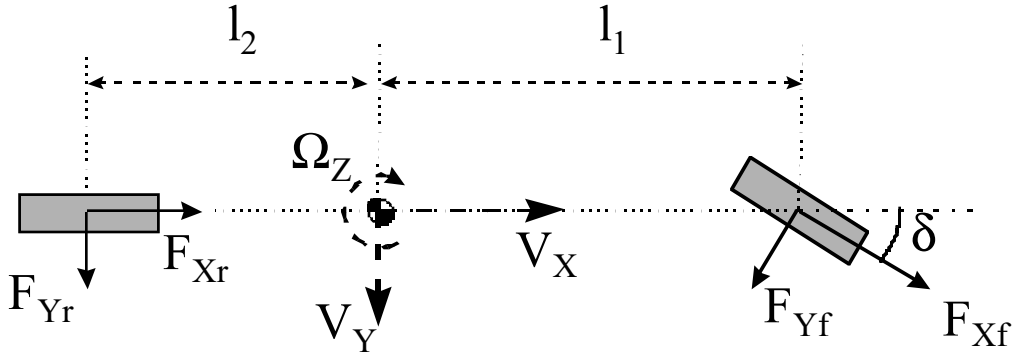

Figure 25 - Bicycle Model Free Body Diagram

$$m\left(\dot{V}_y + V_x\Omega_z\right) = F_{yr} + F_{xf}\sin\delta + F_{yf}\cos\delta \quad , \tag{5.8}$$

$$I_z\dot{\Omega}_z = -l_2F_{yr} + l_1F_{xf}\sin\delta + l_1F_{yf}\cos\delta \quad . \tag{5.9}$$

Note that the reference point for this new set of equations is the vehicle center of mass, not the center of the rear axle.

The difficulty in reducing these equations further lies in computing the lateral forces on the tires. It is proposed by Wong that, for small side slip angles (α), the lateral force on a tire is proportional to this side slip angle[47] (See Figure 26). The following equations

$$F_{yf} = 2C_{\alpha f}\alpha_f \quad , \tag{5.10}$$

$$F_{yr} = 2C_{\alpha r}\alpha_r \quad , \tag{5.11}$$

may then be substituted into Equations 5.7-5.9. Linearizing by making small angle assumptions, assuming a constant V_x, and neglecting higher order terms, the lateral equations again decouple from the longitudinal equations to form the following state-space model:

$$\begin{bmatrix} \dot{V}_y \\ \dot{\Omega}_z \\ \dot{y} \\ \dot{\Psi} \\ \dot{\delta} \end{bmatrix} = \begin{bmatrix} \frac{-2(C_{\alpha r}+C_{\alpha f})}{mV_x} & \frac{2(C_{\alpha r}l_2 - C_{\alpha f}l_1)}{mV_x} - V_x & 0 & 0 & \frac{2C_{\alpha f}}{m} \\ \frac{2(C_{\alpha r}l_2 - C_{\alpha f}l_1)}{I_zV_x} & \frac{-2(C_{\alpha r}l_2^2 + C_{\alpha f}l_1^2)}{I_zV_x} & 0 & 0 & \frac{2C_{\alpha f}l_1}{I_z} \\ 1 & 0 & 0 & V_x & 0 \\ 0 & 1 & 0 & 0 & 0 \\ 0 & 0 & 0 & 0 & 0 \end{bmatrix} \begin{bmatrix} V_y \\ \Omega_z \\ y \\ \Psi \\ \delta \end{bmatrix} + \begin{bmatrix} 0 \\ 0 \\ 0 \\ 0 \\ 1 \end{bmatrix} u \quad . \tag{5.12}$$

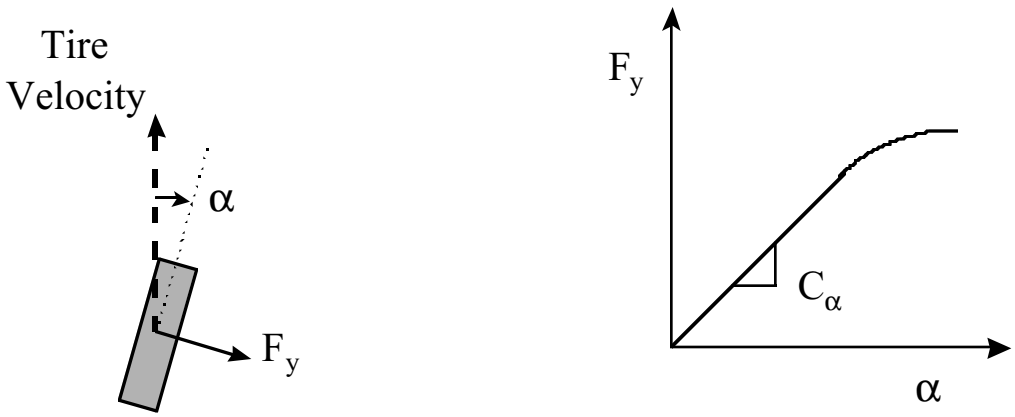

Figure 26 - Wong Tire Slip Model

This model performs significantly better than the Ellis no-slip model for describing land vehicles operating at high speeds. The biggest drawback to this approach is the added complexity. Finding vehicle properties such as mass, moments of inertia, and center of mass location can be difficult – especially for large vehicles. Also, the tire lateral force "constants" ($C_{\alpha f}$, $C_{\alpha r}$) actually vary significantly with tire pressure, tire tread, surface conditions, and forward speed, making them difficult to determine[47]. In fact, when the tire is laterally constrained by friction, these values become infinite.

System identification (on- or off-line) is a reasonable approach to specify a model of this form; however, the state transition matrix is nonlinear in the relevant parameters. The potential exists for a numerically intensive method for parameter identification which may be prone to diverge with poor initial parameter estimates or wide eigenvalue spreads. To eliminate the need for a nonlinear identification algorithm, it is possible to parameterize each unknown element of the state-space matrices individually (e.g. $p_1 = \mathbf{A}_{11} = \frac{-2(C_{\alpha r}+C_{\alpha f})}{mV_x}$), but this does not solve the possible divergence due to poor eigenvalues.

For an automobile under normal driving conditions, forward speeds may reach approximately 30 meters per second. The mass of a typical automobile is approximately 1500 kilograms, and characteristic lengths are on the order of 1 to 2 meters. Typical

values for the lateral slip coefficients in a car are 3000 Newtons per radian at a forward speed of 13.9 meters per second[53].

For a farm vehicle, forward speeds generally lie in the range of 2 to 10 meters per second. The mass of a medium sized-farm vehicle is approximately 7,500 kilograms, and the characteristic lengths are on the order of 1 to 2 meters. To the best knowledge of the author, typical lateral slip coefficient values for a tractor have not previously been published. In fact, it will be shown later in this work that these values are extremely difficult to determine, even when high-bandwidth, high-accuracy measurements of vehicle position, attitude, and front wheel angle are available for system identification.

5.2.3 Wong Model With Hitched Implement

The Wong model, as presented above, makes no provision for a hitch mounted vehicle implement, but this extension can be easily made. Assuming the implement is located a distance l_3 behind the rear axle (see Figure 27), and the forces on the implement are described by the Wong lateral slip model (see Equations 5.10 and 5.11) with coefficient $C_{\alpha h}$, the complete Wong model with hitched implement looks almost identical to the original model,

$$\begin{bmatrix} \dot{V}_y \\ \dot{\Omega}_z \\ \dot{y} \\ \dot{\Psi} \\ \dot{\delta} \end{bmatrix} = \begin{bmatrix} \frac{-2(C_{\alpha r}+C_{\alpha h}+C_{\alpha f})}{mV_x} & \frac{2(C_{\alpha r}l_2+C_{\alpha h}l_4-C_{\alpha f}l_1)}{mV_x}-V_x & 0 & 0 & \frac{2C_{\alpha f}}{m} \\ \frac{2(C_{\alpha r}l_2+C_{\alpha h}l_4-C_{\alpha f}l_1)}{I_zV_x} & \frac{-2(C_{\alpha r}l_2^2+C_{\alpha h}l_4^2+C_{\alpha f}l_1^2)}{I_zV_x} & 0 & 0 & \frac{2C_{\alpha f}l_1}{I_z} \\ 1 & 0 & 0 & V_x & 0 \\ 0 & 1 & 0 & 0 & 0 \\ 0 & 0 & 0 & 0 & 0 \end{bmatrix} \begin{bmatrix} V_y \\ \Omega_z \\ y \\ \Psi \\ \delta \end{bmatrix} + \begin{bmatrix} 0 \\ 0 \\ 0 \\ 0 \\ 1 \end{bmatrix} u \quad , \quad (5.13)$$

where $l_4 \equiv l_2 + l_3$.

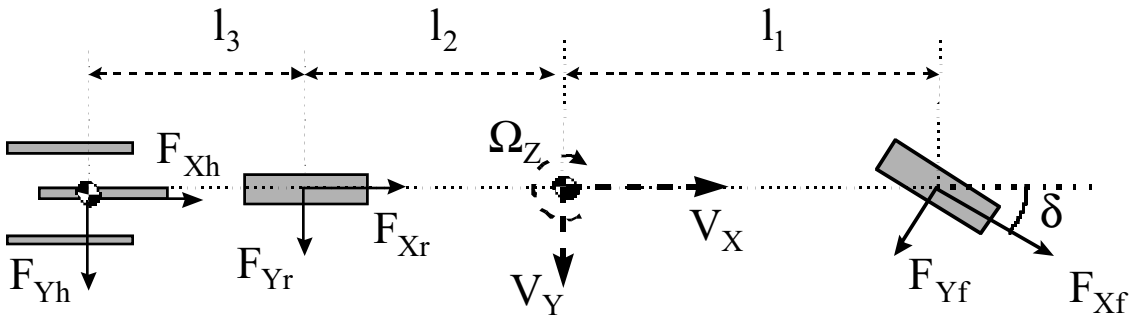

Figure 27 - Free Body Diagram with Hitched Implement

5.2.4 Simplified Wong Model - No Rear Tire Slip

The Ellis and Wong models described above have been used successfully in specific control system applications, but each has significant drawbacks limiting them from use in all circumstances. It is desirable to have models which are more sophisticated than the Ellis model, yet have fewer or more easily identifiable parameters than the Wong model. One approach to developing these theoretical models is to make reasonable assumptions about the system in order to simplify the more complicated Wong model.

One simplification to the complete Wong model is to assume a non-holonomic constraint on the rear tire (i.e. zero rear lateral tire slip) using the previous assumption for the front tire and hitch lateral slip. This is equivalent to taking the limit as $\upsilon_{\alpha r}$ goes to infinity. This assumption is potentially valid for land vehicles with a rear differential which works to eliminate lateral tire slip. The assumption may also hold true for vehicles with large rear tires, vehicles moving at relatively slow speeds over level terrain, or with vehicles with significant vertical loading on the rear tires. A large farm tractor on a flat field fits all of these descriptions, and experience shows that lateral rear tire slip for these vehicles on flat terrain can be very minor, even when pulling a hitched implement.

Summing the moments about the center of the rear axle, the rotation equation of motion is

$$\left(I_z + ml_2^2\right)\dot{\Omega}_z = \left(l_1 + l_2\right)\left(F_{xf}\sin\delta + F_{yf}\cos\delta\right) - l_3 F_{yh} \quad . \tag{5.14}$$

Note that the value for F_{yh} is zero in the absence of a hitched implement.

Substituting Equation 5.10, the linearized version of Equation 5.14 becomes

$$\dot{\Omega}_z = \frac{-2\left(C_{\alpha f}\left(l_1 + l_2\right)^2 + C_{\alpha h} l_3^2\right)}{\left(I_z + m l_2^2\right) V_x}\Omega_z + \frac{2C_{\alpha f}\left(l_1 + l_2\right)}{\left(I_z + m l_2^2\right)}\delta \quad . \tag{5.15}$$

In this new model, the lateral velocity of the vehicle center of mass (V_y) is directly dependent on the vehicle rotation rate by

$$V_y = l_2 \Omega_z \quad . \tag{5.16}$$

Therefore, the state element V_y may be eliminated, and the state-space equations of motion become

$$\begin{bmatrix} \dot{y} \\ \dot{\Psi} \\ \dot{\Omega}_z \\ \dot{\delta} \end{bmatrix} = \begin{bmatrix} 0 & V_x & 0 & 0 \\ 0 & 0 & 1 & 0 \\ 0 & 0 & \frac{-2\left(C_{\alpha f}\left(l_1+l_2\right)^2 + C_{\alpha h} l_3^2\right)}{\left(I_z + m l_2^2\right) V_x} & \frac{2C_{\alpha f}\left(l_1+l_2\right)}{\left(I_z + m l_2^2\right)} \\ 0 & 0 & 0 & 0 \end{bmatrix} \begin{bmatrix} y \\ \Psi \\ \Omega_z \\ \delta \end{bmatrix} + \begin{bmatrix} 0 \\ 0 \\ 0 \\ 1 \end{bmatrix} u \quad , \tag{5.17}$$

where y now describes the lateral deviation of a reference point below the center of the rear axle (recall Figure 23).

A block diagram of this state-space model is shown in Figure 28. In addition to three levels of integration and a constant, velocity-dependent gain, this model exhibits a simple first-order lag response between front wheel angle and vehicle heading rate. This time lag is consistent with visual observation of a farm tractor driving on flat terrain. One interesting note is that in the absence of a hitched implement ($C_{\alpha h} = 0$), the steady state relationship between heading rate and wheel angle is identical to the Ellis model (Equation 5.2, where $L = l_1 + l_2$).

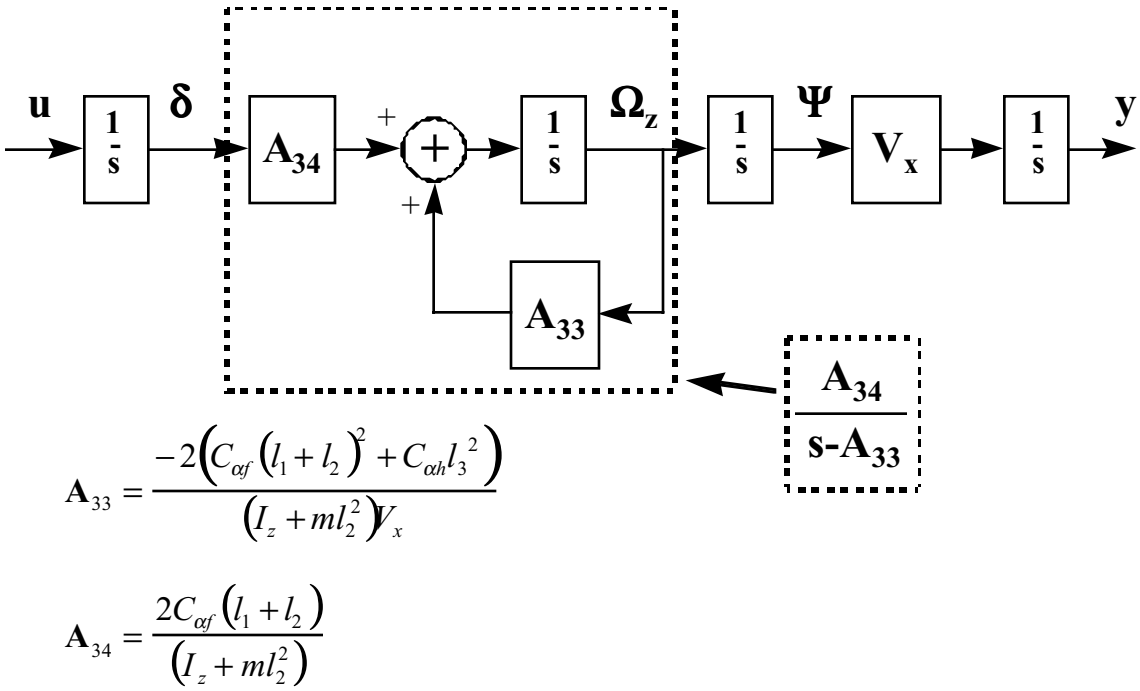

Figure 28 - Simplified Wong Model Block Diagram

5.2.5 Simplified Wong Model - Small Rear Tire Slip

In the case of zero lateral rear tire slip, four states are sufficient to describe land vehicle lateral dynamics; however, if the coefficient $C_{\alpha r}$ is finite, the Wong model shows that five states may be needed to adequately describe vehicle dynamics in the frequency range of interest. To determine the need to model a fifth vehicle state, the eigenvalues of the continuous state transition matrix may be examined to see if any lie outside the desired control system bandwidth or significantly beyond the Nyquist frequency of the discrete control system. It is easy to show that three open-loop eigenvalues are zero, just as in the Ellis model, but the expressions for the remaining two pole locations are algebraically complicated. One solution to this problem is to substitute exact parameter values into the equations to find an exact solution. If the exact values are not know, however, some simplifications may be made based on reasonable expressions for these values to arrive at general conclusions.

Based on visual observations of farm vehicles, one realistic assumption is that the rear tire lateral slip coefficient is finite, but very large compared to the front tire and hitch lateral slip coefficients. A second simplifying assumption is that the velocity component of the $\mathbf{A}_{12}$ term in Equation 5.13 is negligible compared to the component involving lateral slip coefficients. If, for example, we assume a rear tire lateral slip coefficient of 150,000, a characteristic length of 1 meter, a vehicle mass of 7500 kilograms, and a forward velocity of 2 meters per second, we find the assumption is reasonable:

$$\frac{2(C_{\alpha r}l_2 + C_{\alpha h}l_4 - C_{\alpha f}l_1)}{mV_x} \approx \frac{2C_{\alpha r}l_2}{mV_x} = 20 >> V_x \quad , \tag{5.18}$$

If we also reasonably assume that the three characteristic lengths are approximately equal, and these lengths are approximately equal to the vehicle radius of gyration about the vertical axis, the system eigenvalues and eigenvectors may be approximated algebraically. Based on the following assumptions,

$$\varepsilon_f \equiv \frac{C_{\alpha f}}{C_{\alpha r}} << 1, \quad \varepsilon_h \equiv \frac{C_{\alpha h}}{C_{\alpha r}} << 1 \quad , \tag{5.19}$$

$$l_1 \approx l_2 \approx l_3 \equiv l \quad , \tag{5.20}$$

$$I_z \approx ml^2 \quad , \tag{5.21}$$

and canceling out second order terms in epsilon, the approximate eigenvalues and eigenvectors are:

$$\lambda_1 = \frac{-4C_{\alpha r} - 9C_{\alpha h}}{mV_x}, \quad \lambda_2 = \frac{-4C_{\alpha f} - C_{\alpha h}}{mV_x} \quad , \tag{5.22}$$

$$v_1 = \begin{bmatrix} -l\left(1 - \frac{3}{2}\varepsilon_{\alpha h}\right) \\ 1 \end{bmatrix}, \quad v_2 = \begin{bmatrix} l\left(1 + \frac{3}{2}\varepsilon_{\alpha h}\right) \\ 1 \end{bmatrix} \quad . \tag{5.23}$$

Note that for sufficiently large values of $C_{\alpha r}$, the system pole at λ_1 may exceed the frequency range of interest while λ_2 remains unaffected. For the numerical values used in Equation 5.18, λ_1 is approximately -40 radians per second. For a 5 hertz discrete control system, this lies beyond the sampling frequency (31.4 radians per second), and therefore significantly beyond any feasible control system bandwidth.

The mode associated with λ_1 corresponds to how quickly the ratio between V_y and Ω_z reaches its steady-state value, while the mode associated with λ_2 corresponds to the response of V_y and Ω_z to wheel angle inputs. A large value for λ_1 indicates that the steady-state value for V_y may be substituted directly into the equations of motion and, due to its direct dependence on Ω_z, this state may be eliminated.

In the limit as $C_{\alpha r}$ approaches infinity, λ_1 also approaches infinity, and Equations 5.16 and 5.17 exactly describe the steady state V_y to Ω_z ratio and the dynamic equations of motion. For large finite values of λ_1, the *dynamics* associated with this mode may still be neglected, but the *steady-state* ratio of V_y to Ω_z will change slightly. As a result, the center of vehicle rotation on turns will no longer lie at the center of the rear axle. This will cause a slight change in the lateral dynamic equations of motion, which may now be approximated as:

$$\begin{bmatrix} \dot{y} \\ \dot{\Psi} \\ \dot{\Omega}_z \\ \dot{\delta} \end{bmatrix} = \begin{bmatrix} 0 & V_x & c & 0 \\ 0 & 0 & 1 & 0 \\ 0 & 0 & \dfrac{-2\left(C_{\alpha r} l_2^2 + C_{\alpha h} l_4^2 + C_{\alpha f} l_1^2\right) + 2(l_2 - c)\left(C_{\alpha r} l_2 + C_{\alpha h} l_4 - C_{\alpha f} l_1\right)}{I_z V_x} & \dfrac{2 C_{\alpha f} l_1}{I_z} \\ 0 & 0 & 0 & 0 \end{bmatrix} \begin{bmatrix} y \\ \Psi \\ \Omega_z \\ \delta \end{bmatrix} + \begin{bmatrix} 0 \\ 0 \\ 0 \\ 1 \end{bmatrix} u \quad , \qquad (5.24)$$

where c denotes how far back the center of vehicle rotation is relative to the center of the rear axle. This parameter can take on negative or positive values depending on the properties of the tires and the vehicle.

It is worth noting that, if we return to the Wong model and assume that the lateral tire slip coefficients for the front and rear tires are significantly large and that the hitch coefficient is relatively small, it can be shown that the Wong model is well approximated by the three-state Ellis model.

5.3 Bicycle Model Enhancements

The Ellis, Wong, and Wong-based equations described above provide a set of models describing land vehicle lateral dynamics. Several enhancements can be made to these models so they may more accurately reflect a specific land vehicle configuration.

5.3.1 Steering Dynamics

One assumption made in the models described above is a direct front wheel angle rate command. In truth, the response between the computer generated command and the physical wheel angle rate may include significant dynamics. The causes for these dynamics, as well as the methods for identifying them, are discussed in Chapter 6.

One assumption that can be made to simplify the linear steering identification process is one-way coupling between the vehicle states describing steering and other lateral dynamic states. Since vehicle heading and position are unlikely to have a significant effect on vehicle steering, this is almost always a valid assumption. Therefore, the steering system may be described as a system with a single input (wheel angle rate command) and a single output (wheel angle).

A SISO system that is second-order or higher may be described by an infinite number of state-vector definitions. To enforce a unique solution, a special canonical form is often used. Often the observability canonical form is used because the states in this form have physical meaning. The most general observability canonical equation for a third-order system is[54]

$$\begin{bmatrix} \dot{\delta} \\ \ddot{\delta} \\ \dddot{\delta} \end{bmatrix} = \begin{bmatrix} 0 & 1 & 0 \\ 0 & 0 & 1 \\ -a_3 & -a_2 & -a_1 \end{bmatrix} \begin{bmatrix} \delta \\ \dot{\delta} \\ \ddot{\delta} \end{bmatrix} + \begin{bmatrix} \beta_1 \\ \beta_2 \\ \beta_3 \end{bmatrix} u \quad . \tag{5.25}$$

This equation defines a third-order transfer function with three poles and two zeros with an arbitrary steady-state gain:

$$\frac{\delta(s)}{u(s)} = \frac{\beta_1 \left(s^2 + a_1 s + a_2\right) + \beta_2 \left(s + a_1\right) + \beta_3}{s^3 + a_1 s^2 + a_2 s + a_3} \quad . \tag{5.26}$$

For purposes of model simplification, the number of parameters in Equation 5.25 may be reduced in several ways. For one, if it is known that there is one physical integration between input and output, one root of the characteristic equation must be zero, resulting in $a_3 = 0$. Also, if the steering system is calibrated correctly, the steady-state gain from input to output rate will be unity, reducing one degree-of-freedom in the system. Other assumptions which will reduce the number of parameters are to assume only one system zero (resulting in $\beta_1 = 0$) or none (resulting in $\beta_2 = 0$). Of course, using a second-order system model will also serve to reduce the number of free parameters that must be specified to mathematically describe the system.

5.3.2 Sensor Bias States

A simple and powerful change that can be added to any of the above vehicle models is the addition of observable sensor biases. The biases on the heading(ψ) and wheel angle (δ) sensors are both observable when the lateral vehicle position is measured. The states ψ_{bias} and δ_{bias} may be appended to the state vector, producing the following changes in the state-space equations:

$$\mathbf{x}_a = \begin{bmatrix} \mathbf{x} \\ \psi_{\text{bias}} \\ \delta_{\text{bias}} \end{bmatrix} , \tag{5.27}$$

$$\mathbf{A}_a = \left[\begin{array}{c|c} \mathbf{A} & \mathbf{0} \\ \hline \mathbf{0} & \mathbf{0} \end{array}\right], \tag{5.28}$$

$$\mathbf{B}_a = \left[\begin{array}{c} \mathbf{B} \\ \hline \mathbf{0} \end{array}\right], \tag{5.29}$$

$$\mathbf{H}_a = \left[\begin{array}{c|cc} & 0 & 0 \\ \mathbf{H} & 1 & 0 \\ & 0 & 1 \end{array}\right]. \tag{5.30}$$

One interesting note is that, while the sensor bias states are observable, they are *not* controllable, so care must be taken in control law design when these bias states are included.

5.3.3 Integral States

A powerful tool for control system design is integral control. By augmenting the standard vehicle state with an integral state, it is possible to zero out the effect of any residual system biases on the control system output. In most land vehicle lateral control applications, it is desirable to zero the vehicle lateral position (y). This integral state may be appended in the following manner:

$$\mathbf{x}_a = \left[\begin{array}{c} y_{\text{integral}} \\ \hline \mathbf{x} \end{array}\right], \tag{5.31}$$

$$\mathbf{A}_a = \left[\begin{array}{c|ccc} 0 & 1 & 0 & \cdots \\ \hline \mathbf{0} & & \mathbf{A} & \end{array}\right], \tag{5.32}$$

$$\mathbf{B}_a = \left[\begin{array}{c} 0 \\ \hline \mathbf{B} \end{array}\right], \tag{5.33}$$

$$\mathbf{H}_a = \left[\begin{array}{c|c} 0 & \mathbf{H} \end{array}\right]. \tag{5.34}$$

In contrast to the sensor bias states, the integral state is controllable, but is not observable. Care must be taken in estimator design when an integral state is used.

5.4 Final Selected Model

The model selection process is described in detail in Chapter 6. There it will be shown that the final model selected for automatic land vehicle control is a combination of the simplified Wong model with small rear tire slip (4 states), a first-order lag in steering actuator response (1 state), and two sensor biases (2 states), and no integral states, for a combined seven-state model.

Chapter 6

Land Vehicle System Identification

Carrier-phase differential GPS offers very accurate, high bandwidth measurements of vehicle position and attitude. *This ability to sense multiple states with an inexpensive, solid-state sensor makes CDGPS ideal for experimental identification of dynamic systems*. System identification typically involves a trade-off between model complexity and speed of parameter convergence. For a well known, time invariant plant, a controller based on an accurate complex model will usually perform equal to or better than a simpler controller. When the plant model is not known exactly or has time varying parameters, the generality offered by using a simple model may outweigh small performance gains offered by increased complexity.

The system identification methods described in this chapter were selected with the expectation that they will be used in a real-world setting. The goal of this chapter is to pursue a general approach to accurately identify a land vehicle model using CDGPS which will fit into a real-time system identification scheme.

This chapter outlines the general steps required to experimentally characterize a generic land vehicle using CDGPS. These steps include nonlinear steering calibration, positioning antenna lever-arm calibration and correction, disturbance modeling, linear system identification, and mathematical model selection. The validity of this identification method is demonstrated by applying it to the specific case of a John Deere 7800 tractor.

6.1 Steering System Calibration

The first major system identification step for most controls applications is the linearization of inherently nonlinear components. In the case of a land vehicle, the nonlinear components are typically associated with the steering sub-system.

There are three basic general approaches to steering linearization. The most direct method, and the method described in this section, is a lengthy procedure to calibrate the steering sensor and steering valve by post-processing experimental data. This passive nonlinear identification technique involves determining the nonlinear functions that describe the potentiometer and actuator off-line, and using fixed look-up tables to linearize the components. A second method of linearization would use active identification techniques to specify the nonlinear lookup tables in real-time, continuously updating this information in the control system. This method would not require a lengthy calibration process, and may perform at least as well as the first method. An even better method would use linear techniques (such as model reference adaptive control) or nonlinear techniques (such as sliding-mode control) to close the inner steering loop, causing it to behave as a consistent linear system. The steering system would then behave as a black box with known behavior from the perspective of the outer-loop control system.

Figure 29 shows the automatic control scheme based on lookup tables for a land vehicle steering control system. The steering actuator is assumed to have some memoryless nonlinearity (deadband shown) and some dynamics associated with the solenoids or hydraulics driving the actuator. The front wheel angle (^{O}) sensor is also assumed to have

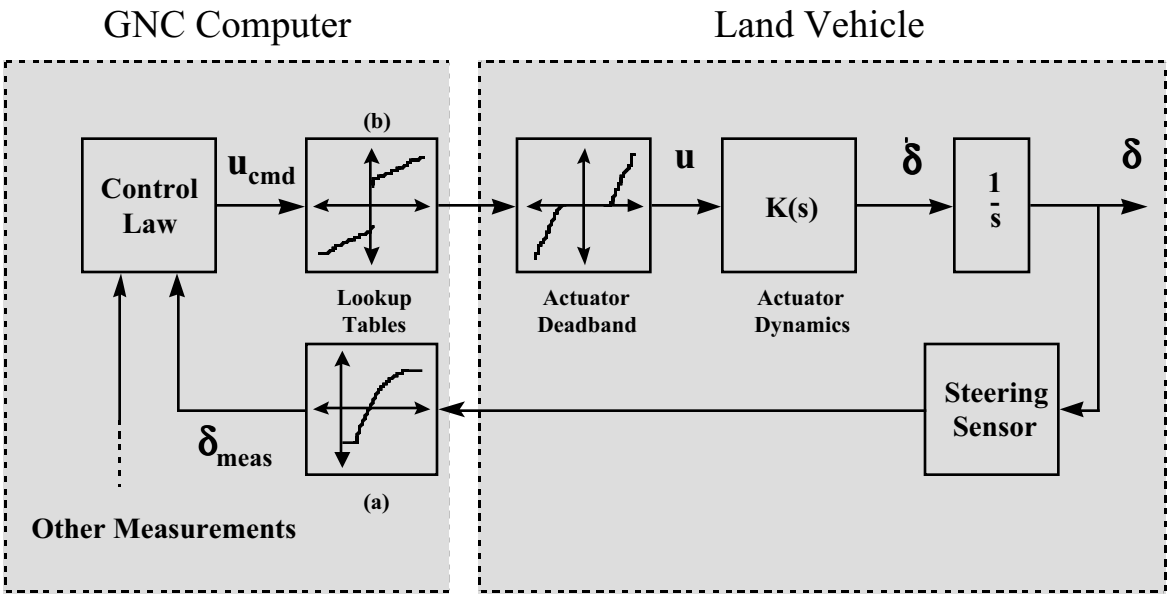

Figure 29 - Tractor Steering System

some memoryless nonlinearity due to sensor imperfections or mounting geometry. The Guidance Navigation and Control (GNC) computer attempts to cancel the effects of the two memoryless nonlinearities using lookup tables. With the ideal lookup tables in place, ignoring disturbance and sensor noise, the nonlinear steering system can be described by the following linear equations:

$$\delta(s) = \frac{K(s)}{s} U_{cmd}(s) \quad , \tag{6.1}$$

$$\delta_{meas} = \delta \quad . \tag{6.2}$$

The calibration of these lookup tables is not trivial. The three steps toward this process are: (1) the direct characterization of steady-state, nonlinear effects in the steering sensor, (2) nonlinear calibration of the actuator, and (3) the identification of an accurate dynamic model to describe the steering system.

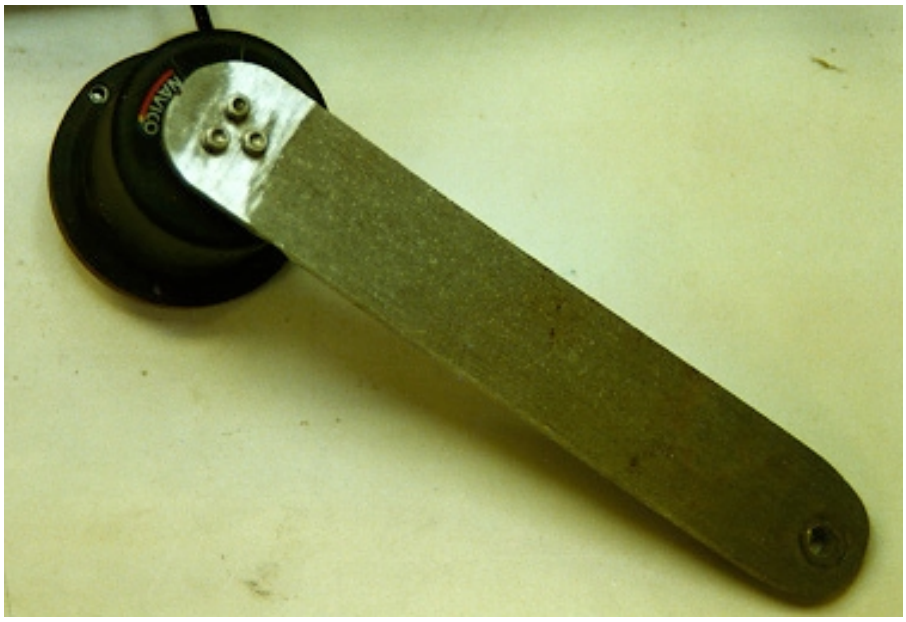

Figure 30 - Golf Cart Steering Sensor

6.1.1 Steering Sensor Linearization

There are a variety of front wheel angle sensors available for land vehicles. Measurements from these sensors are typically not linear for several reasons. For one, the sensor is usually attached to one wheel. In almost all land vehicles, each wheel turns at a different rate, and it is the "effective" wheel angle that is desired. Another source of nonlinearity comes from the geometry of the sensor connection to the vehicle. Finally, the likelihood exists for a sensor imperfection causing an output that is not perfectly proportional to angular or linear displacement input.

Both experimental vehicles in this work had wheel angle sensors with nonlinear behavior. The golf cart used a rotating potentiometer attached between the frame and one tie rod to measure front wheel angle (Figure 30). This sensor was manufactured for use in a Navico WP5000 ship autopilot and a custom mount was built for attachment to the cart. The tractor used a piston potentiometer between the frame and front wheel to sense the front wheel angle (Figure 31). The tractor potentiometer was part of an Orthman row guidance system specifically designed for this line of tractors. Both wheel angle sensors exhibited nonlinear behavior.

The first challenge in specifying the wheel angle sensor lookup table is to define the effective front wheel angle. This value may be arbitrarily chosen as the arithmetic or geometric mean of the left and right wheel angles, but other definitions make more physical sense. In the nonlinear derivations of the Ellis and Wong-based models described in Chapter 5, the steady-state heading rate is directly proportional to the tangent of the effective front wheel angle for a given forward speed. Recall Equation 5.2 from the simple no-slip model,

Figure 31 - Tractor Steering Sensor

$$\dot{\Psi} = \frac{V_{yf}}{L} = \frac{V_x}{L}\tan(\delta) \quad . \tag{5.2}$$

Using this relationship, the nonlinear lookup table (a) from Figure 29 may be constructed to define the effective front wheel angle based on steady-state measurements of raw wheel angle and heading rate.

To experimentally determine the values within this lookup table, a properly instrumented land vehicle may be driven in slow steady circles with a constant front wheel angle while collecting high-bandwidth, precise GPS-based heading data. An example of one such data collection pass taken with the tractor is shown in Figure 32. The effective wheel angle is found by rewriting Equation 5.2:

$$\delta = \tan^{-1}\frac{\Psi_{SS} L}{V_x} \quad . \tag{6.3}$$

The aggregate data collected on the tractor and the interpolated lookup table for the tractor effective front wheel angle are shown in Figure 33.

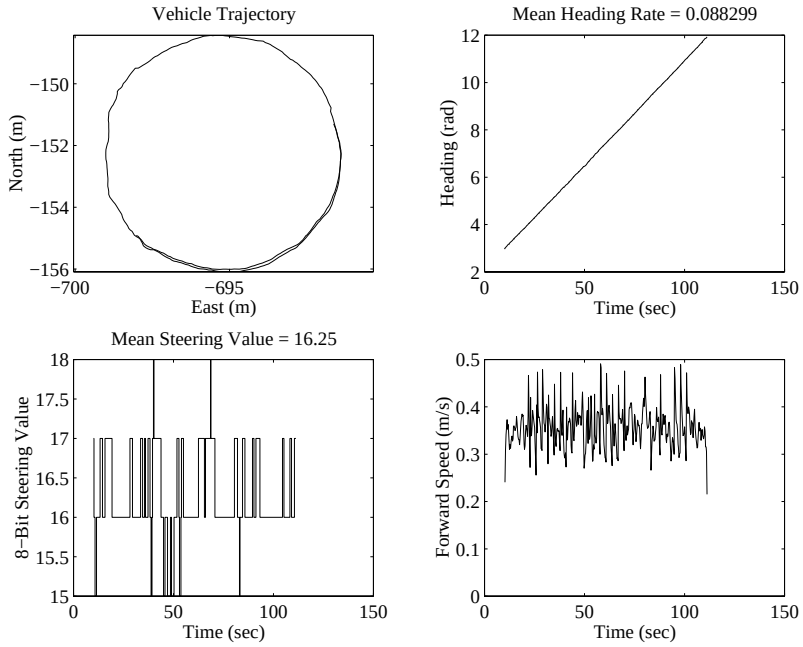

Figure 32 - Steady-State Steering Data Collection Pass

6.1.2 Steering Actuator Linearization

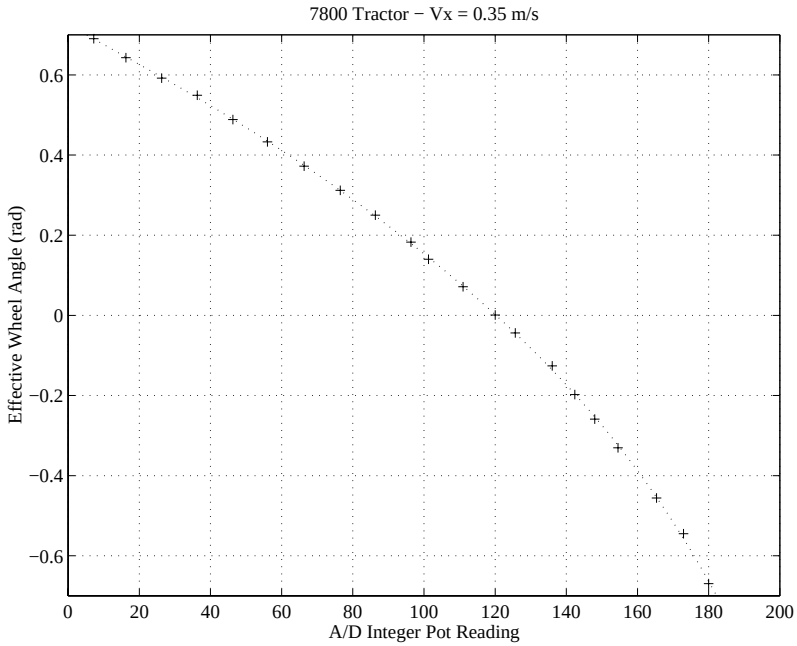

Figure 33 - Tractor Effective Front Wheel Angle Lookup Table

Steering actuators also come in a variety of forms. They may be based on linear or angular actuation, and may be powered by mechanics, electricity, hydraulics, or some combination. Despite their differences, most off-the-shelf land vehicle steering actuators exhibit similar nonlinear behaviors.

In an effort to reduce cost, inexpensive actuators are desirable for production systems. These inexpensive actuators usually have deadband regions and nonlinear active regions, as well as hysteresis or sticktion. While the latter two can usually be negated through effective use of a dither signal, large deadbands and non-proportional active regions require some form of compensation. As was the case with the steering sensor nonlinearity, the nonlinearity in the steering actuator may be corrected through off-line calibration, real-time identification, or inner-loop adaptive or nonlinear control.

Figure 34 - Golf Cart Actuator

Figure 35 - Tractor Actuator

The front wheels of the golf cart were driven by a Navico ship autopilot motor attached to the steering wheel through a rubber drive belt (Figure 34). The motor was supplied by the manufacturer with a high-impedance, pulse-width modulated motor controller providing a wheel angle rate proportional to an input voltage. The front wheels of the tractor, however, were actuated by sending high current through solenoids in an inexpensive, off-the-shelf electro-hydraulic valve (Figure 35). The valve, manufactured by Parker for use in the Orthman row guidance system, exhibited a large deadband region and a nonlinear active region. The tractor steering valve also required pulse-width modulation to minimize transistor heat dissipation, and a large dither signal to provide a memoryless response (i.e. without hysteresis or "sticktion").

Calibration of the steering *actuator* is straightforward once the steering *sensor* is calibrated. The front wheels may be commanded to sweep a large angle with a fixed rate command. The steady-state wheel angle rate (once transients have died out) is then

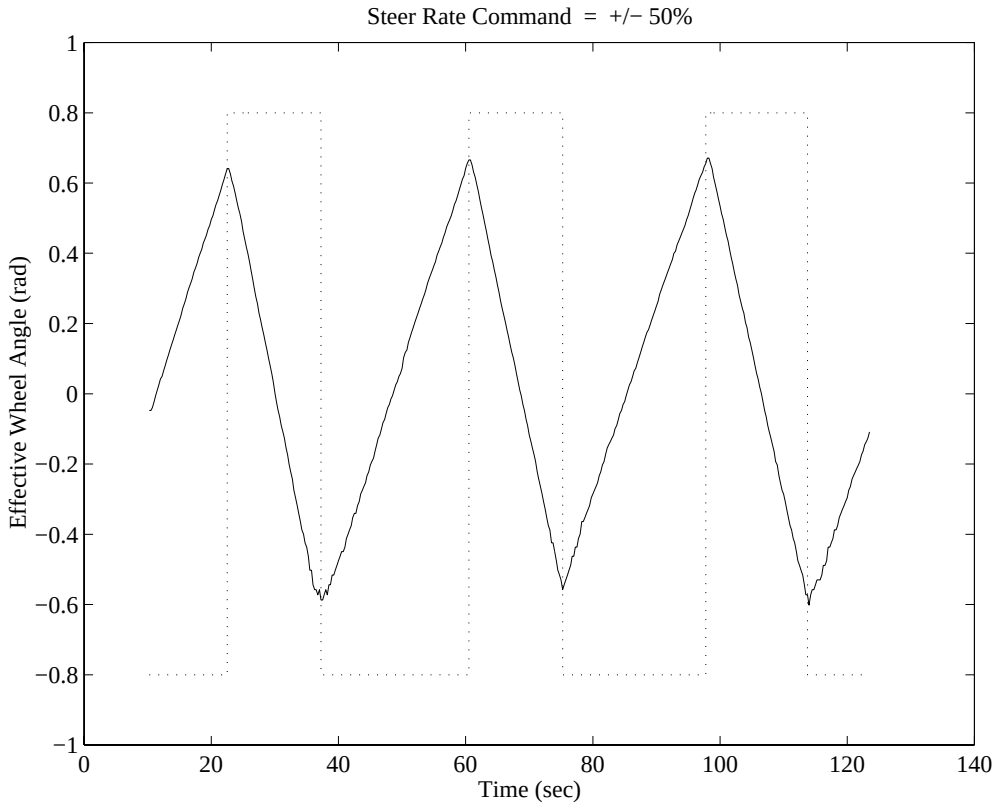

Figure 36 - Steady-State Wheel Angle Rate Data Collection Pass

recorded. This is repeated for many commanded rates and the results are used to create the nonlinear lookup table (b) shown in Figure 29.

One open-loop trial taken on the tractor is shown in Figure 36. Alternating actuator commands were sent at 50% of the maximum left and right turn rates. The mean resulting steady-state wheel angle rates were computed from this data. It is interesting to note that the transients for this actuator were relatively short, so the linear dynamics associated with the steering system is expected to have a fast response. Also, the right and left turn rates were significantly different, illustrating a nonlinearity in the tractor actuator. The results from many actuator calibration tests were combined, and the points were interpolated using spline methods to generate the table shown in Figure 37. This table is directly inverted to generate the steering actuator lookup table.

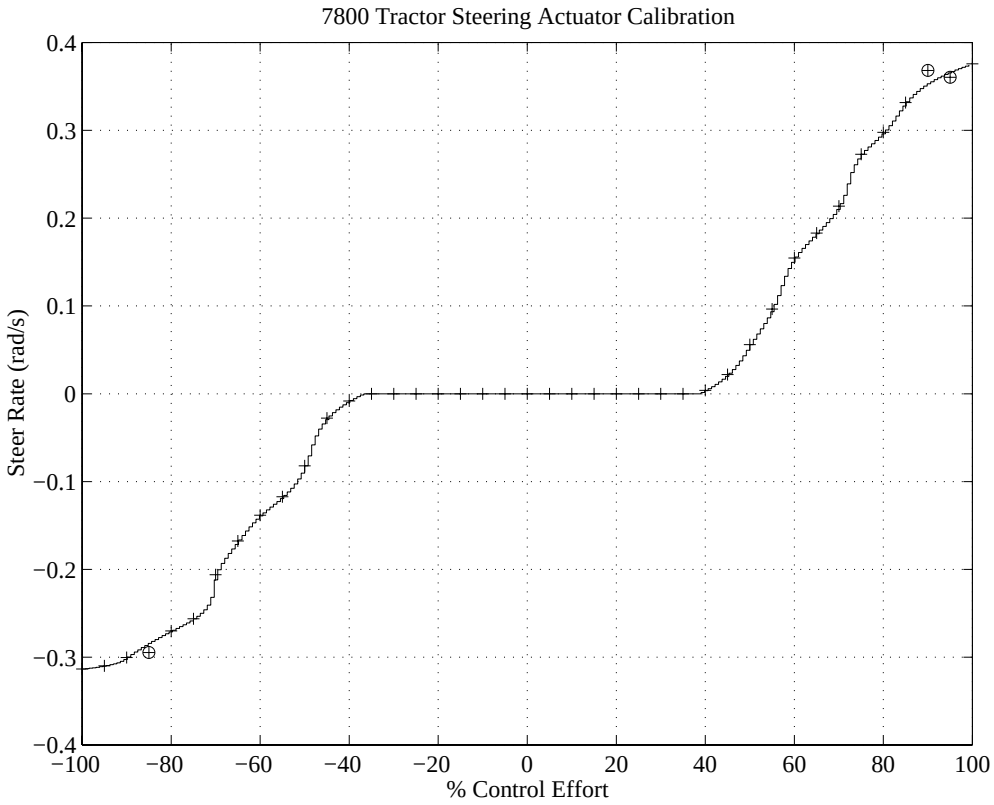

Figure 37 - Tractor Steering Actuator Deadband Table

6.1.3 Characterization of Linear Steering Dynamics

Once the steady-state characteristics of a land vehicle steering sensor and actuator are calibrated, the next step is to identify any *linear* dynamics associated with the steering system. A good, general method for doing this is to make appropriate assumptions about steering dynamics, generate a viable set of models as described in Chapter 5, identify the parameters within these models using empirical data, and select the appropriate model for automatic control. With a strong steering actuator, land vehicle steering dynamics are not generally affected by the non-steering vehicle states associated with heading and position Therefore, the assumption of one way coupling between the steering system and the vehicle dynamics is often appropriate.

Many methods exist for parameter identification using experimental data. One such method is described later in this chapter. The best criteria for model selection varies with

application. If the identified model will be used in a fixed-gain controller, the model exhibiting the maximum robustness or optimal performance properties is desired. If an adaptive control scheme is utilized, the goal may be to minimize the number of free parameters used without a significant sacrifice in performance. In both cases, the "performance" may be measured by running experimental data through a causal estimator and computing the steering state measurement residual.

Several basic assumptions were made regarding the tractor steering system. Since the electro-hydraulic steering actuator was very strong and resistant to external forces, steering one-way coupling was assumed. Also, it was known that the transfer function from input (commanded wheel angle rate) to output (wheel angle) included one integration.

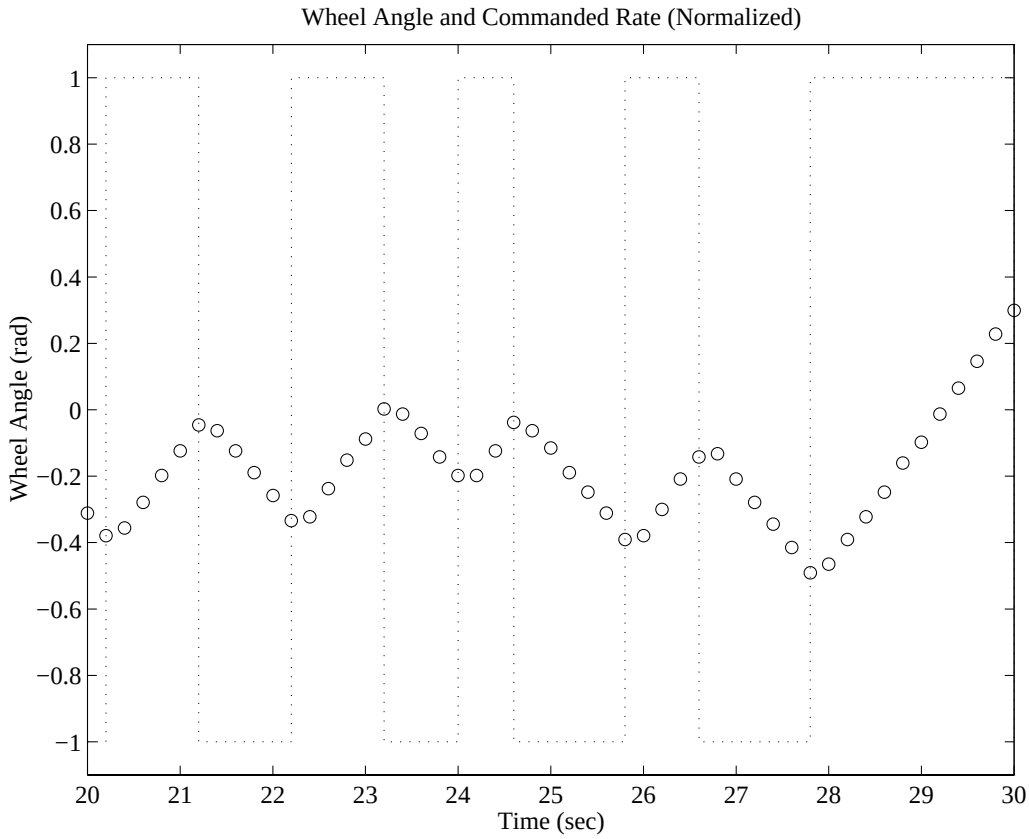

Figure 38 - Tractor Steering Lag

The data from 48 open-loop steering trials were used in post processing to determine the best tractor steering model. A description of these trials is found below and shown in Figure 42. A close-up view of this data shows an apparent steering lag, suggesting that a simple integrator might be inadequate to model the steering system (Figure 38). Based on physical knowledge of the system, the steering actuator is expected to experience a pure time delay from computer processing and serial communications, as well as a dynamic lag caused by the solenoid inductance and the hydraulics. The tractor steering data shows that these effects are significant.

The parameters for seven different steering models were found using each open-loop steering trial independently. The "true" parameters for each model were defined as the mean result from the 48 trials. An estimator gain (L) was established for each "true" model using Linear Quadratic Estimation techniques[55], and the experimental data was run through these estimators to compare steering models.

The seven models explored were:

1. A Simple integrator
2. A Simple integrator with a pure one-sample time delay
3. A Second order type-I system with no zeros, unity steady-state gain
4. A Second order type-I system with no zeros
5. A Second order type-I system with one zero
6. A Third order type-I system with one zero
7. A Third-order type-I system with two zeros

Attempts to identify the parameters of a third-order system with no zeros caused the parameter identification algorithm to diverge.

The resulting estimation measurement residual ($\vartheta_{meas} - \vartheta_{est}$) standard deviations for each model are shown in Table 4.

The three second order models performed significantly better than the simple integrator models, and surprisingly performed slightly better that the third order models. While the higher order model performed better with the case-specific parameters in each individual

Table 4 - Experimental Results for Steering Model Selection

Model No.	Model Description	Free Parameters	Mean Measurement Residual (rad)
1	Integrator	0	0.0480
2	Integrator w/Delay	0	0.0408
3	2^{nd} Order, No Zeros, Unity Gain	1	0.0267
4	2^{nd} Order, No Zeros	2	0.0266
5	2^{nd} Order, One Zero	3	0.0265
6	3^{rd} Order, One Zero	4	0.0280
7	3^{rd} Order, Two Zeros	5	0.0323

case, the third order model with mean parameters performed worse than the simpler second order model with mean parameters. The obvious steering model choice for use in the tractor was model 3, which performed almost identically to more sophisticated models with only one free parameter to identify.

6.2 Positioning Antenna Lever-Arm Correction

Since GPS satellites travel overhead, and L-band signals do not travel well through metal, GPS antennas are typically located on the top side of vehicles. Unfortunately, the goal of most land vehicle control systems is to guide the wheels or an implement that is connected to the ground. Also, the land vehicle dynamic models derived in Chapter 5 describe the land vehicle contact with the ground, not the roof. If a land vehicle experiences significant attitude motion, large errors can occur between the positioning sensor and the point requiring accurate positioning (see Figure 39).

This non-collocated sensing problem is easily solved if the vehicle body may be assumed rigid and three-dimensional attitude measurements are available. By pre-computing the lever-arm from the positioning antenna to the vehicle reference point, a lever-arm correction can be made to create an artificial sensor at the point of interest. The lever-arm correction as described does not take vehicle flexibility into account. While observations

suggest that vehicle flexibility is not significant, validating or invalidating this assumption may be an interesting topic for future research.

6.2.1 Lever-Arm Definition

The TANS Vector receiver conveys 3-D attitude measurements in the conventional 3-2-1 Euler Angle format used for aircraft and spacecraft. Defining $\bar{\mathbf{r}}$ as the lever-arm vector from the vehicle reference point to the positioning antenna in body axes, the location of the control point in local coordinates can be found by

$$\begin{bmatrix} N \\ E \\ D \end{bmatrix}_{REF} = \begin{bmatrix} N \\ E \\ D \end{bmatrix}_{ANT} - \Phi\,\Theta\,\Psi \begin{bmatrix} r_x \\ r_y \\ r_z \end{bmatrix}, \tag{6.4}$$

where $\boldsymbol{\Phi}$, $\boldsymbol{\Theta}$, and $\boldsymbol{\Psi}$ are the standard orthonormal Euler Angle roll, pitch and yaw matrices respectively. The reference point position and antenna position are expressed in a North-East-Down frame, and r_x, r_y, and r_z are components of the lever-arm vector $\mathbf{r}$ in the body frame.

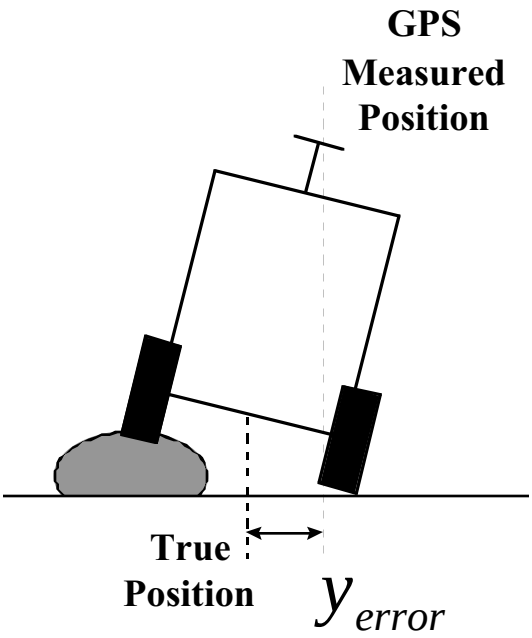

Figure 39 - Attitude Induced Lever-Arm Error

For a land vehicle on relatively flat terrain (small roll and pitch angles), the equations may be linearized for faster computation:

$$N_{REF} = N_{ANT} - (r_x + r_z\theta)\cos\psi + (r_y - r_z\phi)\sin\psi \quad , \tag{6.5}$$

$$E_{REF} = E_{ANT} - (r_x + r_z\theta)\sin\psi - (r_y - r_z\phi)\cos\psi \quad , \tag{6.6}$$

$$D_{REF} = D_{ANT} + r_x\theta - r_y\phi - r_z \quad . \tag{6.7}$$

For the 7800 tractor, the vehicle reference point was defined as the point on the ground directly below center of rear axle. This point was chosen to allow coordinate system consistency between controllers used for different implement configurations.

6.2.2 Lever-Arm Calibration

The most obvious method for calibration of the positioning antenna lever-arm is direct measurement. For the 7800 tractor, all 3 dimensions of the lever-arm were first found

using a tape measure. The horizontal lever-arm components r_x and r_y were later improved using the four-antenna static baseline survey performed by the TANS Vector attitude receiver. Since two GPS antennas were aligned with high accuracy along the longitudinal axis of the vehicle, the longitudinal and lateral position of the primary positioning antenna could be found very accurately using this survey.

It is proposed that, when all three axes of attitude and position measurements are taken concurrently, it may be possible to find components of the positioning antenna lever-arm in post-processing or in real-time using experimental data. For a vehicle traveling in a nearly straight line, Equation 6.6 may be reduced to give the vehicle antenna lateral position y_{ANT} as a function of the vehicle reference point lateral position y_{REF}, the antenna lever-arm, and the vehicle attitude. If we assume small heading deviations from the desired line, and neglect second order terms,

$$y_{ANT} = y_{REF} + r_y + r_x\psi - r_z\phi \quad . \tag{6.8}$$

An arbitrary error term may be defined as

$$\varepsilon = y_{ANT} - r_y - r_x\psi - w\phi \quad , \tag{6.9}$$

where in this case, w is simply a scalar constant whose significance will be seen shortly.

Substituting Equation 6.8, this error term may be rewritten as

$$\varepsilon = y_{REF} - (r_z + w)\phi \quad . \tag{6.10}$$

If we square this equation and take the expected value of both sides, Equation 6.10 becomes

$$E\left[\varepsilon^2\right] = E\left[y_{REF}^2\right] - 2(r_z + w)E\left[y_{REF}\phi\right] + (r_z + w)^2 E\left[\phi^2\right] \quad . \tag{6.11}$$

If the land vehicle is traveling over terrain which is on average flat, the expected value of $y_{REF}\phi$ should be zero. From this, it can be shown that the value of w which minimizes the expected value of the square of the defined error term is $w = -r_z$.

Given that the error in Equation 6.9 is a function of known constants and measurements, methods exist to compute the w that minimizes $E[\varepsilon^2]$ in post-processing (e.g. the Wiener-Hopf Solution[56]), or converges to the optimal w in real-time (e.g. the LMS algorithm[57]).

Real-time sequential estimation of the vertical lever-arm component is straightforward using the LMS algorithm. Figure 40 shows a schematic of how the error term may be computed in real-time and fed back at each epoch to update the estimate of w . Skipping the derivation, the LMS algorithm is

$$\bar{\mathbf{w}}_{k+1} = \bar{\mathbf{w}}_k + 2\mu\varepsilon_k\bar{\mathbf{x}}_k \ , \tag{6.12}$$

where for our example, $\bar{\mathbf{x}}_k$ is simply the scalar measurement of ϕ_k , and $\bar{\mathbf{w}}_k$ is a scalar. The

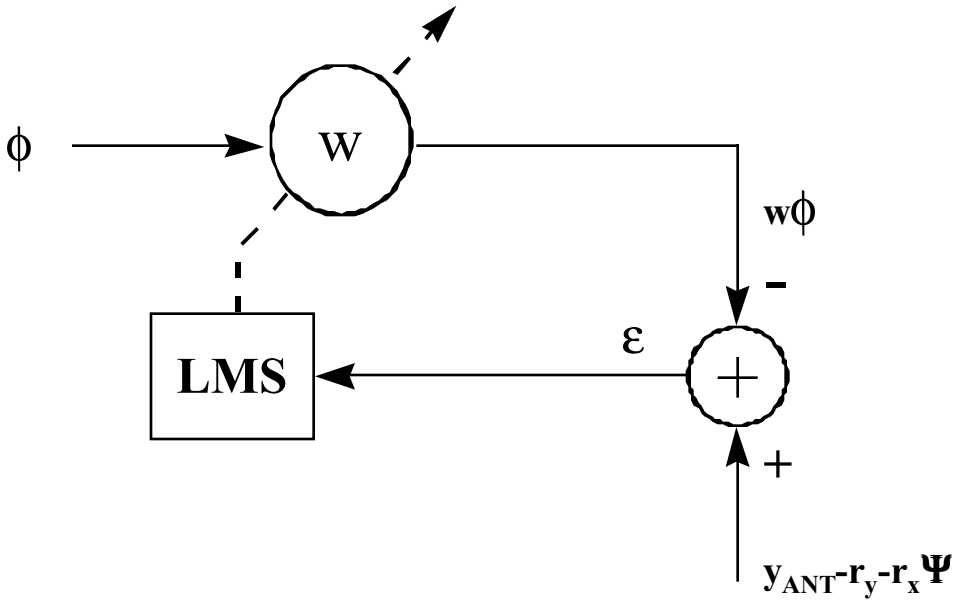

Figure 40 - LMS Algorithm for Vertical Lever-Arm Estimation

value μ is a design parameter which must be chosen carefully. Small values of μ will cause the estimate of w to converge very slowly to the correct value, while large values of μ will result in large estimation errors (misadjustment) or, worse yet, may cause the algorithm to diverge. A typical value selected for μ is

$$\mu = \frac{0.1}{\text{trace}\left(E\left[\bar{\mathbf{x}}\,\bar{\mathbf{x}}^T\right]\right)} \quad . \tag{6.13}$$

To guarantee convergence stability, the numerator of Equation 6.13 must lie between zero and one.

Figure 41 shows the performance of the LMS algorithm applied to experimental data taken on the 7800 tractor. The measurements from approximately 20 line-following trials were stacked together to create over 30 minutes of data for post-processing. The Wiener method was used to determine the "true" value for the vertical lever-arm component. It is interesting to note that the solution obtained using the Wiener method differed from the value determined using the tape measure by only a few centimeters. The LMS algorithm was applied to the same data sequentially to determine how a real-time system would have performed. Three trials were run with a constant value for μ, and one was run with a μ value that decreased over time.

It can be seen from the plots that for large convergence parameters, the lever-arm estimate converges quickly, but the noise on this estimate is very large. For smaller μ values, the estimate is less noisy but it converges extremely slowly. The lower-right plot attempts to vary the value of μ, taking advantage of the fast convergence of a high μ when the estimate is poor, and reducing the value of this parameter when the solution is more accurate.

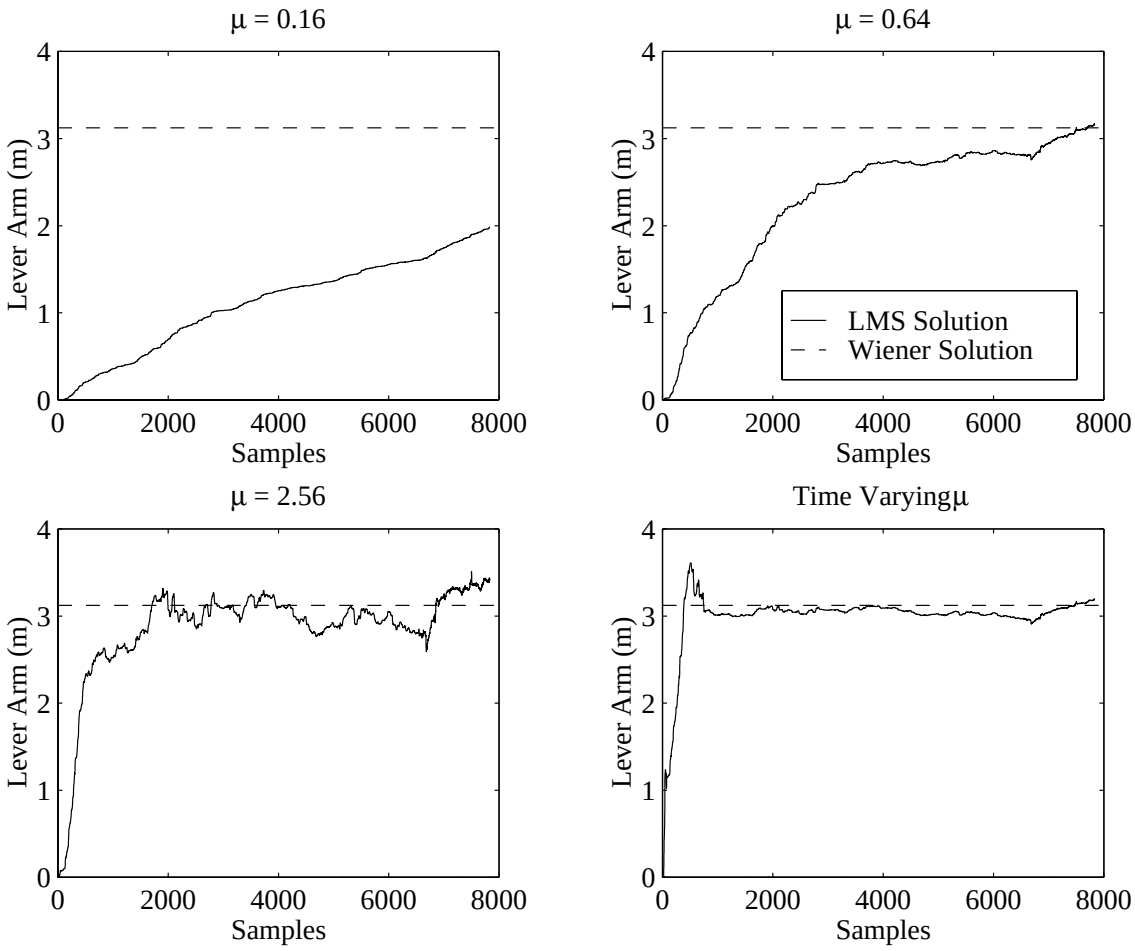

Figure 41 - LMS Convergence of Vertical lever-arm Component

While these analyses were performed in post-processing, they demonstrate the possibility of performing the lever-arm calibration in real-time. The algorithm suggested here only attempts to solve for the vertical component of the lever-arm, which is typically the largest and most difficult to measure. It may be possible to estimate all three components of the vehicle antenna lever-arm in real-time given all three dimensions of position and attitude measurements. The generalization of the algorithm described here is an interesting topic for future research.

6.2.3 Lever Arm Errors

Additional errors creep into the vehicle lateral position measurements as a result of the real-time lever-arm correction. If we assume uncorrelated attitude and position measurements, we can quantify the effect of noisy attitude measurements and inexact lever-arm calibration on lateral position measurement.

The linearized error equations yield the following measurement equation:

$$y_{meas} = y + v_{pos} + r_z v_\phi + \delta r_z \phi + r_x v_\psi + \delta r_y \quad . \tag{6.14}$$

Table 5 shows the typical or expected values of these quantities for the tractor used in these experiments. Note that vehicle lever-arm motion causes approximately a 30% increase in the lateral position measurement standard deviation (from 1.0 to 1.3 centimeters) when the lever-arm is correctly taken into account. If the lever-arm is not taken into account, the lateral error standard deviation reaches approximately 6 centimeters. If this additional error is not taken into account during control system design, the resulting controller is likely to go unstable.

Table 5 - Approximate Lever Arm Values for 7800 Tractor Configuration

Quantity	(units)	Typical or Expected Value (1-σ)	Error Contribution With Correction	Error Contribution Without Correction
v_{pos}	**(cm)**	1.0	**1.0**	**1.0**
φ	(rad)	0.017		
r_z	(cm)	350		5.95
v_ϕ	(rad)	0.0017		
r_z	(cm)	350	0.6	
φ	(rad)	0.017		
or_z	(cm)	2.0	0.03	
v_ψ	(rad)	0.0017		
r_x	(cm)	68	0.1	
or_y	(cm)	0.5	0.5	
RMS Total			**1.3 cm**	**6.0 cm**

6.3 Linear System Identification

After characterizing the necessary nonlinear vehicle components and calibrating the rigid body lever-arm, a land vehicle can be well approximated as a linear dynamic system about fixed operating points. The procedure for designing the vehicle automatic control system begins with the process of linear system identification.

For the purpose of designing a controller using standard linear techniques, either a transfer function or state-space representation of the land vehicle is desired. Many methods exit to identify a transfer function for continuous (s-plane) and discrete (z-plane) "single-input single-output" (SISO) systems[58]; however, transfer function descriptions are not well suited to describe the general case of vehicles with multiple sensor outputs (SIMO), multiple actuator inputs (MISO), or both (MIMO). State-space techniques, on the other hand, offer a simple way to describe SIMO, MISO, and MIMO systems while enabling powerful optimal and robust control system design tools. The current drawback to state-space techniques is the general lack of methods for system identification (on-line or off-line) for state-space models.

6.3.1 Comparison of Basic System Identification Techniques

There are two basic approaches to state-space system identification. These approaches can be simply labeled as (1) "black-box" or general system identification, which assumes no prior knowledge about system dynamics, and (2) parameter identification, which aims to identify parameters in a pre-specified dynamic model.

General system identification techniques are extremely flexible. They can be used for any system with measurable inputs and outputs. A single "black-box" identification algorithm is able to identify the dynamics of a tractor, an airplane, or an electrical circuit without modifying the algorithm, making it simple for an unsophisticated operator to use. Also,

general techniques are not prone to modeling errors or false assumptions which can arise when a specialized model is assumed.

Parameter identification techniques require some assumptions about the dynamic system, but they have several advantages over general system identification. When a good model is used, a parameter identification algorithm has fewer degrees of freedom available, making it potentially faster and more accurate then the more general algorithms. Also, by defining physically meaningful states and identifying physically meaningful parameters, it becomes possible to extrapolate the dynamics of an identified system to predict performance in regimes where data has never been collected. For example, the results from two data runs collected on a vehicle driving 1 meter per second and 1.5 meters per second may be extrapolated to generate a model for a vehicle driving at 2.0 meters per second, or possibly even driving backwards at 0.5 meters per second. This is not true for more generic algorithms. For these reasons, a parameter identification algorithm was chosen for use in this work.

6.3.2 Off-Line Identification Through Optimal Smoothing

The method selected for parameter identification in this work was based on a method recently presented in a Ph.D. dissertation by Idan[59], which was built upon earlier work by Cox and Bryson[60]. Assuming a discretized plant with zero-mean disturbance and sensor noise and no control effort feed-through to measurements, the equations of motion describing plant dynamics may be written as:

$$\mathbf{x}_{k+1} = \Phi(\mathbf{p})\mathbf{x}_k + \Gamma(\mathbf{p})\mathbf{u}_k + \Gamma_w(\mathbf{p})\mathbf{w}_k \quad , \tag{6.15}$$

$$\mathbf{z}_k = \mathbf{H}(\mathbf{p})\mathbf{x}_k + \mathbf{v}_k \quad , \tag{6.16}$$

where $\mathbf{x}_k$, $\mathbf{u}_k$, and $\mathbf{z}_k$ are the vehicle state, control, and measurement vectors at epoch k, $\mathbf{\Phi}, \mathbf{\Gamma}, \mathbf{\Gamma}_w$, and $\mathbf{H}$ are the state-space model matrices, $\mathbf{p}$ is the parameter vector, and $\mathbf{w}_k$ and $\mathbf{v}_k$ are the disturbance and measurement noise vectors.

For identification purposes, a performance measure is defined in the standard way with an additional term for an initial estimate of the parameters ($\mathbf{p}_0$)

$$J \equiv \tfrac{1}{2}\left(\mathbf{p}-\mathbf{p}_0\right)^T \mathbf{P}_0 \left(\mathbf{p}-\mathbf{p}_0\right) + \tfrac{1}{2}[\mathbf{x}(0)-\mathbf{x}_0]^T \mathbf{X}_0 [\mathbf{x}(0)-\mathbf{x}_0] + \tfrac{1}{2}\sum_{k=0}^{N-1}\left[\mathbf{w}_k^T \mathbf{Q}^{-1} \mathbf{w}_k + \mathbf{v}_{k+1}^T \mathbf{R}^{-1} \mathbf{v}_{k+1}\right], \tag{6.17}$$

where the weighting matrices $\mathbf{P}_0, \mathbf{X}_0, \mathbf{Q}$, and $\mathbf{R}$ are design parameters which ideally represent uncertainties in the initial state and parameter estimates and noise variances.

Following the standard approach to dynamic optimization[61], the constraint Equation 6.15 is adjoined to the cost function of Equation 6.17 using Lagrange multipliers to form

$$\mathcal{J} = J + \sum_{k=0}^{N-1} \lambda_{k+1}^T \left[\Phi(\mathbf{p})\mathbf{x}_k + \Gamma(\mathbf{p})\mathbf{u}_k + \Gamma_w(\mathbf{p})\mathbf{w}_k - \mathbf{x}_{k+1}\right]. \tag{6.18}$$

Minimizing $\mathcal{J}$ is equivalent to minimizing J subject to the dynamic constraints. The first variation of $\mathcal{J}$ relative to the unknowns in the problem is given by

$$\delta\mathcal{J} = \sum_{k=0}^{N} \frac{\partial \mathcal{J}}{\partial \mathbf{x}_k}\delta\mathbf{x}_k + \sum_{k=0}^{N-1} \frac{\partial \mathcal{J}}{\partial \mathbf{w}_k}\delta\mathbf{w}_k + \frac{\partial \mathcal{J}}{\partial \mathbf{p}}\delta\mathbf{p}. \tag{6.19}$$

The method for finding the minimum $\mathcal{J}$ is an iterative process. First, the parameter estimate is held fixed while $\mathbf{x}_k$ and $\mathbf{w}_k$ are found by solving the standard Linear Two Point Boundary Value Problem (LTPBVP). Once this smoothing process is complete,

$$\frac{\partial \mathcal{J}}{\partial \mathbf{x}_k} = \frac{\partial \mathcal{J}}{\partial \mathbf{w}_k} = 0, \tag{6.20}$$

and Equation 6.19 becomes

$$\delta \bar{J} = \frac{\partial \bar{J}}{\partial \mathbf{p}} \delta \mathbf{p} \quad , \tag{6.21}$$

The gradient of $\bar{J}$ with respect to the parameters may be found as a function of $\mathbf{x}_k$, $\mathbf{w}_k$, and the partial derivatives of the state-space dynamic matrices with respect to the parameters.

Unfortunately, the value of $\mathbf{p}$ to minimize $\bar{J}$ cannot be found immediately, because as $\mathbf{p}$ is updated, the form of the dynamic model changes, requiring new estimate of the optimal $\mathbf{x}_k$ and $\mathbf{w}_k$. The actual smoothing algorithm uses a sophisticated method to take a small step towards the optimal solution for $\mathbf{p}$, then begins the next iteration by re-solving the LTPBVP. This iterative process continues until the estimate of $\mathbf{p}$ converges and the gradient is driven to zero.

The biggest difficulty in this process is the computation of the derivatives of the state-space matrices with respect to the parameters. Since continuous differential equations may be written to match physics more closely than discrete difference equations, most vehicle models, including the ones used in this work, are presented and parameterized in continuous form. It is desirable to keep and identify the continuous model so that a control system of any sample rate may be designed based on the same model without identifying a separate system model.

A solution to the matrix differentiation problem is found in a Ph.D. dissertation by Keller[62]. This solution allows easy computation of the partial derivatives of discrete state-space matrices when the associated continuous state-space matrices are linear in the parameters $\mathbf{p}$. The algorithm is able to make the following conversion:

$$\mathbf{A(p), B(p), p}, T_s \rightarrow \Phi, \Gamma, \frac{\partial \Phi}{\partial \mathbf{p}}, \frac{\partial \Gamma}{\partial \mathbf{p}} \quad , \tag{6.22}$$

where T_s is the sample time for the discrete controller.

6.3.3 Real-Time Parameter Identification

The previous section describes a method for identifying vehicle parameters in one long post-processing batch. It may be desirable for some land vehicles to continuously update the estimate of these parameters in real-time.

The operating conditions of some land vehicles change unpredictably over time. These parameter variations may be accounted for in two ways when designing an automatic controller. A fixed-gain, fixed model controller may be used which is robust to a known range of plant variations, or an adaptive controller may be used which continuously updates vehicle parameter estimates and adjusts the automatic control algorithm accordingly. While the robust control design tends to result in a simpler control law with fewer computations, a well designed adaptive controller has the potential for much better performance.

It is believed that significant parameter variations are likely to occur in the specific case of farm vehicles. Changing soil conditions, forward speeds, implement types, and terrain slope will all cause difficulties for a fixed gain controller. An adaptive controller that accounts for these effects may simply gain schedule on forward velocity and other measurements, or it may use more sophisticated means such as Extended Kalman Filter[63] estimation with real-time LQR control law generation. The area of adaptive control of land vehicles has substantial potential for future research.

6.4 Land Vehicle Model Selection and Validation

In addition to finding optimal parameters for a singe state-space model, experimental data may be used to assess and compare the validity of multiple land vehicle models. Model selection involves an engineering trade-off between model complexity and modeling

accuracy. A very simple model allows easy real-time state and parameter estimation, but is unlikely to accurately model a true system. More complicated systems may be more accurate, but the increased number of parameters make these systems more difficult to mathematically identify.

A good procedure is to choose a set of viable dynamic models, collect open-loop data with strong control signal inputs to excite all system dynamic modes, approximate disturbance and sensor noise values from this data, and optimally identify parameters within each model. By processing the experimental data through causal estimators based on each model, the measurement residuals may be compared as an indication of the relative model accuracies.

6.5 Tractor Parameter Identification

The parameter identification technique described in Section 6.3 was combined with the general model selection method of Section 6.4 and applied to the John Deere 7800 tractor to arrive at an appropriate mathematical model for automatic control. The specific processes of data collection, noise modeling, parameter identification, and final model selection are described below.

6.5.1 Data Collection

The data collected for the identification of the tractor steering system (shown in Figure 42) was also used to identify the full tractor system dynamics. A strong pseudo-random control input $\mathbf{u}$ was used for "persistent excitation"[58] in an effort to excite all modes of the system for accurate identification. The commands were entered manually by a human driver while approximately following a straight line. The lateral position and heading measurements shown in the figure are linearized about the best-fit line through the data. A total of 49 trials were run with various implements and at varying forward velocities.

6.5.2 Noise Modeling

Recall the general linearized, discrete equations of motion describing vehicle motion found

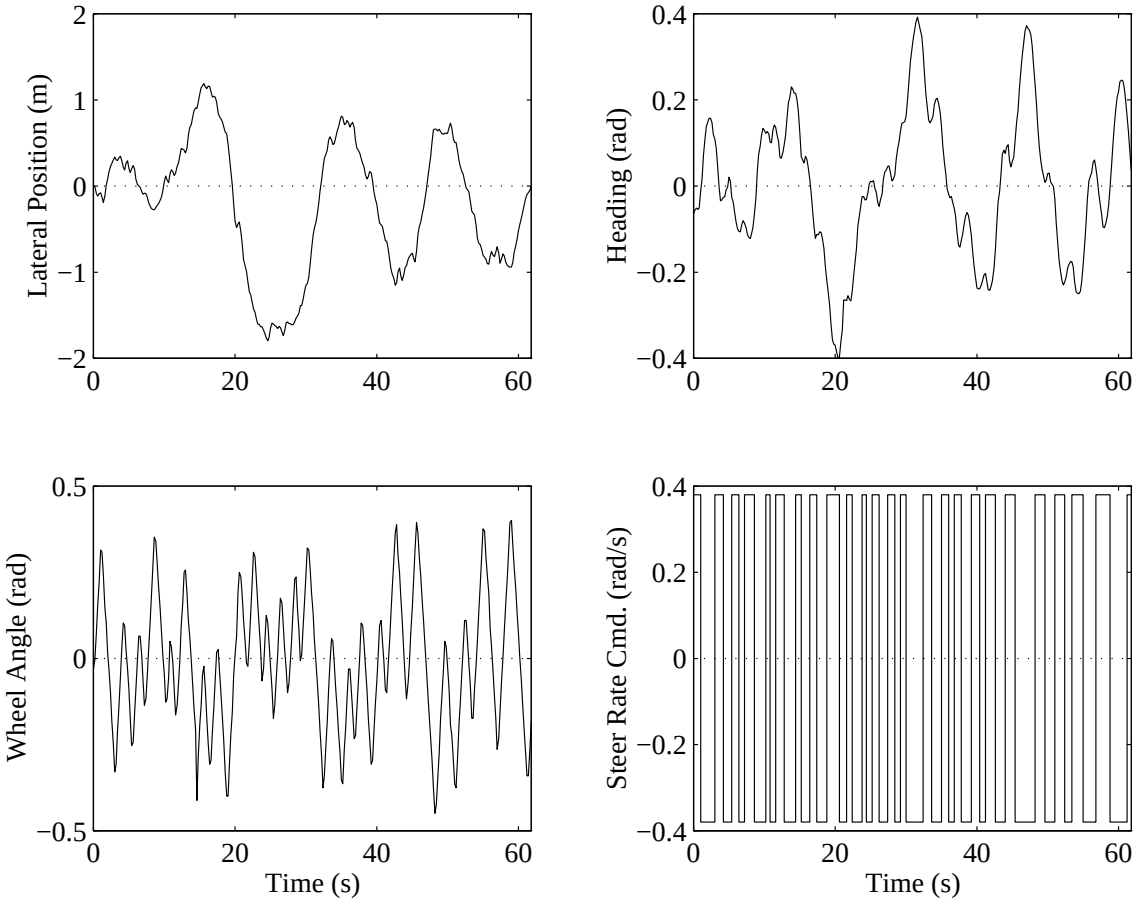

Figure 42 - Tractor Open-Loop Steering Data

in Equations 6.15 and 6.16.

$$\mathbf{x}_{k+1} = \Phi(\mathbf{p})\mathbf{x}_k + \Gamma(\mathbf{p})\mathbf{u}_k + \Gamma_w(\mathbf{p})\mathbf{w}_k \quad , \tag{6.15}$$

$$\mathbf{z}_k = \mathbf{H}(\mathbf{p})\mathbf{x}_k + \mathbf{v}_k \quad , \tag{6.16}$$

The optimal parameter identification techniques described above require specific knowledge and assumptions regarding the statistical properties of the sensor noise ($\mathbf{v}_k$) and vehicle disturbances ($\mathbf{w}_k$) in order to accurately model the plant using collected data.

It is usual to assume the noise vectors are zero mean, independent of each other, independent between samples, and follow a Gaussian random distribution with a fixed and known covariance ($E\left[\mathbf{w}_k\mathbf{w}_k^{\mathrm{T}}\right]=\mathbf{W}$, $E\left[\mathbf{v}_k\mathbf{v}_k^{\mathrm{T}}\right]=\mathbf{V}$). Arriving at numerical values for the covariance matrices usually requires some combination of experimental data, analysis, and engineering judgment. Since information about measurement and disturbance cross-correlation is normally unavailable, **W** and **V** are often selected as diagonal matrices.[64]

The sensor covariance values are almost always easier to determine than the plant disturbances. The three sensor measurements utilized on the tractor for automatic control were front wheel angle (δ), heading (Ψ), and lateral position (y). The analog front wheel angle sensor measurement was encoded by the interface microprocessor as an 8-bit value for processing by the controls computer. Observations revealed that the primary error on this sensor was due to quantization. Based on the wheel angle look-up table described above, the mean quantization level (q) for the sensor was found, and since the steering measurement generally changed quickly during these tests, the sensor error was modeled as a uniform distribution with a variance of $\frac{q^2}{12}$ as described by Franklin, Powell, and Workman.[64]

The heading and lateral position sensor noise variances were found by taking GPS measurements with the tractor in a stationary position and computing the standard

deviation based on the data. Since tractor dynamics are relatively slow compared to the carrier-phase tracking loops in the GPS receivers, these noise values were assumed valid for a moving tractor. The final measurement noise covariance matrix used for parameter identification and estimator design was:

$$\mathbf{V} = \begin{bmatrix} \sigma_{Vy}^2 & 0 & 0 \\ 0 & \sigma_{V\Psi}^2 & 0 \\ 0 & 0 & \sigma_{V\delta}^2 \end{bmatrix} \tag{6.23}$$

where the standard deviation values σ_{Vy}, $\sigma_{V\Psi}$, and $\sigma_{V\delta}$ are found in Table 6.

Vehicle disturbance characterization is significantly more challenging than sensor error modeling. The difficulty is that the vehicle model identification process is driven by the covariance estimate **W**, but **W** is partially a result of the vehicle modeling process. Often in estimator design, a rough approximation of a diagonal **W** is initially used and the values are later tweaked as design parameters[64]; however, it is desirable to arrive at the best noise model possible for the best estimator and system identification performance[59]. With a wealth of open-loop experimental data available for the tractor, a method was desired to estimate **W** based on data from these experiments. Figure 43 shows one possible iterative identification process which finds vehicle model parameters based on an assumed **W**, then updates **W** based on the new vehicle model. While this method seems practical, analysis has shown this process is unreliable and often diverges.

To arrive at a fairly conservative but realistic approximation of **W**, the Ellis model was used with an accurate model of **V**. Defining $\mathbf{I}_w$ of Equation 6.15 and $\mathbf{H}$ of Equation 6.16 as 3-by-3 identity matrices, Equation 6.16 can be rewritten

$$\mathbf{x}_k = \mathbf{z}_k - \mathbf{v}_k \ . \tag{6.24}$$

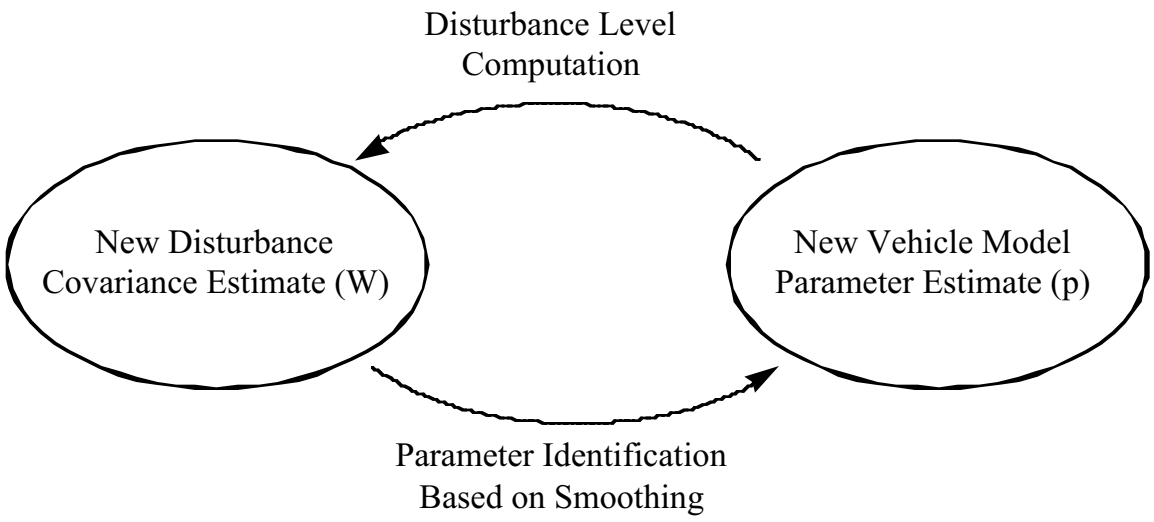

Figure 43 - Iterative Process of Parameter and Disturbance Identification

This relation may then be substituted in Equation 6.15 to become

$$\mathbf{z}_{k+1} - \mathbf{v}_{k+1} = \Phi(\mathbf{z}_k - \mathbf{v}_k) + \Gamma\mathbf{u}_k + \mathbf{w}_k \quad . \tag{6.25}$$

Collecting known terms on the left side and random terms on the right, the equation becomes

$$\mathbf{z}_{k+1} - \Phi\mathbf{z}_k - \Gamma\mathbf{u}_k = \mathbf{v}_{k+1} - \Phi\mathbf{v}_k + \mathbf{w}_k \quad . \tag{6.26}$$

Squaring both sides and taking the expected value, the noise terms may be separated by assuming $E[\mathbf{v}_k\mathbf{v}_{k+1}^T] = 0$, $E[\mathbf{v}_k\mathbf{w}_k^T] = 0$, and $E[\mathbf{v}_{k+1}\mathbf{w}_k^T] = 0$, giving

$$E\left[(\mathbf{z}_{k+1} - \Phi\mathbf{z}_k - \Gamma\mathbf{u}_k)(\mathbf{z}_{k+1} - \Phi\mathbf{z}_k - \Gamma\mathbf{u}_k)^T\right] = \mathbf{V} + \Phi\mathbf{V}\Phi^T + \mathbf{W} \quad . \tag{6.27}$$

Since the left side of Equation 6.27 can be found empirically, and **V** is known, we can solve for **W** explicitly from experimental data. Using experimental data, the resulting **W** matrix was found to be:

$$\mathbf{W} = 0.001 \times \begin{bmatrix} 0.5473 & -0.0463 & 0.1694 \\ -0.0463 & 0.1452 & -0.0497 \\ 0.1694 & -0.0497 & 2.2278 \end{bmatrix} . \tag{6.28}$$

The normalized eigenvectors of this matrix are:

$$v_1 = \begin{bmatrix} 0.99 \\ -0.10 \\ -0.10 \end{bmatrix}, \quad v_2 = \begin{bmatrix} 0.11 \\ 0.99 \\ 0.02 \end{bmatrix}, \quad v_3 = \begin{bmatrix} 0.10 \\ -0.03 \\ 0.99 \end{bmatrix}. \tag{6.28a}$$

Since these eigenvectors show that the cross correlation terms in the disturbance matrix are relatively small, and since the goal of this exercise is to arrive at a rough approximation of the disturbance noise values using a vehicle dynamic model that is known to be false, we may simplify the estimate of **W** by eliminating the cross terms. The experimentally determined standard deviation values σ_{Wy}, $\sigma_{W\psi}$, and $\sigma_{W\delta}$ are found in Table 6. When higher order models were examined, these same three noise values were used with a modified $\mathbf{I}_w'$ matrix.

It is expected that the value for **W** will vary for different vehicles, implements, fields, forward speeds, and operating conditions. The values shown here are conservative values for a relatively rough field at fairly slow speeds. Modifications may be required when designing controllers for use in different conditions.

Table 6 - Tractor Sensor and Disturbance Noise Values

	Sensor Noise (1-σ)	Disturbance Noise (1-σ, 5 Hz)
y	**0.5 cm.**	**2.33 cm.**
Ψ	**0.0014 rad.**	**0.0087 rad.**
δ	**0.0023 rad.**	**0.0467 rad.**

6.5.3 Off-Line Parameter Identification and Model Selection

The optimal parameters for four continuous state-space land vehicle models were found by processing open-loop tractor data using the optimal smoothing technique described above. Each of the following models was identified with heading and wheel angle sensor bias states.

- Ellis Model with no steering dynamics (Section 5.2.2)
- Ellis Model with single steering lag state (see Table 4, model 3)
- Simplified Wong model with zero lateral rear tire slip (Section 5.2.4)
- Simplified Wong model with small lateral rear tire slip (Section 5.2.5)

The resulting measurement residuals from the four identified models are shown in Table 7, and described in detail in Appendix A.

Surprisingly, parameter identification attempts using the direct Wong model diverged for all data sets. A closer examination of the post-processing results showed that the eigenvalue associated with the relationship between V_y and ω_z (λ_1 of Equation 5.22) grew without bound as the cost function of Equation 6.17 declined, leading to the conclusion that the dynamics associated with this eigenvalue was not identifiable using the available collection of data points. The successful convergence of the algorithm for all other models supports this suspicion.

Table 7 - Model Identification Aggregate Measurement Residual Results

Vehicle Model	y (cm)	Ψ (deg)	δ (deg)
Ellis	2.34	0.36	2.73
Ellis with Steering Lag State	2.34	0.36	1.43
Simplified Wong - No Rear Lateral Tire Slip	2.33	0.31	1.42
Simplified Wong - Small Rear Lateral Tire Slip	2.26	0.31	1.42

The simplified Wong model with small lateral tire slip was chosen for automatic control system design. With appended sensor bias states, this seven-state model has the general form of Equations 6.29 and 6.30, where the parameters p_1 to p_5 have a non-linear dependence on vehicle tire slip parameters, forward velocity, characteristic lengths, and inertia parameters as described in Chapter 5 (see Appendix A).

$$\begin{bmatrix} \dot{y} \\ \dot{\Psi} \\ \dot{\Omega}_z \\ \dot{\delta} \\ \dot{\omega} \\ \dot{\bar{\Psi}}_{\text{bias}} \\ \dot{\delta}_{\text{bias}} \end{bmatrix} = \left[\begin{array}{ccccc:cc} 0 & p_1 & p_2 & 0 & 0 & 0 & 0 \\ 0 & 0 & 1 & 0 & 0 & 0 & 0 \\ 0 & 0 & -p_3 & p_4 & 0 & 0 & 0 \\ 0 & 0 & 0 & 0 & 1 & 0 & 0 \\ 0 & 0 & 0 & 0 & -p_5 & 0 & 0 \\ \hdashline 0 & 0 & 0 & 0 & 0 & 0 & 0 \\ 0 & 0 & 0 & 0 & 0 & 0 & 0 \end{array}\right] \begin{bmatrix} y \\ \Psi \\ \Omega_z \\ \delta \\ \omega \\ \bar{\Psi}_{\text{bias}} \\ \delta_{\text{bias}} \end{bmatrix} + \begin{bmatrix} 0 \\ 0 \\ 0 \\ 0 \\ p_5 \\ \hdashline 0 \\ 0 \end{bmatrix} u \quad , \tag{6.29}$$

$$\mathbf{z} = \left[\begin{array}{ccccc:cc} 1 & 0 & 0 & 0 & 0 & 0 & 0 \\ 0 & 1 & 0 & 0 & 0 & 1 & 0 \\ 0 & 0 & 0 & 1 & 0 & 0 & 1 \end{array}\right] \begin{bmatrix} y \\ \Psi \\ \Omega_z \\ \delta \\ \omega \\ \bar{\Psi}_{\text{bias}} \\ \delta_{\text{bias}} \end{bmatrix} \quad , \tag{6.30}$$

Based on this model, the optimal parameter estimates from all 48 trials were compared to assess the relationship between the parameters and the vehicle forward velocity and hitch load. The plots from these trials are shown in Appendix A. Only parameters p_1 and p_4 showed a strong dependence on forward vehicle velocity, and in both cases the dependence was approximately linear. Surprisingly, none of the parameters exhibited a strong correlation with hitch load. The time constants associated with the steering lag and the heading lag were both on the order of 0.2 seconds, which agrees with visual inspection of the data and experience driving the tractor.

While the relatively low measurement residuals from this model suggested that it may be appropriate for automatic control over a variety of conditions, automatic control system results based on this model are needed to provide the ultimate validation.

Chapter 7

Land Vehicle Control Design

After characterizing the nonlinear land vehicle components, modeling the disturbances, and selecting and identifying the general linear state-space model, a wide range of design techniques may be used to generate a viable vehicle controller. In this chapter, a detailed analysis of the three-state simple Ellis model (Equation 5.5) and the 7800 tractor five-state model (Equation 6.29, excluding bias states) are explored, and experimental results from the golf cart and tractor are presented.

7.1 Linear Three-State Land Vehicle Model

Before exploring the intricacies of MIMO control for a large dynamic system with many states, much can be learned about a complex system by looking at simple special cases. The simplest model may provide some fundamental properties of the system, even if the model itself is not entirely realistic. Also, the limiting case may sometimes be used as a sanity check to verify the need for a more sophisticated model in a specific application.

7.1.1 Classical SISO Analysis

Recall from Chapter 5 (Equation 5.5) that the continuous form of linearized equations of motion for the simple three-state vehicle model are

$$\begin{bmatrix} \dot{y} \\ \dot{\Psi} \\ \dot{\delta} \end{bmatrix} = \begin{bmatrix} 0 & V_x & 0 \\ 0 & 0 & \frac{V_x}{L} \\ 0 & 0 & 0 \end{bmatrix} \begin{bmatrix} y \\ \Psi \\ \delta \end{bmatrix} + \begin{bmatrix} 0 \\ 0 \\ 1 \end{bmatrix} u \quad . \tag{7.1}$$

The desired output for most land vehicle automatic control applications is the lateral position of the vehicle. If we take this value, y, as the plant output and u as the plant input, we may find the single-input single output (SISO) continuous transfer function in the following manner

$$\frac{Y(s)}{U(s)} = \mathbf{C}(s\mathbf{I} - \mathbf{A})^{-1}\mathbf{B} = \frac{\frac{V_x^2}{L}}{s^3} \quad . \tag{7.2}$$

The basic form of the equation is a triple integrator with no zeros.

Without the use of an estimator, Bode analysis shows that a compensator with at least two zeros is required to provide the positive phase margin needed for a stable SISO controller. In other words, over some range of frequencies, two differentiations of the lateral position would be required for successful automatic control. These differentiations could be performed by a SISO double lead controller, but this would amplify the noise on the lateral position sensor in the region of lead compensation.

A second possibility is to effectively supply the compensator zeros by utilizing the measurements of additional vehicle states. This would better reject the noise on the lateral position measurement, and both mathematics and common sense dictate that extra measurements should be used when they are available.

For the implementation described in this chapter, MIMO control system design tools were used with a full-state estimator and full-state feedback control law. All appropriate and available measurements were used by the estimator.

7.1.2 MIMO Control Design

Because of its real-world robustness properties and its implementation simplicity, a Linear Quadratic Regulator (LQR) was used as the baseline MIMO linear controller in this work[55]. The LQR technique computes the full-state feedback control algorithm that minimizes the cost function

$$J = \int_{t=0}^{\infty} [\mathbf{x}(t)^T \mathbf{Q}\mathbf{x}(t) + \mathbf{u}(t)^T \mathbf{R}\mathbf{u}(t)]dt \quad , \tag{7.3}$$

subject to the dynamic constraints of the continuous state-space equations of motion. It turns out that for a linear, time-invariant, controllable plant, the control law minimizing this quadratic cost function is always a linear combinations of the state vector elements:

$$\mathbf{u}_{opt}(t) = -\mathbf{K}_{opt}\mathbf{x}(t) \quad . \tag{7.4}$$

In the case of the Ellis land vehicle model, when all three states are measured or somehow estimated from measurements, a stabilizing controller with good performance may be obtained without explicit differentiation of the lateral position.

One way to view this form of control is as a series of successive loop closures. The equations for the transfer function between command input and vehicle states Ψ and o are shown below:

$$\frac{\Psi(s)}{U(s)} = \mathbf{C}(s\mathbf{I} - \mathbf{A})^{-1}\mathbf{B} = \frac{v_x}{s^2} \quad , \tag{7.5}$$

$$\frac{o(s)}{U(s)} = \mathbf{C}(s\mathbf{I} - \mathbf{A})^{-1}\mathbf{B} = \frac{1}{s} \quad . \tag{7.6}$$

Using root-locus analysis, it can be shown that by successively closing the steering, heading, and lateral position loops, constant feedback gains are sufficient to force the system poles arbitrarily far into the stable left half of the s-plane.

7.1.3 Forward Velocity Compensation

The linear state-space equations of motion for the Ellis three-state model (7.1) exhibit a strong dependence on the vehicle forward velocity. This shows that, as expected, the dynamic behavior of even the simplest land vehicle is highly dependent on the vehicle's forward speed. The LQR techniques described above may be used to arrive at a controller for a fixed speed, but it is desirable to implement a controller which will work well at any achievable forward velocity.

The optimal gain matrix $\mathbf{K}$ may be found for individual values of forward speed; however,

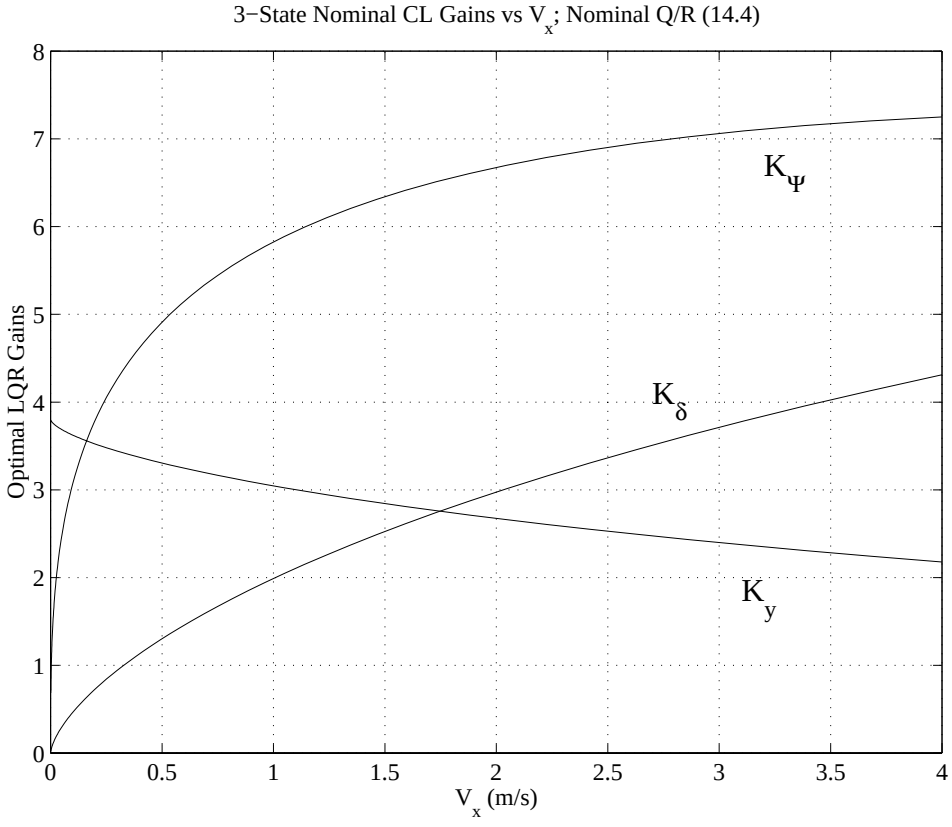

Figure 44 - Optimal Closed-Loop Gains for Simple Three-State Plant

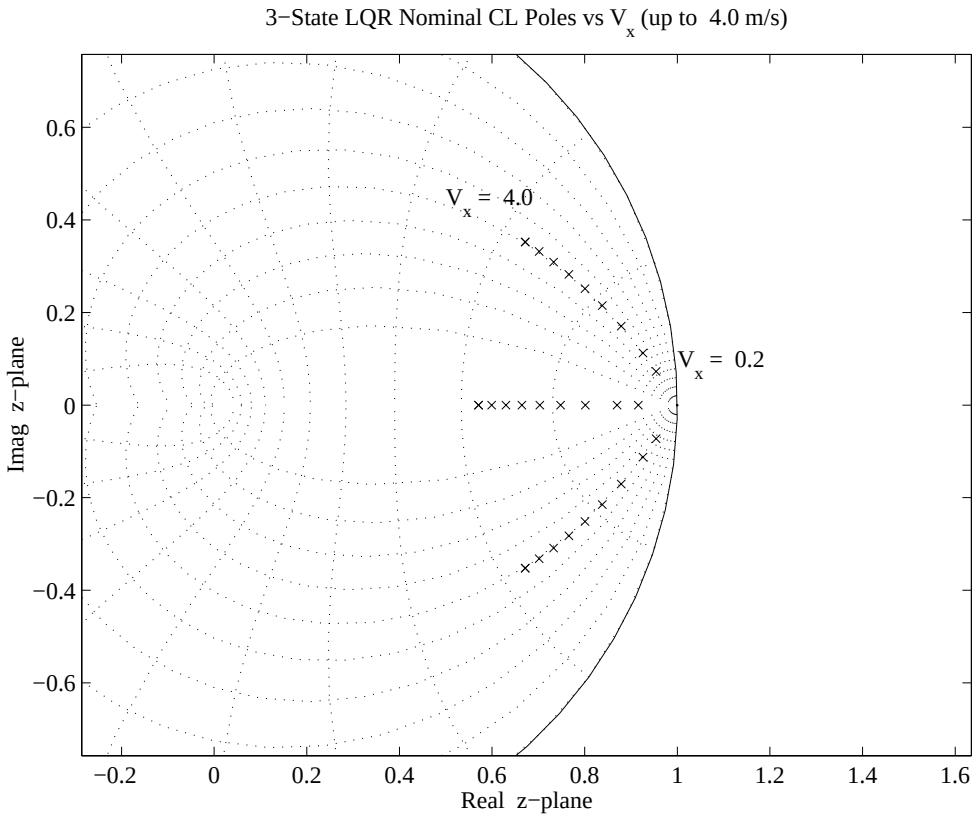

Figure 45 - Optimal Closed-Loop Pole Locations vs. Forward Velocity

arriving at a closed-form solution for $\mathbf{K}(V_x)$ is impractical for dynamic models higher than second order. A plot of the gains for specified $\mathbf{Q}$ and $\mathbf{R}$ values is shown in Figure 44. The closed-loop pole locations using these gains are shown in Figure 45.

On solution to the velocity scaling problem is to update the linear gains of the system in real-time by gain-scheduling on forward velocity, which is a measurable vehicle state. This could be done using a look-up table or by computing the LQR gains in real-time.

A second approach to this problem yields a simpler controller that scales linearly with velocity. Taking the linearized equations of motion that form state-space Equation 7.1, and dividing through on both sides by the forward velocity ($\frac{dx}{dt}$), the following equations result:

$$\frac{dy}{dx} = \Psi \ , \tag{7.7}$$

$$\frac{d\Psi}{dx} = \frac{1}{L}\delta \ , \tag{7.8}$$

$$\frac{d\delta}{dx} = \frac{1}{V_x}u \ . \tag{7.9}$$

The forward velocity term now only appears in one of the three equations of motion. By defining a control law which scales linearly with velocity, we may eliminate this time varying term altogether. A good choice for this controller is to find the LQR gain matrix $\mathbf{K}$ for some nominal forward speed $V_{x,\text{nom}}$, and define the control law as

$$u = -\frac{V_x}{V_{x,\text{nom}}}\mathbf{Kx} \ . \tag{7.10}$$

The resulting state-space equations become

$$\frac{d}{dx}\begin{bmatrix} y \\ \Psi \\ \delta \end{bmatrix} = \begin{bmatrix} 0 & 1 & 0 \\ 0 & 0 & \frac{1}{L} \\ 0 & 0 & 0 \end{bmatrix}\begin{bmatrix} y \\ \Psi \\ \delta \end{bmatrix} + \begin{bmatrix} 0 \\ 0 \\ 1 \end{bmatrix}\tilde{u} \ , \tag{7.11}$$

where the new control effort is defined as

$$\tilde{u} \equiv \frac{u}{V_x} \ . \tag{7.12}$$

The control law may then be written

$$\tilde{u} = -\mathbf{Kx} \ , \tag{7.13}$$

where the new gain matrix is a constant defined by

$$\tilde{\mathbf{K}} \equiv \frac{\mathbf{K}}{V_{x,\text{nom}}} \ . \tag{7.14}$$

This spatial derivative form for the equations of motion is much more elegant than the time derivative form of the equations. The trajectory followed by a land vehicle is dependent only on the control effort $\tilde{u}$. With the controller gain matrix $\tilde{\mathbf{K}}$ defined, the vehicle will follow the same trajectory *regardless of forward speed*.

Despite its elegance, this controller suffers from a major drawback which limits its use in any practical application. As the forward velocity of a vehicle increases, more control effort is needed to achieve the same $\tilde{u}$. Unfortunately, physical actuators always have a finite limit to their performance. Bryson's Rule[55] is typically used in LQR design to directly apply the physical actuator limit into the design parameter $\mathbf{R}$, and the maximum desired state deviation into the design parameter $\mathbf{Q}$. As a result, the maximum state

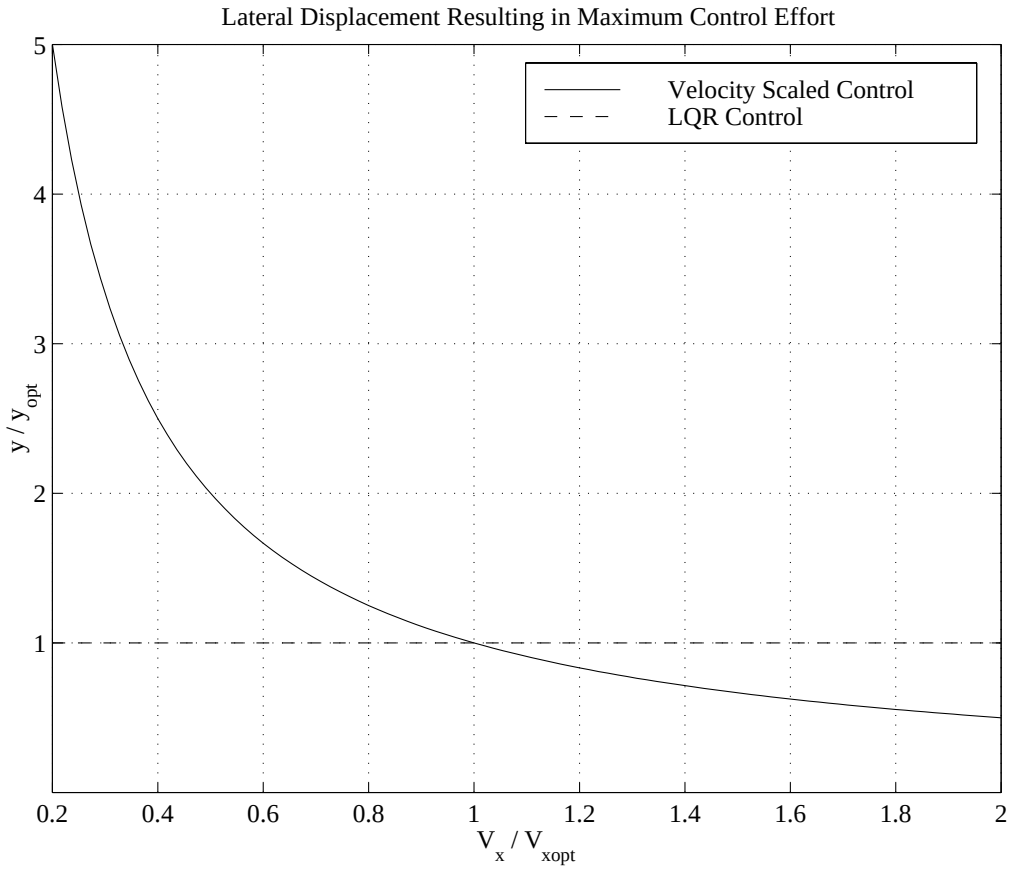

Figure 46 - A Comparison of Velocity Scaled and LQR Gain Scheduled Control

deviation resulting in maximum control effort is fixed.

For the velocity scaled controller, the lateral displacement resulting in a maximum commanded wheel angle rate will vary significantly with velocity. As shown in Figure 46, less lateral deviation is tolerated at higher velocities for this controller. It can also be shown that, at slower velocities, the response time for a velocity scaled controller is significantly slower than it should be for optimal performance. For these reasons, the control systems implemented in this work were designed for a specific vehicle forward velocity.

7.1.4 Effects of Discretization

In most modern control systems, control signal generation is performed digitally, with measurements taken and commands issued at discrete times. This discretization can have a significant effect on control system performance, and must normally be accounted for in control system design using one of the many methods available[64].

The controllers in this work were directly designed in the discrete domain using a zero-order hold equivalent for the plant model. The resulting equations of motion for the three-state model are

$$\begin{bmatrix} y \\ \Psi \\ \delta \end{bmatrix}_{k+1} = \begin{bmatrix} 1 & V_x T_s & \frac{V_x^2 T_s^2}{2L} \\ 0 & 1 & \frac{V_x T_s}{L} \\ 0 & 0 & 1 \end{bmatrix} \begin{bmatrix} y \\ \Psi \\ \delta \end{bmatrix}_k + \begin{bmatrix} \frac{V_x^2 T_s^3}{6L} \\ \frac{V_x T_s^2}{2L} \\ T_s \end{bmatrix} u_k \quad , \tag{7.15}$$

where T_s is the sample period, and k is one sample epoch. The single-input single-output discrete transfer function from control input to lateral position output is

$$\frac{Y(z)}{U(z)} = \mathbf{C}(z\mathbf{I} - \Phi)^{-1}\Gamma = \frac{V_x T_s}{6L} \cdot \frac{z^2 + 4z + 1}{(z-1)^3} \cdot \tag{7.16}$$

The exact formulas for the discrete state-space matrices and transfer functions are shown here. For more complicated dynamic models, such as the five-state model for the John Deere 7800 tractor, these discrete system values may be found numerically from the continuous system values using commercially available software tools such at MATLAB.

The lateral position transfer function shows two system zeros at $-2 \pm \sqrt{3}$ that were not present in the continuous transfer function. These zeros do not provide lead to the system. In fact, as expected, the net effect of the discretization is an increased lag at higher frequencies[64]. For the discrete transfer function shown, the uncompensated frequency response phase is always below -270°.

For the controllers in this work, a special form of the LQR algorithm was used to minimize the *continuous* cost function of Equation 7.3 given the *discrete* constraint Equation 7.15. This algorithm provides the discrete control system gains for full-state feedback.

7.2 Linear Five-State Land Vehicle Model

In Chapter 6 (Table 7) it was determined that the best approach for land vehicle state estimation used a five-state simplified Wong model with assumed small rear lateral tire slip and two additional sensor bias states. This section explores the need for a more sophisticated model from a control system perspective, and discusses the need for state estimation.

7.2.1 Results of Poor Modeling

A very simple analysis shows that the three-state Ellis model is inadequate for control of the John Deere 7800 tractor used in this work. Figure 47 shows the optimal closed-loop pole locations for the three-state feedback controller applied to the nominal three-state plant for varying levels of ζ at a forward speed of 2.5 meters per second. The closed-

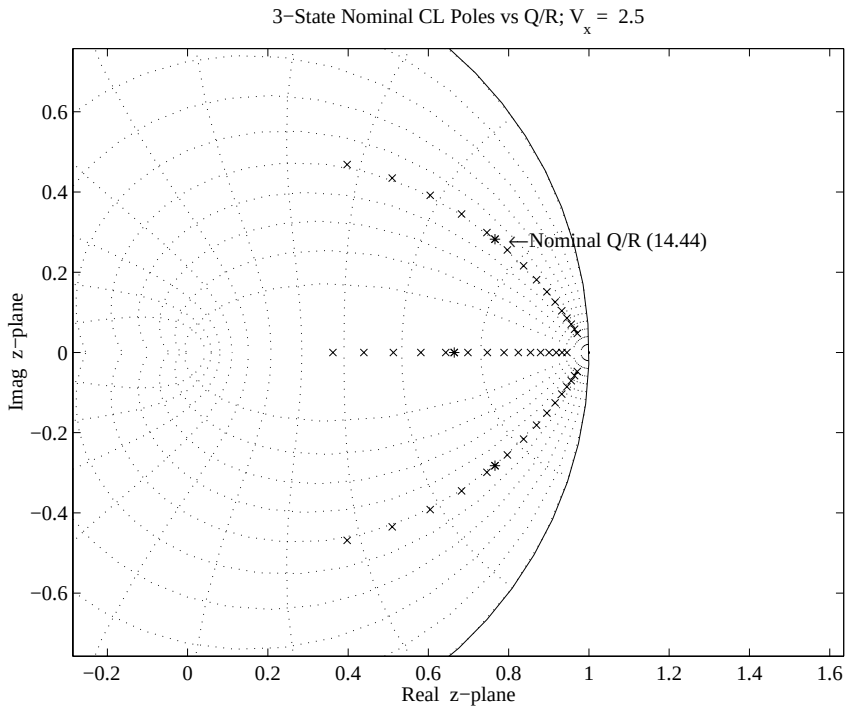

Figure 47 - Optimal Closed-Loop Pole Locations vs. Q/R

loop pole locations for the same controller applied to the identified five-state tractor model are shown in Figure 48. Note that for non-aggressive control (small $\frac{Q}{R}$), the two are very similar. However, if the cost on control effort is reduced to produce a more aggressive controller, performance is significantly degraded as a result of poor modeling, and the closed-loop system may actually be driven to instability. The two figures show the pole locations for the nominal $\frac{Q}{R}$ values used on the tractor. These poles in fact lie outside the unit circle for the poorly modeled case.

7.2.2 Estimator Design

With only three measurements available in these experiments, some form of processing was required to provide estimates of all five states required for full-state LQR feedback. The tool used to find the optimal state estimate based on sensor and disturbance noise properties was the Linear Quadratic Estimator (LQE). Details regarding estimator design are found in Section 7.3.1 (golf cart) and 7.4.2 (tractor).

7.3 Golf Cart Experimentation

The initial land vehicle closed-loop experiments in this project were performed using the golf cart described above. The purpose of these tests was to demonstrate land vehicle automatic control on a small, manageable platform. This section describes the control design assumptions, simulation results, and experimental results from this vehicle.

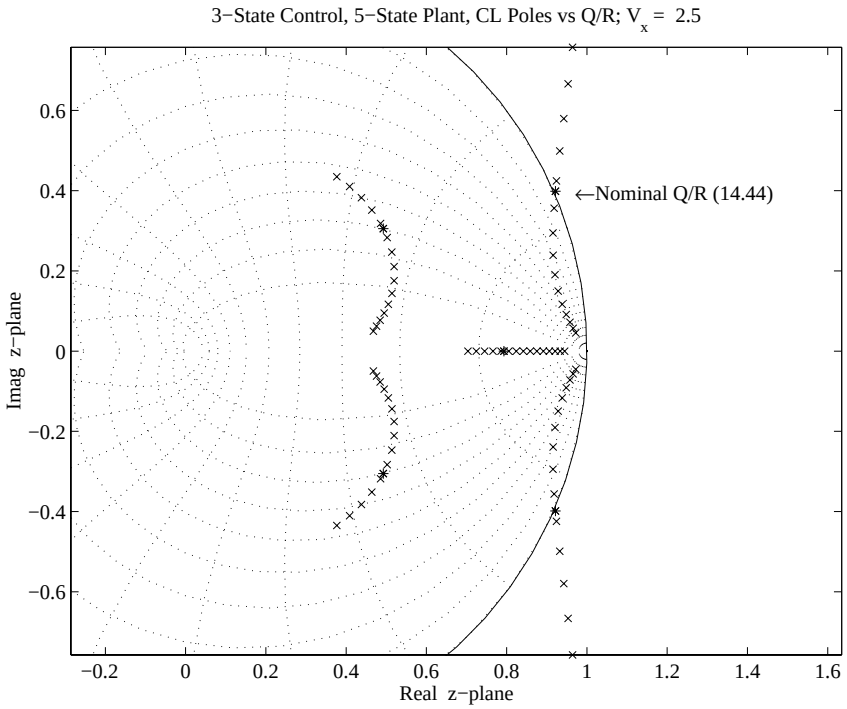

Figure 48 - Actual Closed-Loop Pole Locations vs. Q/R

Table 8 - Golf Cart Sensor and Disturbance Noise Values

	Sensor Noise (1-σ)	Disturbance Noise (1-σ, 4 Hz)
y	2.0 cm.	0.1 cm.
Ψ	0.3 deg.	0.06 deg.
δ	0.3 deg.	0.3 deg.
Ψ_{bias}	-	0.006 deg.
δ_{bias}	-	0.006 deg.

7.3.1 Golf Cart Controller Simulation

Initial open-loop golf cart experiments suggested that the Ellis three-state model was adequate to describe the dynamics of this particular land vehicle driving at a speed of two meters per second on a grass surface. Therefore, this model was used for the simulation and control system work described here.

Based on the Ellis model, a straight line controller was simulated using LQR techniques. The state cost matrices used to compute the regulator gains weighted only the vehicle lateral position deviation and control effort using Bryson's rule:

$$\mathbf{Q} = \begin{bmatrix} \frac{1}{y_{max}^2} & 0 & 0 \\ 0 & 0 & 0 \\ 0 & 0 & 0 \end{bmatrix}, \tag{7.17}$$

$$\mathbf{R} = \left[\frac{1}{u_{max}^2}\right]. \tag{7.18}$$

Where u_{max}, the maximum control effort available using the Navico steering actuator, was $\pm 2.3^{\circ}$ / sec., and y_{max}, the desired maximum lateral deviation, was designed as 0.1 meters.

The purpose of the simulation was to arrive at an anticipated value for control system accuracy, and to assess the importance of vehicle state and sensor bias estimation. Two cases were explored in the simulation. In one case, the control signal sent to the vehicle was a linear combination of the *measured* vehicle states ("No Estimator" case). In the second, the heading and front wheel angle sensor biases were appended to the vehicle state, which was *estimated* in real-time using Linear Quadratic Estimation ("Estimator" case). The measurement and disturbance values used to determine the Linear Quadratic Estimator gains are shown in Table 8. The same regulator gains, sensor noise, and process noise were used in both simulation cases.

Figure 49 shows the results from the first 200 meters of both simulation cases with an initial lateral displacement of 0.3 meters, and with heading and wheel angle sensor biases of 0.5°. This simulation was run for a 10 kilometer path to gather the statistical data shown in Table 9.

Table 9 - Statistical Golf Cart Simulation Results

	"Estimator" (mean $\pm 1\sigma$)	"No Estimator" (mean $\pm 1\sigma$)
y (cm)	0.0 ± 3.2	-8.8 ± 3.7
u (deg/s)	0.0 ± 0.47	0.0 ± 0.98
Ψ_{bias} Estimate(deg)	0.0 ± 0.07	N/A
δ_{bias} Estimate (deg)	0.0 ± 0.04	N/A

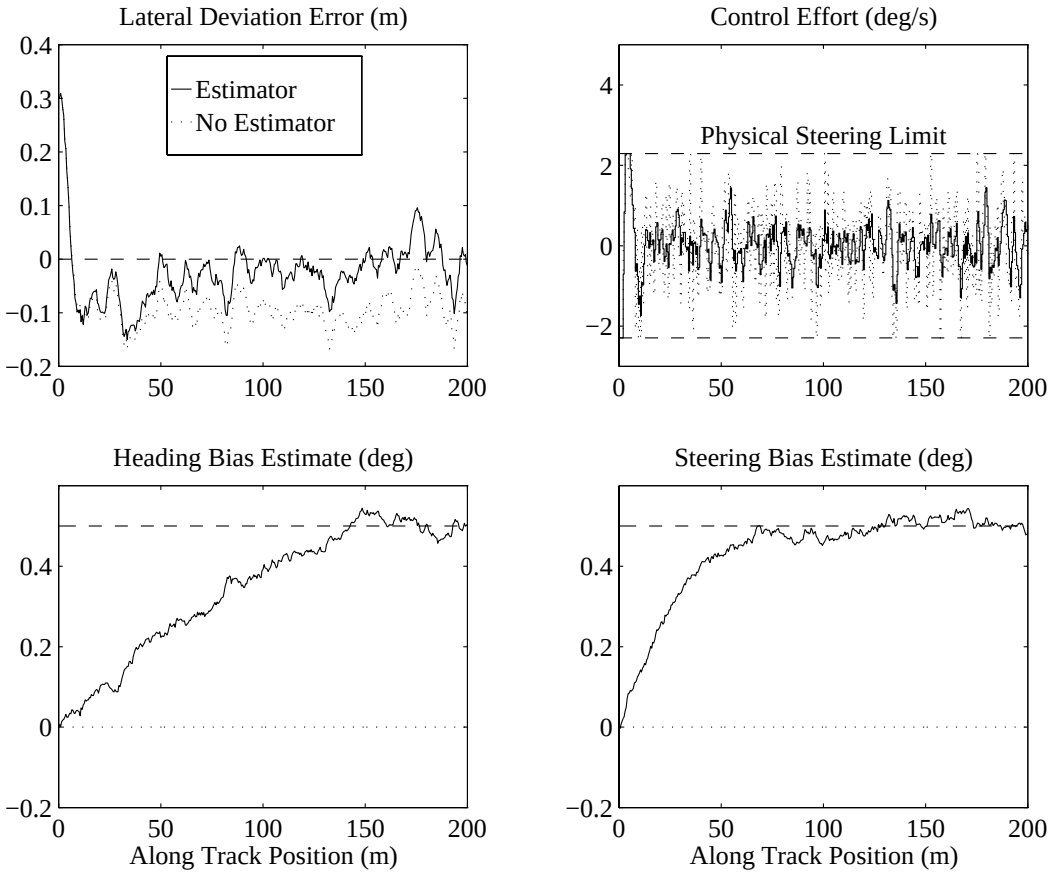

Figure 49 - Golf Cart Simulation results

This simulation shows that the controller based on the optimal estimator had three major advantages. For one, the control effort utilized by the controller with estimator was half the level of the control without the estimator. Secondly, it was found that a relatively small sensor bias error results in a significant lateral position bias when these errors are not estimated in real-time. The simulated 0.5° sensor biases produced almost a 9 centimeter offset in the vehicle line-tracking ability. Finally, the lateral position standard deviation was reduced by over 10% when the estimator was used to optimally filter the raw measurements.

7.3.2 Golf Cart Controller Testing

Golf cart experimentation took place on a large grass field at Stanford University known as "The Oval". Since a 10 kilometer data collection run was not possible on this field, two control modes were designed for the cart – a straight line following mode and a u-turn mode.

The technique used for golf cart straight line following control was the Linear Quadratic Regulator and Estimator used in simulation. Sensing and control were both performed at 4 hertz. The measurement of the vehicle positioning antenna was used for feedback (i.e. no lever-arm correction was implemented). Vehicle CDGPS position was initialized by starting each test from a fixed, known location. While this method was not truly repeatable, it was adequate for control system testing.

The u-turn controller was a modified version of the straight line controller with a nominal feed-forward command designed to track the turn. The feed-forward path was designed to require up to 75% of the actuator authority, leaving at least 25% for feedback about the nominal trajectory. The path was numerically stored as a discrete set of nominal states and feed-forward control commands, as shown in Figure 50.

Two basic tests were performed on the golf cart. For the first test, a number of trials were

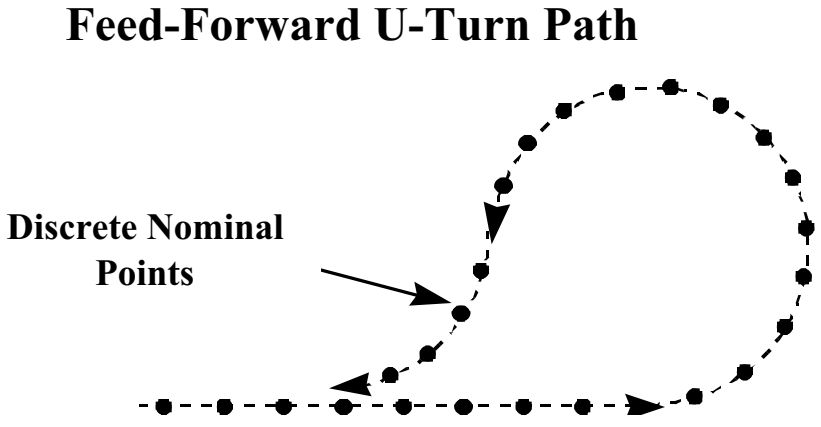

Figure 50 - Feed-Forward U-Turn Path

performed in which the vehicle was commanded to follow a straight line 100 meters long. Of fifteen trials, three were unable to acquire the line on initialization due to a poor initial state when the controller was activated. Of the twelve trials that were able to acquire the line, three more resulted in eventual system instability or saturated actuation producing a widely varying vehicle path. The results from the nine successful passes are shown in Figure 51. The lateral position error from these passes was zero mean with a 5.0 centimeter standard deviation. The control effort was also zero mean with a standard deviation of 1.26 degrees per second. Due to higher than expected disturbances (see Section 7.3.3), these numbers are significantly higher than the 3.2 centimeter lateral position standard deviation and 0.47 degrees per second control effort standard deviation predicted in simulation.

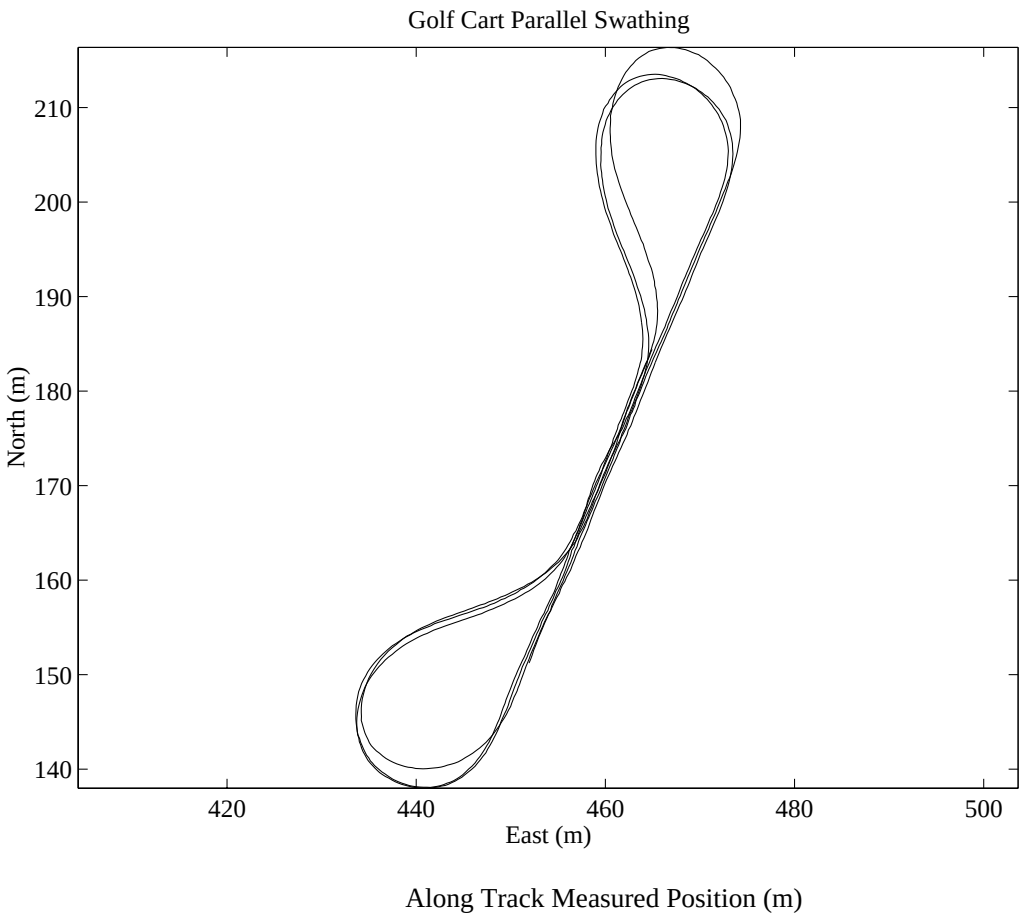

Figure 52 - Golf Cart Experimental Swathing
Figure 51 - Golf Cart Line Following Experimental Results

It is reassuring to note that the ratio of lateral position error to control effort ($\frac{1}{R}$) is almost identical to the design value (see Equations 7.17 and 7.18). This suggests that lowering this ratio by decreasing the cost on lateral position error (or, equivalently, by increasing the cost on control effort) may prevent the actuator from hard-limiting and provide better control system stability.

The purpose of the second test was to simulate parallel swath following. The goal was to perform multiple line tracking trials with rows spaced 30 centimeters apart. After several attempts, the trajectory shown in Figure 52 was achieved, however, instability on the turns resulted in many unsuccessful initial trials. The failure to follow the path was

caused by the actuator's inability to tightly track the feed-forward trajectory without saturation.

7.3.3 Golf Cart Lessons Learned

Several important lessons were learned through implementation of the land vehicle controller on the golf cart. These discoveries were the direct result of physical experimentation, and would have been easily overlooked in a strictly computer-based simulation.

Perhaps the most interesting outcome of the successful golf cart line following experiments was the high level of noise correlation between trials, which is easily seen in Figure 51. This path repeatability was not attributable to measurement errors, and the

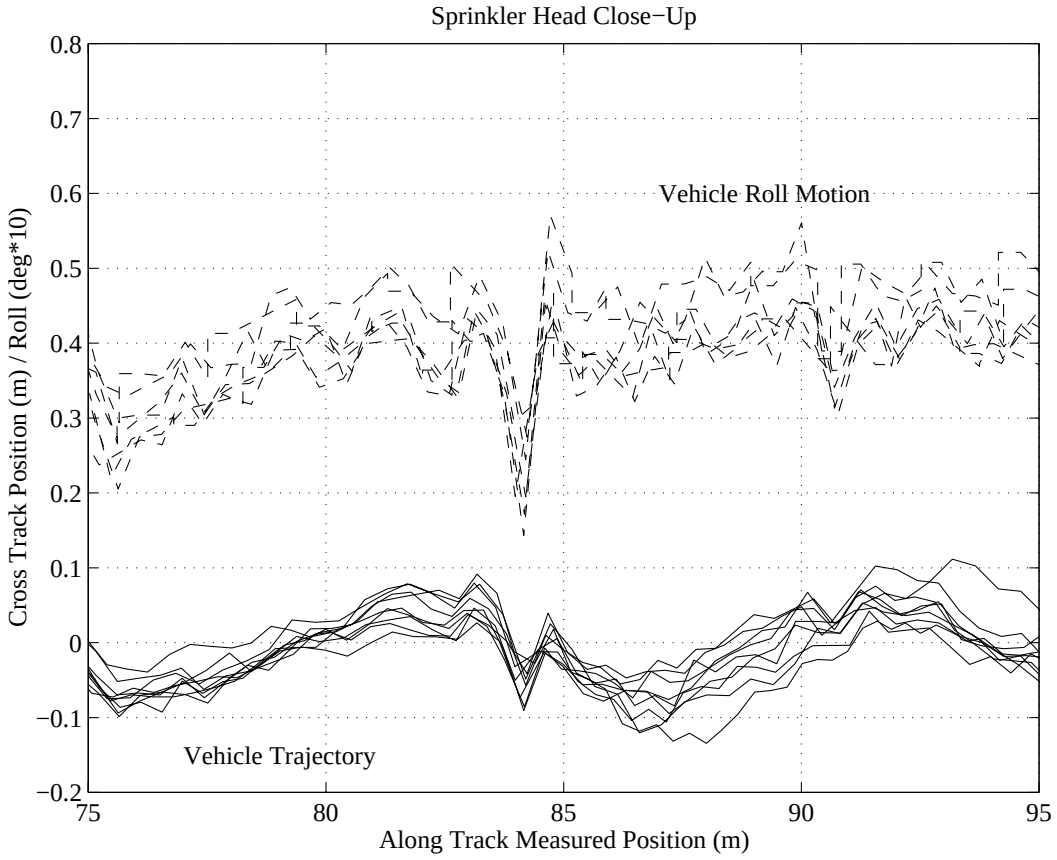

Figure 53 - Close-Up of Golf Cart Line Following Experimental Results

level of the recurring disturbances did not appear to be consistent with those expected on the smooth grass field. Upon examination, it was found that the sharpest and most repeatable disturbance took place when the golf cart hit the same sprinkler head on each pass. A closer examination of the data about this point led to the understanding that, because a lever-arm correction was not implemented, the roll motion of the golf cart was causing the errors (See Figure 53).

This lever-arm induced lateral disturbance noise accounted for the higher than simulated lateral position and control effort standard deviations during successful line following. The three diverging passes were also an indirect result of this unaccounted lever-arm. For these cases, the roll motion produced large enough errors to saturate the steering actuator, creating nonlinear behavior that caused the controller to diverge.

Another major problem discovered during golf cart experimentation was the controller's poor robustness during line acquisition, u-turns, and large, unanticipated row-following lateral errors. The vehicle was capable of tracking a straight line only when the vehicle state was within tight limits, and u-turns were completely unreliable. The experiments clearly showed that a hybrid controller was required to handle off-nominal and initialization conditions.

Finally, many of the problems with the golf cart were the result of a *very* limited actuator. The maximum front wheel angle rate using the golf cart steering actuator was approximately 2.3°/second – requiring 25 seconds for a transition from a hard left turn to a hard right turn. A stronger actuator was desired for further experimentation.

7.4 Tractor Experimentation

Based on the limited control system success demonstrated on the golf cart, work was performed to implement an improved system on a more realistic platform – the John Deere 7800 farm tractor. The automatic control of a genuine farm vehicle was the primary

focus of this project, and these experiments mark the culmination of the research efforts presented in this thesis.

7.4.1 Expert Human Driver Results

To measure the success and utility of an automatic tractor steering system, it is important to understand the capabilities of human tractor operators. Even if a tractor controller is not as fast or as accurate as a human driver, the control system offers certain advantages, including reduced driver fatigue, low-visibility operation, and the elimination of some costly farm vehicle accessories. If it is more accurate or faster than a human, greater efficiency improvements due to reduced row overlap and cost-effective tape irrigation become possible, and the potential to save money for farmers is dramatically improved.

To test the potential capabilities of a human driver, Oscar, the best human tractor operator available on one large farm in the southwestern United States, was chosen for experimentation. The vehicle navigation system on the 7800 tractor was initialized, the automatic control system was disengaged, and Oscar was instructed to maneuver the tractor in a long, straight line with a 10-row bedder in the ground – a task considered difficult by farmers. In accordance with his usual practices, Oscar used no flags or other cumbersome field markers to define his row.

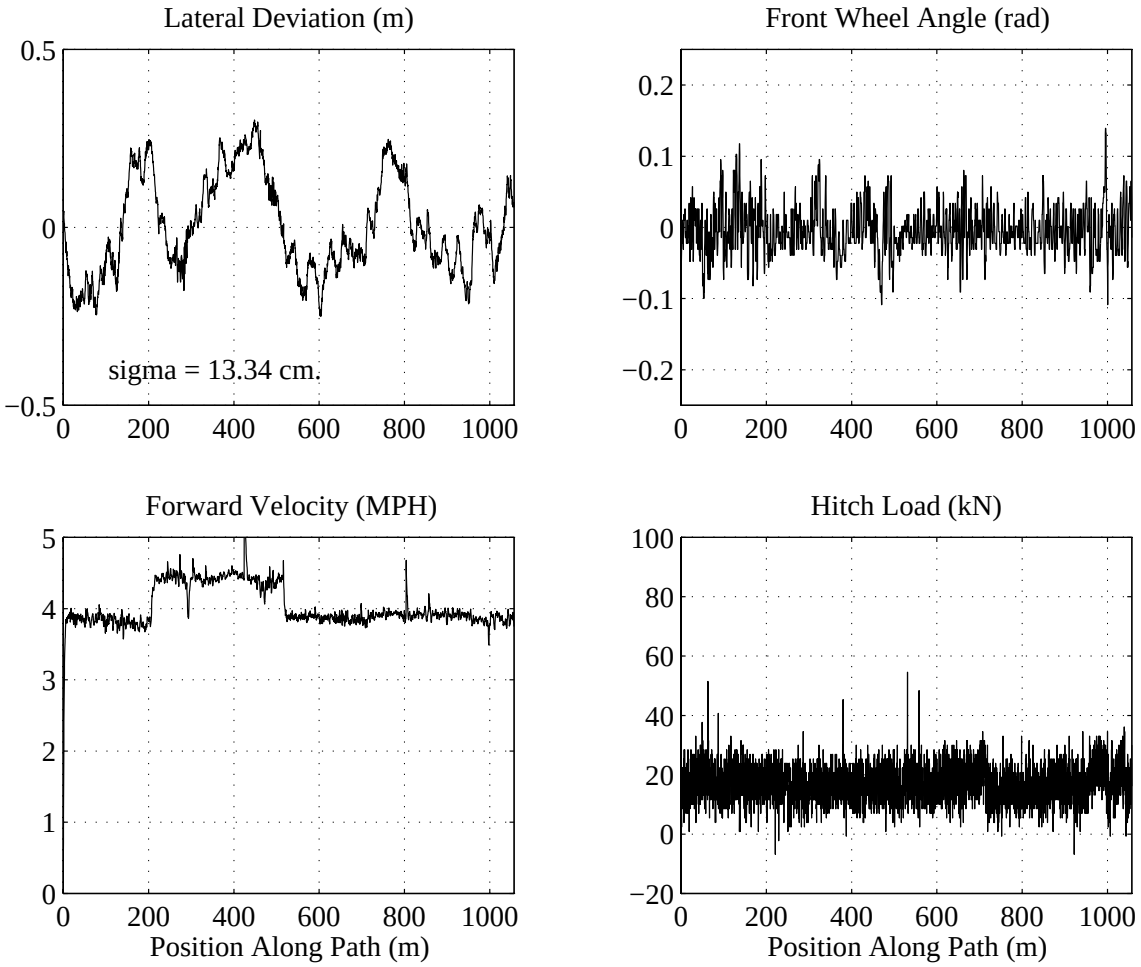

Figure 54 - Expert Driver Results for Line 1

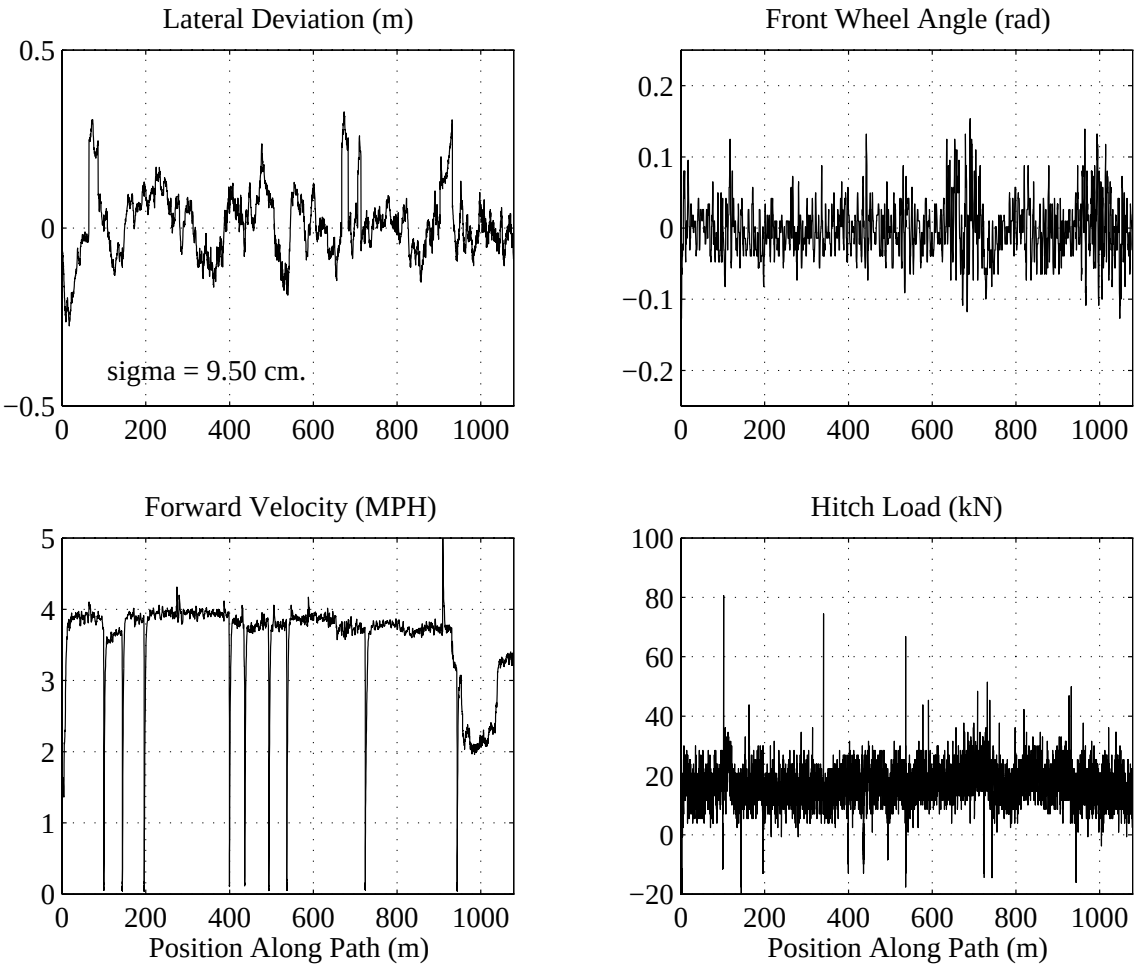

Figure 55 - Expert Driver Results for Line 2

After several short "warm-up" passes, Oscar executed two long rows, both exceeding 1000 meters in length. The results from these passes are shown in Figure 54 and Figure 55. Both runs were driven at approximately the typical speed of 1.8 meters per second (4 miles per hour). The standard deviation errors from the best-fit straight line through these paths were 13.34 centimeters for line 1 and 9.50 centimeters for line 2. Oscar was assumed to have zero mean error.

It is interesting to note that, for line 2, the wind was blowing from behind the tractor at a speed slightly higher than the tractor operating speed. As a result, dust from the bedder

frequently obscured Oscars vision (See Figure 3), requiring him to stop the vehicle until the resulting dust cloud had blown away from the tractor.

These forward speed and vehicle accuracy results define a major goal for tractor and implement automatic control research and development. They may be viewed in the eye of a farmer as the "pay-back point". When these results can be surpassed by an automatic farm vehicle controller, it will become easy to justify investing in a piece of hardware to perform automatic control. The stage has been set for a friendly, yet highly important competition: "Oscar vs. The Machine".

7.4.2 Tractor Control Regimes

The tractor controller was designed after testing was completed on the golf cart. Knowledge and lessons learned from golf cart experiments were used to redesign several aspects of the land vehicle controller. In addition to adding the lever-arm correction, a variety of control regimes were added to provide a cushion for any divergent controllers, provide initialization on the first row, and provide robust, seamless transition between lines, including u-turns. The resulting controller was a combination of linear and nonlinear control laws designed to supply maximum accuracy, maximum speed, or maximum robustness depending on the phase of operation. This complete controller included automatic switching between control regimes.

The first new control law, rapid acquisition of Closed-Loop Heading, was designed as a building block for higher-level control regimes. The goal of this controller was to achieve a desired heading in minimum time. Since this controller was implemented only when centimeter-level lateral deviation accuracy was not required, the simple 3-state Ellis model was used for design. Sensor biases were not estimated in automatic control regimes based on closed-loop heading.

Using the three-state land vehicle model assumption, it can be shown that the minimum time state trajectory to acquire a heading is the bang-bang solution. The possible Ψ -δ trajectories for bang-bang control may be easily shown on a phase plane diagram for a given control signal u. The bottom two elements of Equation 7.1, combined with the relation

$$\ddot{\Psi} = \dot{\Psi}\frac{d\dot{\Psi}}{d\Psi}, \tag{7.19}$$

may be reduced to

$$\delta^2 = \frac{2Lu}{V_x}\Psi + C, \tag{7.20}$$

where C is a constant of integration defined by the initial conditions.

The standard bang-bang control law with parabolic switching curve shown in Figure 56 reflects what a human driver would do on a wide turn. The front wheel is turned to its maximum angle, and is straightened out just in time to arrive near the desired heading when the wheel angle reaches zero. Note from the figure that a small linear control region is included to eliminate chattering by the controller while zeroing out small errors near the desired heading. This controller was used as a building block for Waypoint Following and Line Acquisition (including u-turns).

A second controller mode, Waypoint Following, was also added as a high level control mode. This controller utilized the Closed-Loop Heading controller, setting the desired heading based on the vehicle position relative to a desired waypoint. This control law was implemented to perform a mode transition when the vehicle entered a pre-defined

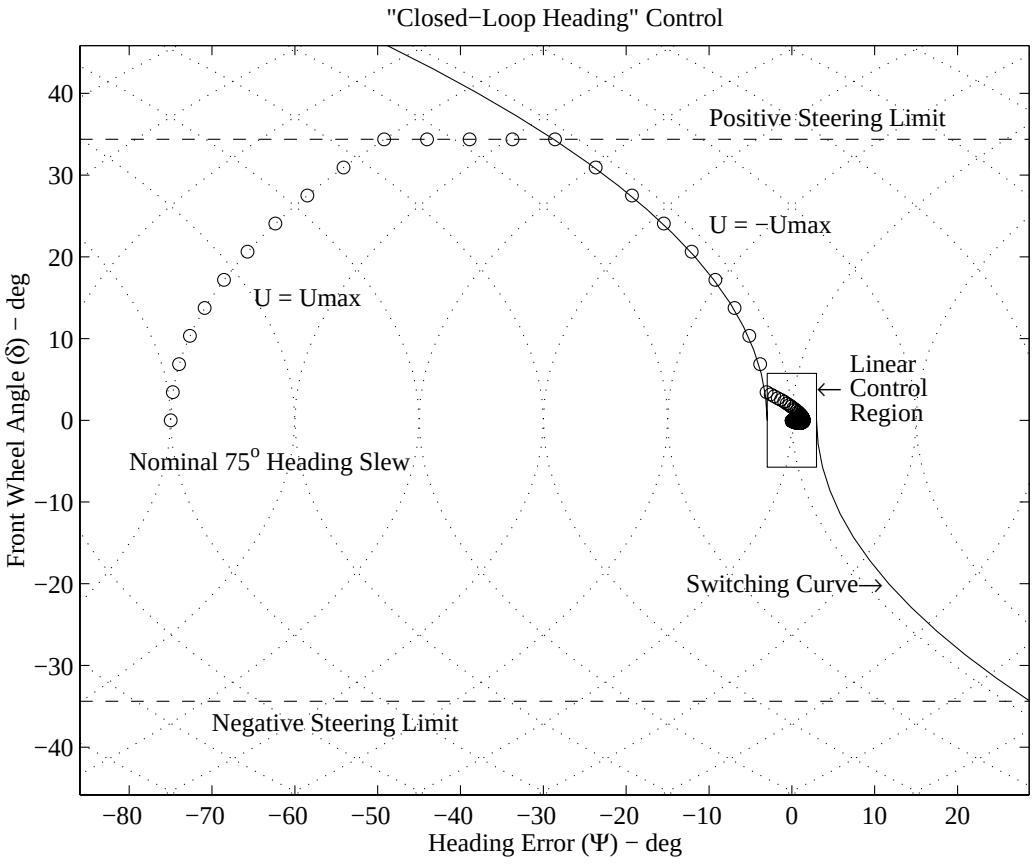

Figure 56 - Bang-Bang Closed-Loop Heading Controller

waypoint radius. This mode switch would cause the vehicle to follow the next waypoint or, after the final waypoint is reached, acquire a straight line. The waypoint transition radius was set larger than the land vehicle turn radius to avoid the possibility of encircling the waypoint indefinitely.

The third general control law added to the high level control system was a Line Acquisition controller. This heuristic algorithm was also based on the Closed-Loop Heading controller. Its purpose was to allow a general asymptotic approach to a desired line regardless of the initial vehicle state. Such a Line Acquisition controller was useful for acquiring the first row, as well as making end-of-row u-turns. The commanded heading was related to lateral position deviation by the following relationship:

$$\Psi_{cmd} = -\tan^{-1}(ky) \quad . \tag{7.21}$$

This equation was selected to command a heading perpendicular to the desired row for very large lateral position deviations (y), and parallel to the row for very small position errors. The value of k was chosen to allow the vehicle to smoothly but quickly transition onto the line.

The original golf cart Tight Line Controller based on LQR techniques was used with some minor changes: the lever-arm correction was included in the measurement output equation, the five-state land vehicle model was implemented, and the maximum control effort was set to 20 degrees per second to correspond with the tractor actuator. An LQE estimator was implemented which estimated the five vehicle states along with two sensor bias states. The disturbance values used in the estimator are shown in Table 6.

7.4.3 Tractor Closed-Loop Experimental Results

To demonstrate automatic control of a farm tractor, a path was selected to display all control system modes. Waypoints were set up to bring the vehicle to the beginning of the initial row, the specialized control law was used for line acquisition, the LQR controller was used to follow 4 rows, 50 meters long and 3 meters apart, and u-turns were automatically performed between the rows.

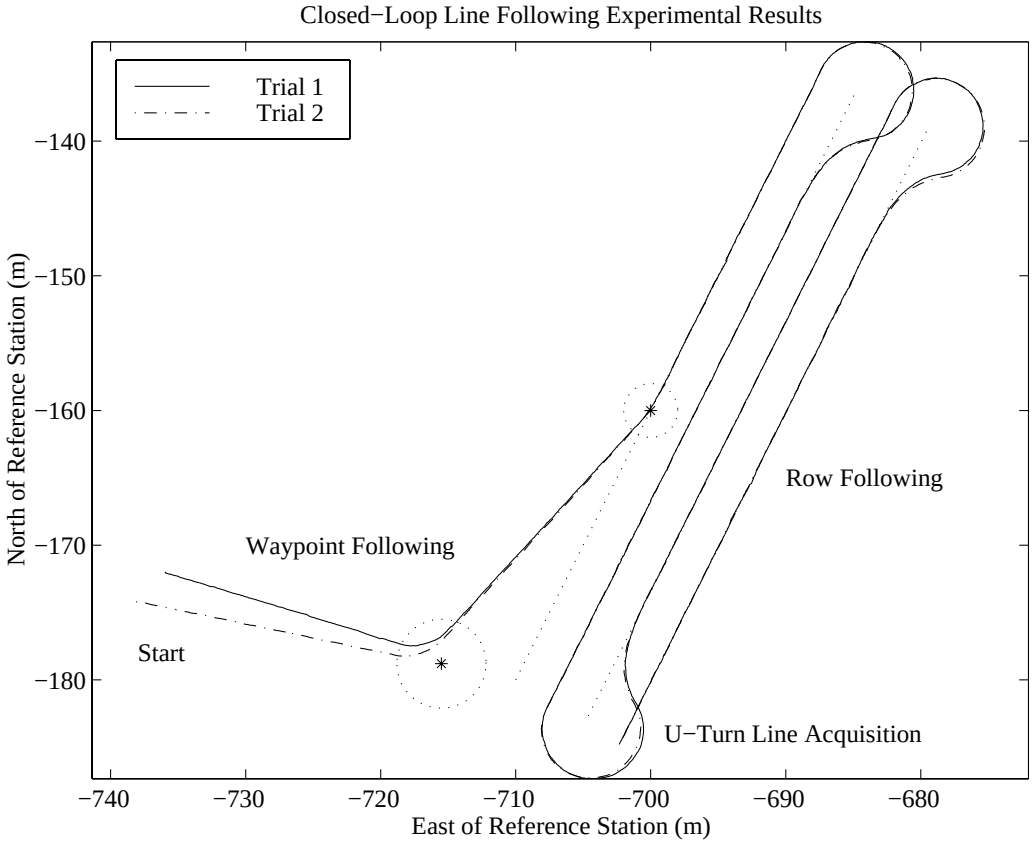

Figure 57 - John Deere 7800 Automatic Control Trajectory

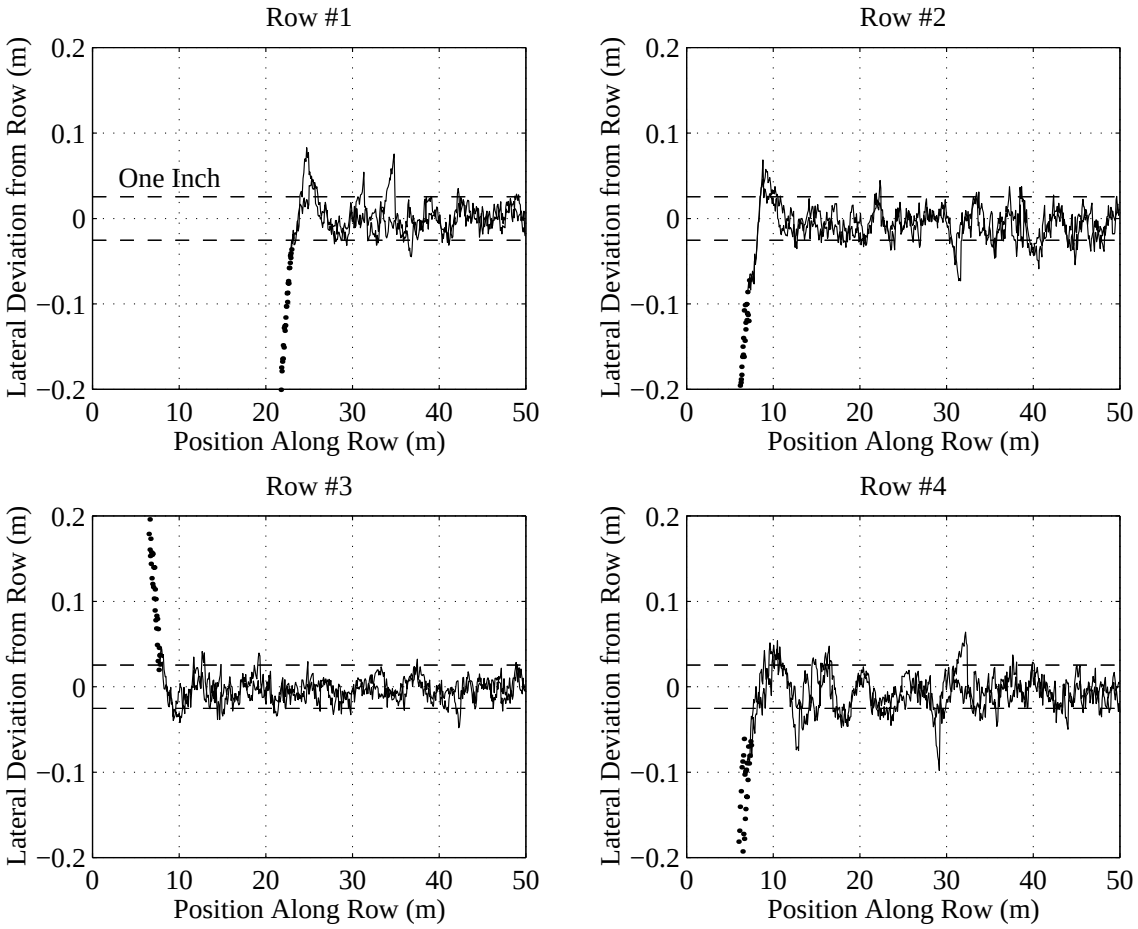

Figure 58 - John Deere 7800 Automatic Control Rows

Fixed-gain controllers were used for three specific tractor operating conditions: first gear (0.35 meters per second) with no implement, ninth gear (1.6 meters per second) with no implement, and first gear with a three-shank sub-soiler in the ground during row following. Figure 57 shows the GPS measured position for two *fully automatic control* trials with the tractor in first gear with no implement.

From the scale of the plots in Figure 57, the lateral position error is not easily discernible. The measurements along each row were transformed into path coordinates and plotted in Figure 58. This figure shows a close-up view of all four rows for both trials. From the

Table 10 - Automatic Control System Statistics

	Error Statistics (mean +/- 1σ)	Row Following Controller Reliability
First Gear No Implement	**-0.4 +/- 1.9 cm.**	**8 out of 8**
Ninth Gear No Implement	**-0.7 +/- 4.4 cm.**	**8 out of 8**
First Gear Hitched Sub-Soiler	**-1.0 +/- 2.0 cm.**	**4 out of 4**

plots it can be seen that the lateral displacement error was within one inch for most of the time. The numerical results for all three operating conditions is shows in Table 10. Two trials were run for each operating condition with no implement. After the first trial with the sub-soiler, this sturdy implement came in contact with an equally sturdy ancient underground pipe, and the "immovable object" won. The sub-soiler was badly damaged, and only one trial was ultimately performed with the implement.

Further experimentation performed in collaboration with other Stanford students have corroborated the accuracies and control system integrity shown in Table 10, and have extended the control system to a wider range of tractor operating regimes.

The figures and tables above show the CDGPS *measurements* used by the automatic control system. Therefore, these plots and mathematical results represent the errors induced by the control system, but do not reflect any navigation system errors. For example, a constant bias in the navigation solution would not appear in these results since a position measurement bias is not observable given the sensors available on the tractor.

To determine the total system accuracy of the control system, the *true* vehicle position is required. The position measurements offered by CDGPS are so accurate that it is very difficult to find a better sensor for comparison. A simple test was devised to find the approximate total system accuracy along straight rows.

A 60 meter length of rope was tightly stretched over the field, and the two ends were surveyed using the tractor CDGPS system. This navigation system was then reset and reinitialized through satellite motion or by starting at a fixed, known location. A ten centimeter wide wooden pointer was connected to the bottom of the tractor with markings located one centimeter apart. A video camera was mounted to the tractor and aimed at this pointer. The tractor control system was then commanded to drive with the center of the pointer over the rope. Trials were run without an implement in first gear and in ninth gear.

CDGPS position measurements were collected while video was taken. The video tape was later examined on a second-by-second basis and the image of the pointer over the

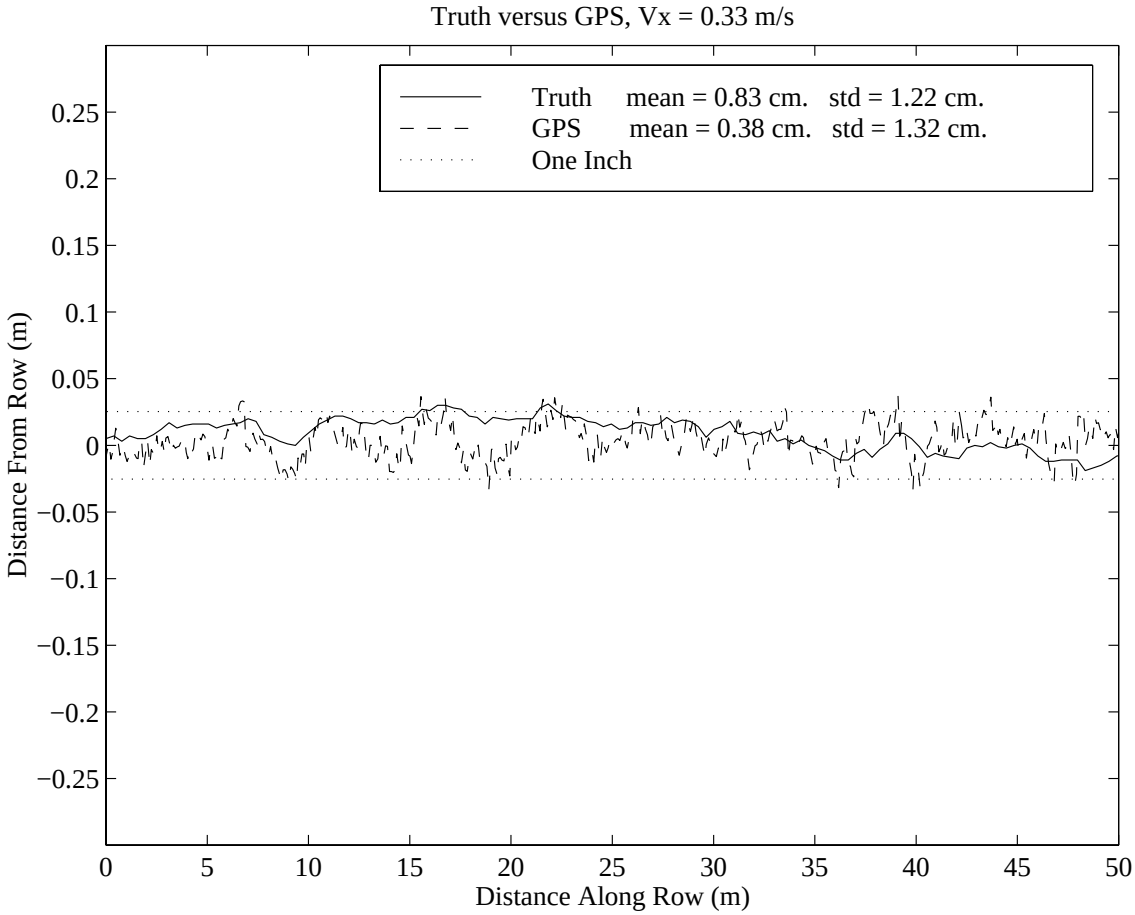

Figure 59 - First Gear CDGPS and Video "Truth" Comparison

rope was used to arrive at a measurement of “truth”. The comparison of the video measurements and CDGPS measurements for each forward speed are shown in Figure 59 and Figure 60.

The bias between the CDGPS and video measurements was less than a centimeter for both trials, verifying that the CDGPS initialization was repeatable between trials and for the rope survey. The plots show that CDGPS is significantly noisier than the video measurements for both cases. The statistics verify that the standard deviation of the CDPGS measurements was in fact higher than the true lateral position standard deviation as measured by the pointer. This suggests that the total system error was smaller than the CDGPS measured lateral position error due to the linear state estimation and the physical filtering due to plant dynamics.

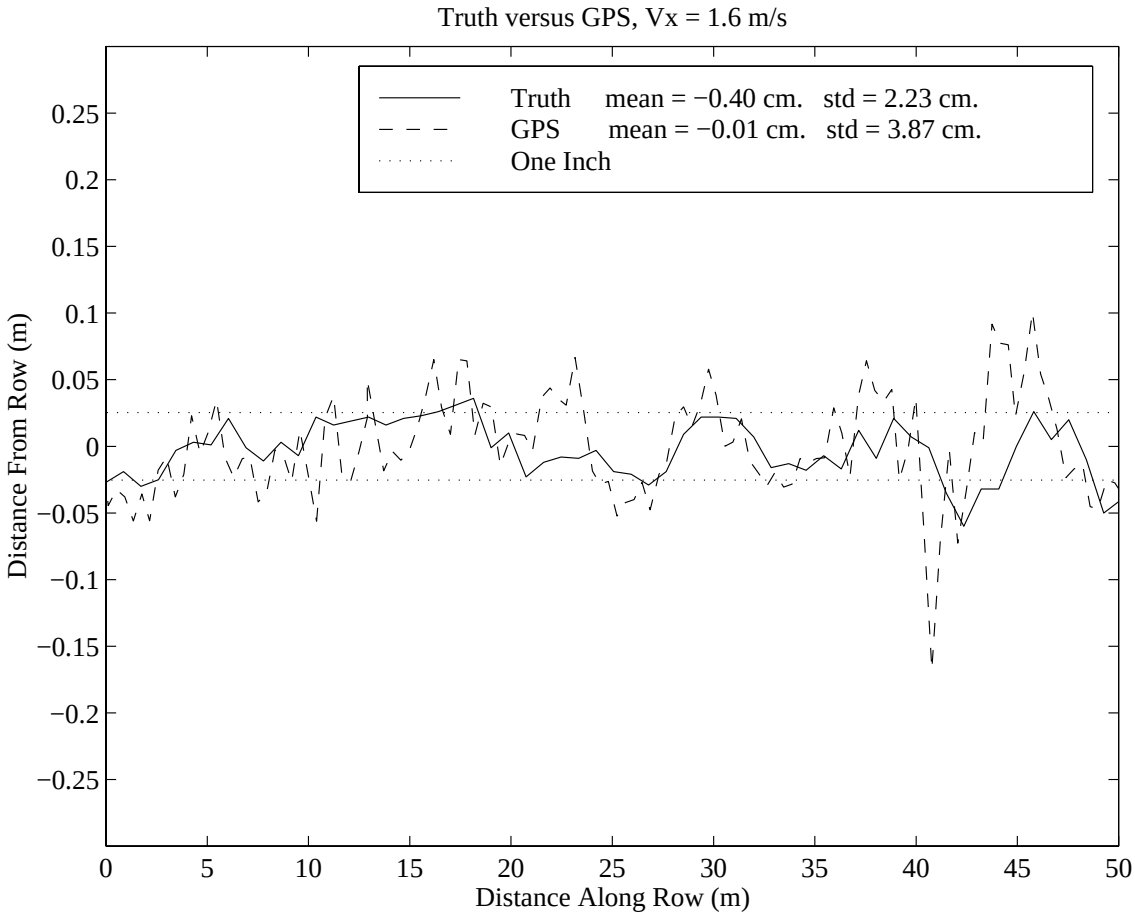

Figure 60 - Ninth Gear CDGPS and Video "Truth" Comparison

One possible criticism of this test method is that the CDGPS sensor was used to survey the position of the rope. In practice, most land vehicle applications will require a survey of the region of control interest prior to vehicle operations within this region. This survey will often be performed using CDPGS. For example, a farmer will probably drive around fields while taking CDGPS measurements to define their borders. While the rope test does not demonstrate the absolute accuracy of the system, it does show repeatability of the system, which is just as important.

The resolution of the video camera filming the rope was on the order of a few millimeters, making it a good method to measure truth; however, a possible cause of error during rope

tests was lateral deviations of the rope on the ground. Although the rope was stretched tightly, slowly varying errors in the straightness of the rope could be on the order of a centimeter or two. A better method for truth comparison would be the use of a laser.

7.4.4 Tractor Experimental Conclusions

In conclusion, centimeter-level control system accuracy and repeatable centimeter-level total system accuracy were demonstrated on a John Deere 7800 farm tractor. Three specific operating conditions were demonstrated with 1σ control system lateral deviation accuracies better than 5 centimeters in all cases. A robust controller was designed to follow waypoints, begin rows, perform u-turns, and ensure stability in the case of larger than expected disturbances.

More testing is clearly needed since these tests were performed in one field with either no implement or one specific implement. Also, each test was established specifically for a desired operating condition with no flexibility in the control system gains. Some testing has been performed in conjunction with other Stanford students with more flexible controllers, new implements, and new field conditions with promising results. These results will be presented in future Doctoral dissertations.

Chapter 8

Alternate Sensor Simulations

The previous chapters in this thesis describe a careful study of land vehicle dynamics and the successful demonstration of an accurate steering control system using a fixed set of highly accurate sensors. To design a commercial product for farm vehicle automatic control, different sensor combinations must be explored in simulation and experimentally; the set of sensors providing acceptable accuracy and robustness at minimal cost is desired. This chapter serves as the first step in this process. The simulated lateral position accuracy is computed for various sensor combinations, and the relative cost of these combinations is compared.

8.1 Simulation Assumptions

Because this thesis is only concerned with high accuracy GPS control of land vehicles, the simulations described below all assume centimeter-level CDGPS measurements of the tractor main positioning antenna. The other four sensors simulated were a CDGPS attitude receiver, a flux gate compass, a yaw rate gyroscope, and a front wheel angle

potentiometer. A total of 16 simulation cases were run to explore each possible sensor combination.

For the simulation truth model, the John Deere 7800 tractor five-state linearized model was used with a forward speed of 1.0 meters per second and the disturbance properties found experimentally on the tractor. Each sensor was modeled with a *quickly varying* random noise component and a *slowly changing* bias. The bias was modeled as the output of a pure integrator driven by Gaussian white noise (also known as a random walk process).

The random noise values for the CDGPS attitude receiver and the steering potentiometer were determined experimentally as described above, and were assumed to have negligible sensor bias drift. The noise driving the slowly varying bias values for these two sensors was assumed to be very small, since both sensors are expected to have a relatively fixed bias. The noise and bias drift values used to describe the simulated compass and gyroscope were taken from a Ph.D. dissertation by Eric Abbott[65]. All values are all shown in Table 11.

A Linear Quadratic Regulator and Estimator were assumed in the simulation. The regulator was designed based on a desired maximum lateral position deviation of 0.1 meters and a maximum wheel rate command identical to the John Deere 7800 tractor. The estimator was designed using the five-state model with one additional state for each non-

Table 11 - Simulated Sensor Noise Characteristics

Sensor	Sensor Random Measurement Noise (1-σ)	Sensor Bias Disturbance Noise (1-σ)
CDGPS with correction	1.3 cm.	-
CDGPS without correction	6.0 cm.	-
CDGPS Attitude Azimuth	1.7×10^{-3} rad	1.0×10^{-10} rad
Compass Azimuth	3.4×10^{-2} rad	7.8×10^{-4} rad
Gyro Azimuth Rate	4.7×10^{-4} rad/s	2.0×10^{-9} rad/s
Potentiometer Wheel Angle	2.6×10^{-3} rad	1.0×10^{-10} rad

positioning sensor bias. The "truth" disturbance and sensor noise covariances from Table 11 were assumed by the estimator. The lever-arm correction for the lateral position was applied only when roll measurements were available using CDGPS attitude. The simulated truth model and the simulated control system were both run at five hertz.

8.2 Simulation Results

For each sensor combination, a closed-loop linear simulation of straight line following was run for 100,000 samples. The accuracy statistics based on the simulated "truth" values are shown in Table 12, along with the approximate cost of each sensor combination. The tabulated values represent the steady-state estimates and do not include the effects of initial errors in vehicle state estimate. All sensor combinations resulted in a lateral position bias error of less than one millimeter.

One quick method of sensor assessment involves comparing the effect each sensor has on the total lateral position error when used independently. The use of a steering potentiometer or a yaw rate gyro had the effect of reducing the true lateral positioning

Table 12 - Simulated Lateral Position Accuracy for Various Sensor Combinations

Trial No.	CDGPS Attitude ($2000)	Compass Yaw ($250)	Gyro Yaw Rate ($100)	Pot Steering ($50)	Added Sensor Cost	Lateral Position cm, 1-σ	Control Effort rad/s, 1-σ
1	No	No	No	No	$0	11.4	0.303
2	No	No	No	Yes	$50	4.2	0.090
3	No	No	Yes	No	$100	4.2	0.103
4	No	No	Yes	Yes	$150	3.8	0.084
5	No	Yes	No	No	$250	7.3	0.209
6	No	Yes	No	Yes	$300	3.9	0.086
7	No	Yes	Yes	No	$350	3.9	0.100
8	No	Yes	Yes	Yes	$400	3.7	0.083
9	Yes	No	No	No	$2000	3.3	0.109
10	Yes	No	No	Yes	$2050	2.7	0.076
11	Yes	No	Yes	No	$2100	2.9	0.093
12	Yes	No	Yes	Yes	$2150	2.6	0.076
13	Yes	Yes	No	No	$2250	3.3	0.108
14	Yes	Yes	No	Yes	$2300	2.7	0.077
15	Yes	Yes	Yes	No	$2350	2.9	0.093
16	Yes	Yes	Yes	Yes	$2400	2.6	0.076

error from 11.4 centimeters to 4.2 centimeters. The compass was slightly less effective, reducing the error to 7.3 centimeters. The error reductions provided by these three sensors fundamentally resulted from the addition of lead information. The CDGPS attitude receiver caused the lateral position error to plummet to 3.3 centimeters. This improvement was caused by a combination of the lead information provided by heading measurements and the incorporation of the roll motion lever arm correction.

Further analysis shows that the CDGPS attitude system and compass acting together (cases 13-16) produce the same lateral position accuracy as the CDGPS attitude system without a compass (9-12). Also, all cases which included CDGPS attitude with no compass (9-12), show much better accuracy than cases with the compass and no CDGPS attitude (5-8). This effect is most likely due to lever-arm correction. In fact, the compass does not improve the total system accuracy by more than 3 millimeters unless it is the only sensor used beyond the basic CDGPS.

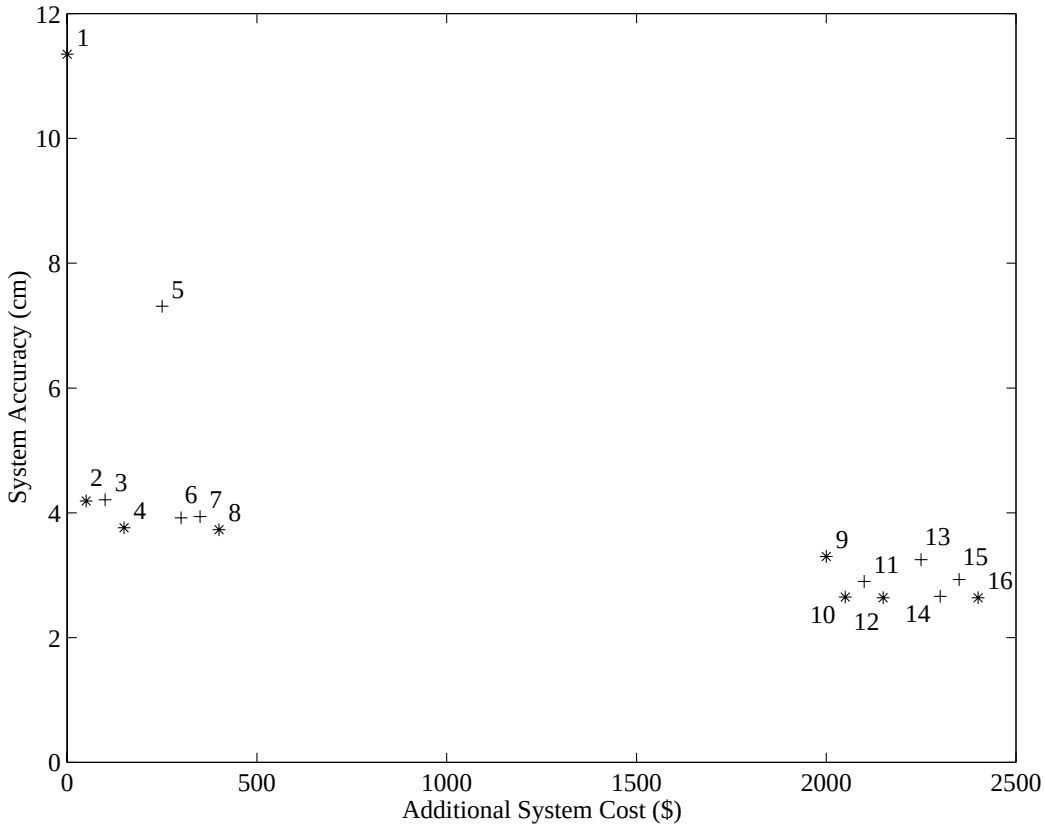

Figure 61 - Simulated Cost versus Accuracy Trade-Off

A plot of approximate additional system cost (above the price of the CDGPS system) versus simulated control system accuracy is shown in Figure 61. The points denoted with asterisks show the best accuracy system within a given cost. It is important to note that a minimal level of vehicle roll motion was assumed in all of these simulations. If the vehicle roll motion were significantly larger due to hills or large bumps, the error would be significantly worse for all trials without a CDGPS attitude sensor.

The control system effort required for a given set of sensors is almost as important as the control system accuracy. If a control system generates relatively small control signals, the $\mathbf{Q}$ and $\mathbf{R}$ matrices in the LQR algorithm may be changed to improve performance at the cost of additional control effort. Table 12 shows that, in general, as the sensors allow more accurate tracking of vehicle lateral position, the amount of control effort required is

reduced. One interesting note is that the yaw rate gyroscope and steering potentiometer have roughly the same effect on system accuracy; however, the control effort exerted with the gyro is higher than with the potentiometer. This is due to the fact that a steering sensor inherently provides more system lead information than a yaw rate sensor for the five-state vehicle model used in this simulation.

It is extremely important to note that this basic study addresses control system accuracy under nominal operation only. The issues of real-time system identification for adaptive control and the possibility of sensor outages are not included in the simulation. It is also important to note that these are simulation results only, and they have not been verified experimentally. All of these issues merit further analysis, simulation, and experimentation.

Chapter 9

Conclusions and Recommendations

9.1 Conclusions

This thesis describes the theoretical and experimental research behind the first successful demonstration of automatic land vehicle control using CDGPS. To accomplish this task, a number of specific research contributions were made.

- A single-pseudolite solution to the CDGPS initialization problem was studied and experimentally demonstrated, with a resulting navigation system accuracy of better than 5 centimeters.

- An original and highly general set of land vehicle models was developed for use in automatic control system applications.

- A Yamaha Fleetmaster golf cart was automatically steered with a row-following lateral position standard deviation of 5.0 centimeters using CDGPS.

- A general experimental method to linearize highly nonlinear land vehicle steering components was proposed and experimentally demonstrated on a farm tractor.

- A model for a John Deere 7800 farm tractor was selected and identified using a relatively general optimal parameter identification techniques and experimental data.

- A robust control system complete with waypoint following, line acquisition, row following, and u-turn capabilities was demonstrated on the 7800 farm tractor with a lateral position accuracy (mean plus two-sigma) over a rough field of 4.2 centimeters in first gear with no implement, 9.5 centimeters in ninth gear with no implement, and 5.0 centimeters in first gear with a three-shank ripper. These CDGPS control system accuracies were verified using quantitative video data collection techniques.

- A highly talented expert human driver was evaluated using CDGPS and found to have a best-case two-sigma driving accuracy of 19.0 centimeters over a smooth, prepared field in ninth gear with a ten-row bedder.

- A series of simulations were run to explore the use of various sensor combinations for automatic control of the farm tractor. Through the use of CDGPS attitude, a yaw compass, a yaw rate gyro, and/or a steering potentiometer, a tractor traveling at 1.0 meter per second over a fairly rough field can expect to improve control system accuracy from 11.4 centimeters (1-σ) to as low as 2.6 centimeters.

The most obvious and most important conclusion that can be drawn from this thesis is that centimeter-level automatic control of land vehicles using CDGPS is feasible – today. The preceding chapters in this document show that the technical issues relating to land vehicle control are not easy to solve; however, with continued university research and a concerted development effort, this technology will soon find itself in real-world land vehicle applications.

9.2 Recommendations for Future Work

This thesis describes the first step toward a practical, intelligent automatic control system for land vehicles based on carrier-phase differential GPS. While the system described in this work already holds enormous potential to assist farmers after modest development, this project also offers a wealth of opportunities for continued research at Stanford University.

• **GPS Navigation Research:** Several issues relating to pseudolite usage should be explored. In this work, a single pseudolite was used for a short period of time to initialize land vehicle CDGPS navigation. Areas of future research may include the use of a single pseudolite for extended periods at long range to augment the availability and integrity of the GPS satellite constellation. Also, the use of a dipole pseudolite transmit antenna for reduced cost and multipath reduction should be explored experimentally.

• **"Low-Level" Automatic Control:** This work also opens up countless opportunities for research in the area of automatic control. At the sensor level, accuracy, availability, and robustness properties of new sensor and actuator combinations could be explored and implemented experimentally, including inclinometer sensors and roll and pitch gyroscopes. In the user interface arena, the development and testing of a graphical display for human-in-the-loop automatic control of land vehicles is desperately needed. On the automatic controls side, new capabilities could be added to the current experimental system by including the automatic control of a vehicle with a towed implement, successful control on hilly terrain, or the ability to follow arcs, spirals, and other arbitrary curved paths. A controller is also needed that is robust to real-time vehicle parameter variations.

• **"High-Level" Automatic Control:** At a slightly more sophisticated level, a number of high-level robotic functions may also be addressed for future research. Such topics include

real-time path planning to reach a desired state, adaptive contour plowing, adaptive and guaranteed row overlap, and possibly even path planning over an entire field.

9.3 Closing

The automatic control of land vehicles has been a goal for many years. With the recent development of low-cost, high-precision satellite navigation technologies, automatic land vehicle steering systems are finding their way into countless industries. One of the first industries to take full advantage of this newfound navigation capability will almost surely be agriculture. Most farms provide an environment highly suitable for satellite navigation, and most farmers will quickly realize the financial benefits to be gained by utilizing this technology. Within the next few years, automatic farming will dramatically affect the entire farming industry, improving the quality of life on farms as well as the quality of food production throughout the world.

Appendix A

Parameter Identification Results

The resulting measurement residuals for the four land vehicle dynamic models described in Chapter 6 are shown below. For each of the 24 trials plotted, the optimal parameters were identified using the Idan method, and the data was processed through a causal estimator based on these parameters. The resulting measurement residuals were then compared for model selection purposes.

As expected, lateral position and heading estimates become significantly worse at higher speeds for all models. An interesting note is that the Wong-based models, which allow for front lateral tire slip, perform dramatically better in heading estimation than the Ellis-based models at high speeds. The only noticeable improvement in lateral position residual comes with the allowance for small amounts of rear tire lateral slip.

It can be seen that the addition of a steering dynamic lag term has a significant effect on the performance of the estimator, reducing the steering measurement residual almost in half. The overall wheel angle measurement residual is relatively consistent between high and low speeds.

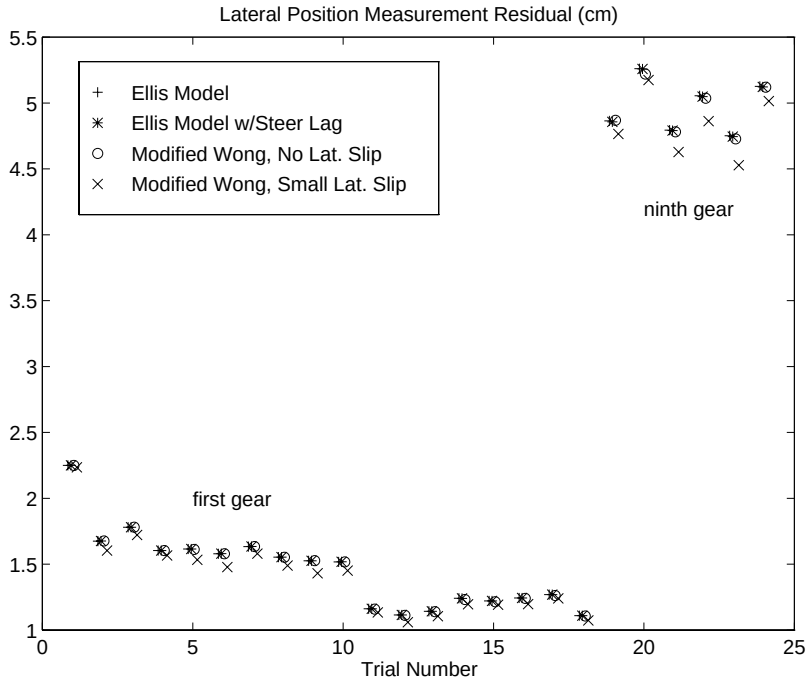

Figure 62 - Lateral Position Measurement Residual Comparison

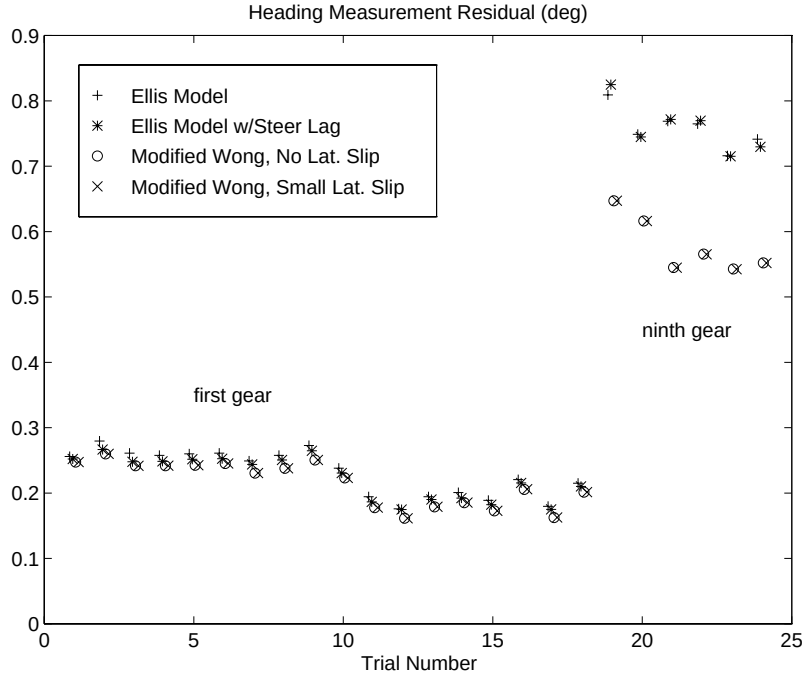

Figure 63 - Heading Measurement Residual Comparison

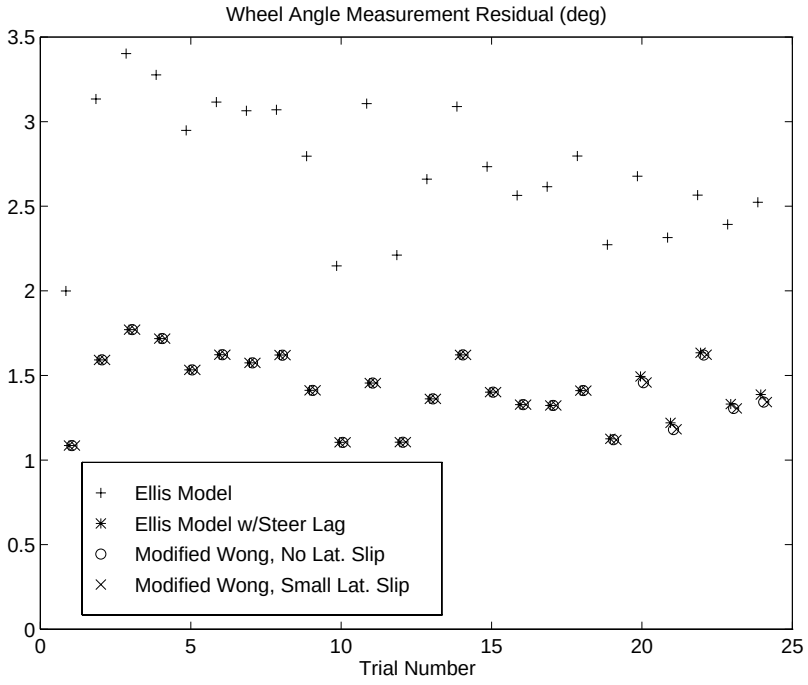

Figure 64 - Heading Measurement Residual Comparison

The identified parameter estimates for the seven-state model, using all 48 open-loop trials as described in Chapter 6, are shown in this appendix. Each parameter is plotted independently as a function of vehicle forward speed and hitch load. The following vehicle model was used

$$\begin{bmatrix} \dot{y} \\ \dot{\Psi} \\ \dot{\Omega}_z \\ \dot{\delta} \\ \dot{\omega} \\ \dot{\Psi}_{\text{bias}} \\ \dot{\delta}_{\text{bias}} \end{bmatrix} = \left[\begin{array}{ccccc|cc} 0 & p_1 & p_2 & 0 & 0 & 0 & 0 \\ 0 & 0 & 1 & 0 & 0 & 0 & 0 \\ 0 & 0 & -p_3 & p_4 & 0 & 0 & 0 \\ 0 & 0 & 0 & 0 & 1 & 0 & 0 \\ 0 & 0 & 0 & 0 & -p_5 & 0 & 0 \\ \hline 0 & 0 & 0 & 0 & 0 & 0 & 0 \\ 0 & 0 & 0 & 0 & 0 & 0 & 0 \end{array}\right] \begin{bmatrix} y \\ \Psi \\ \Omega_z \\ \delta \\ \omega \\ \Psi_{\text{bias}} \\ \delta_{\text{bias}} \end{bmatrix} + \begin{bmatrix} 0 \\ 0 \\ 0 \\ 0 \\ p_5 \\ 0 \\ 0 \end{bmatrix} u \quad . \tag{A.1}$$

Based in the theory described in Chapter 5, these parameters have the following expected values:

$$p_1 \approx V_x \ , \tag{A.2}$$

$$p_2 \approx c \ , \tag{A.3}$$

$$p_3 \approx \frac{2\left(C_{\alpha r} l_2^2 + C_{\alpha h} l_4^2 + C_{\alpha f} l_1^2\right) - 2\left(l_2 - c\right)\left(C_{\alpha r} l_2 + C_{\alpha h} l_4 - C_{\alpha f} l_1\right)}{I_z V_x} \ , \tag{A.4}$$

$$p_4 \approx \frac{2 C_{\alpha f} l_1}{I_z} \ , \tag{A.5}$$

$$p_5 \approx \frac{1}{\tau_{steering}} \ , \tag{A.6}$$

where c denotes the distance from the vehicle rear axle to the center of vehicle rotation.

Note that the relatively consistent value for the parameter p_3 and the linear velocity dependence of the parameter p_4 suggest that the lateral tire slip coefficients are linearly dependent on forward velocity.

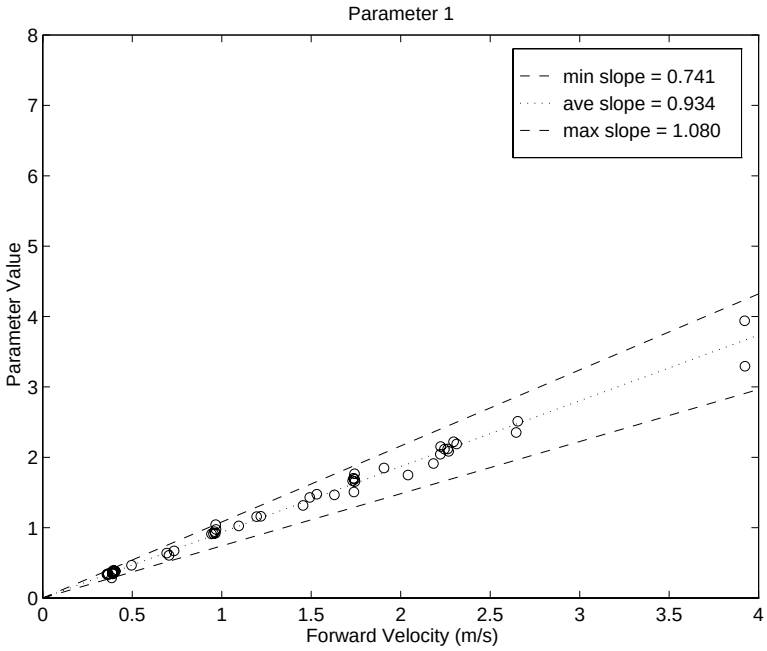

Figure 65 - Parameter 1 Versus Forward Velocity

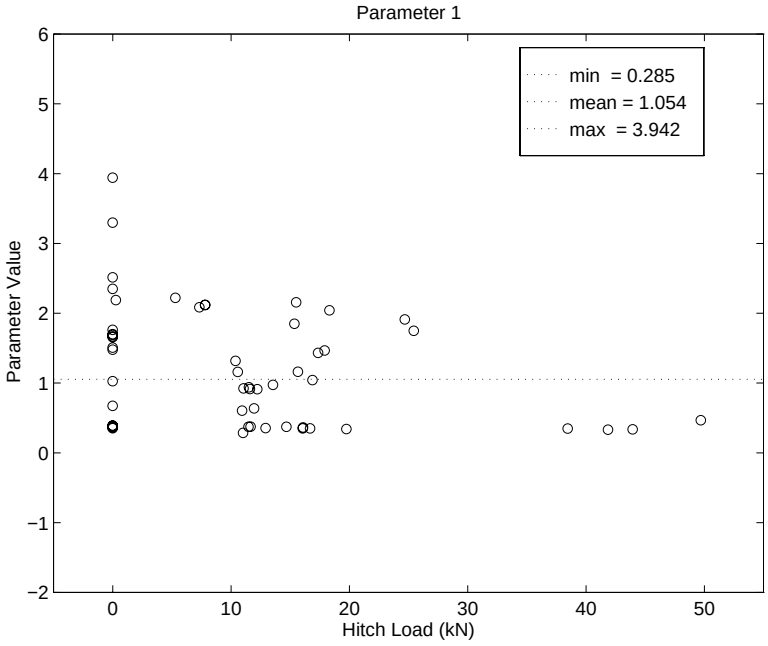

Figure 66 - Parameter 1 Versus Hitch Load

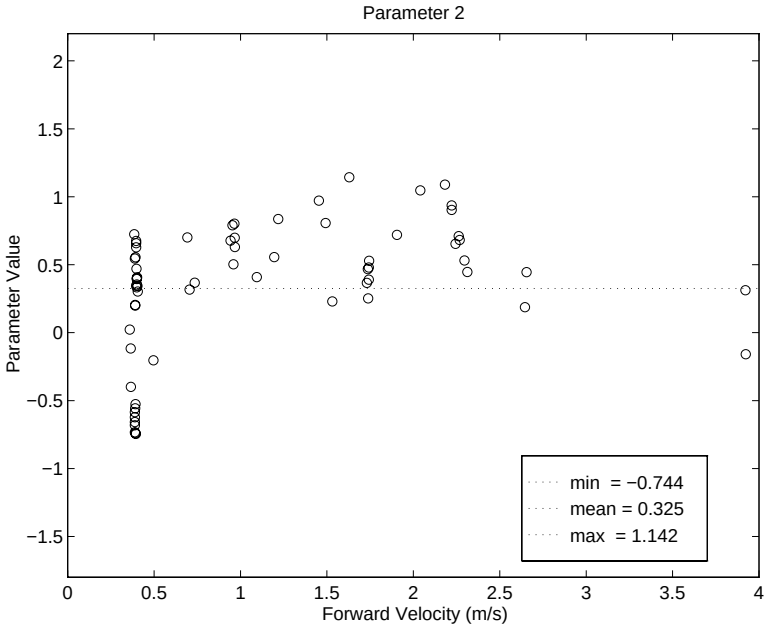

Figure 67 - Parameter 2 Versus Forward Velocity

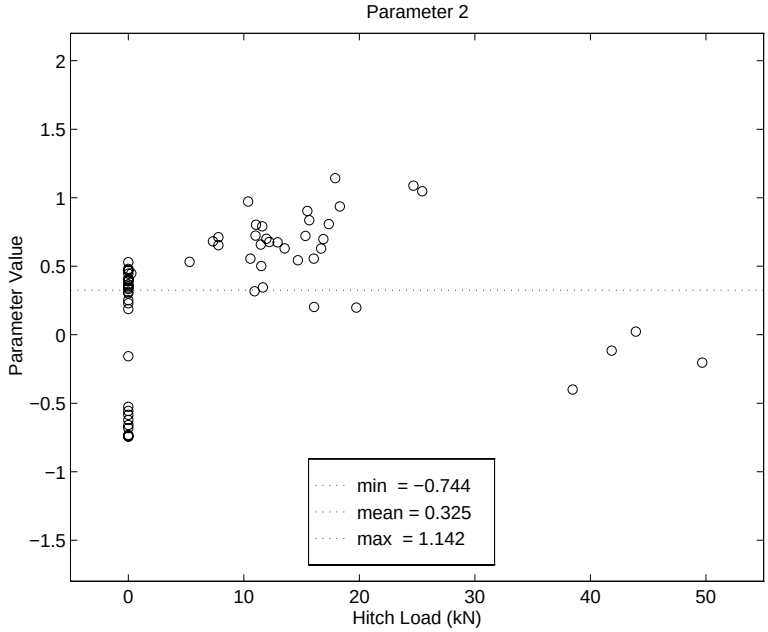

Figure 68 - Parameter 2 Versus Hitch Load

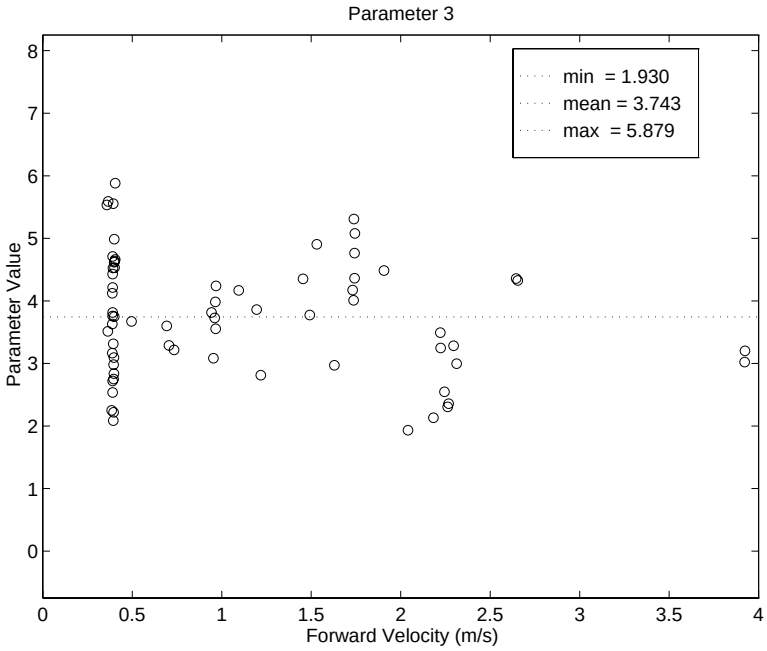

Figure 69 - Parameter 3 Versus Forward Velocity

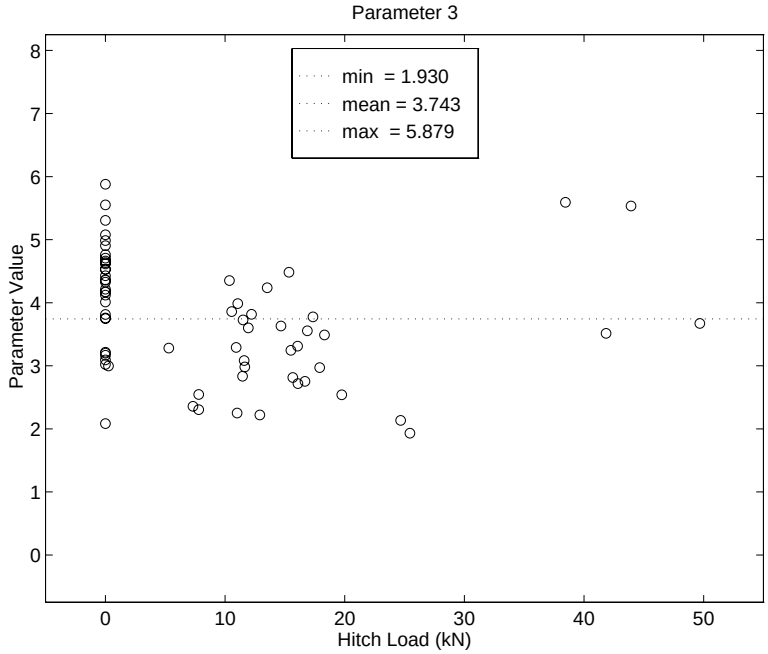

Figure 70 - Parameter 3 Versus Hitch Load

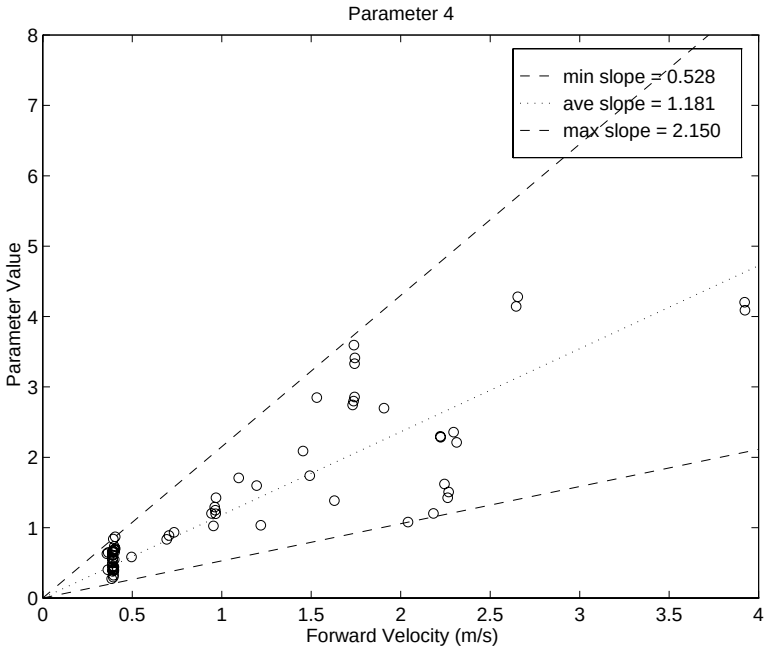

Figure 71 - Parameter 4 Versus Forward Velocity

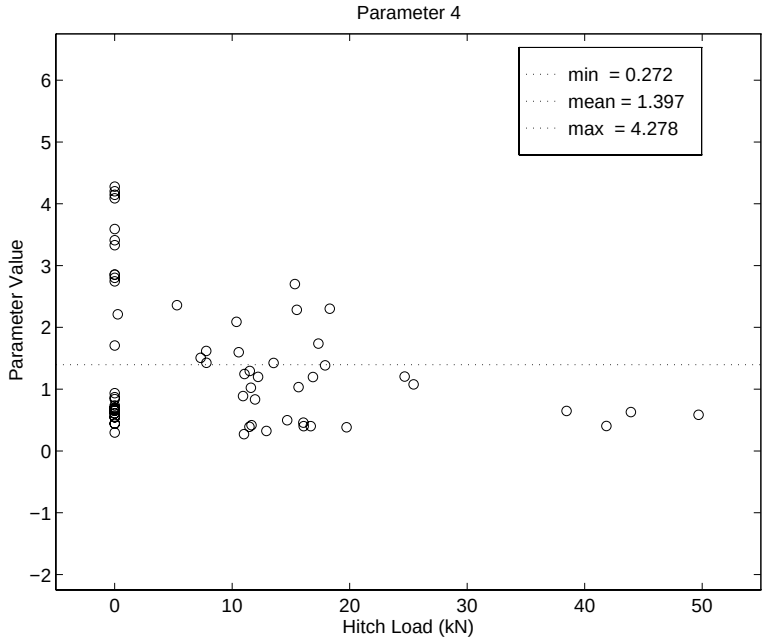

Figure 72 - Parameter 4 Versus Hitch Load

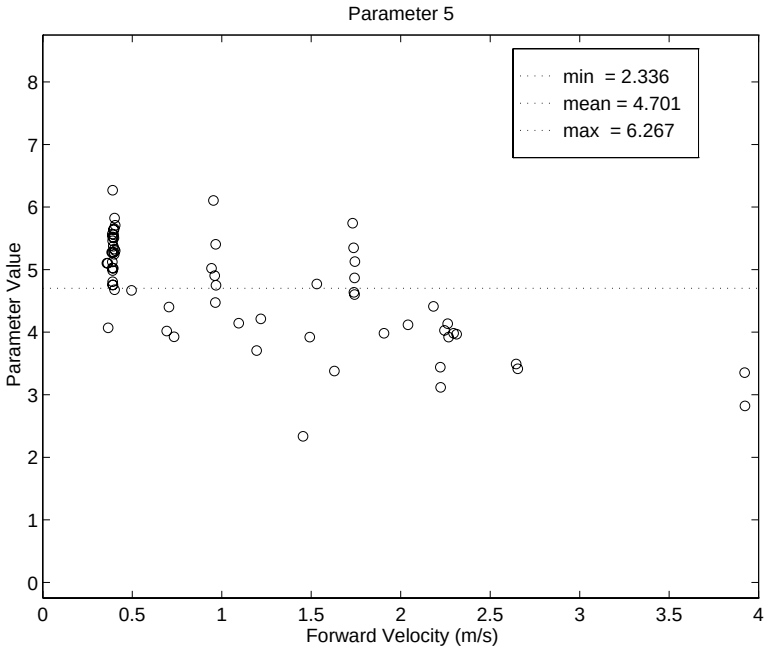

Figure 73 - Parameter 5 Versus Forward Velocity

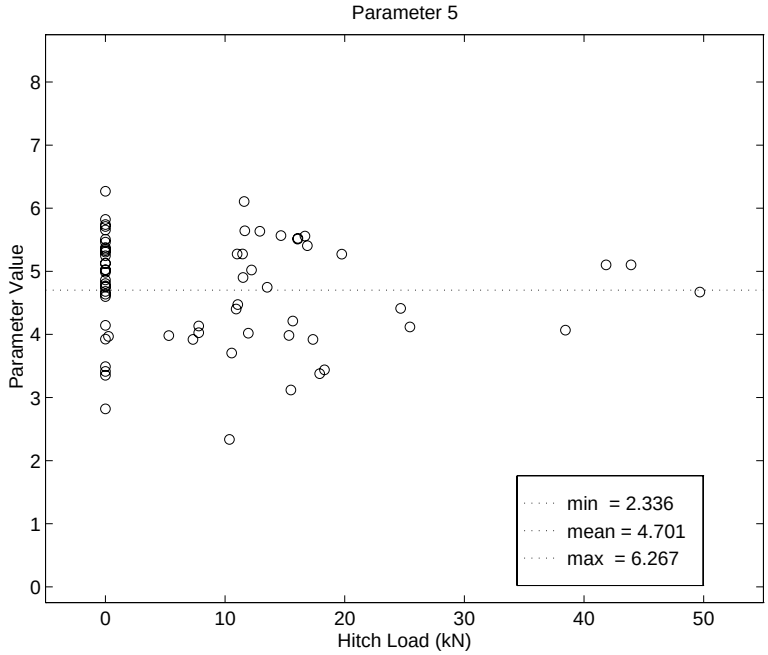

Figure 74 - Parameter 5 Versus Hitch Load

References

[1] B.W. Parkinson and J.J. Spilker, eds. *Global Positioning System: Theory and Applications*. Two Volumes. American Institute of Aeronautics and Astronautics, Inc. Washington, DC, 1996.

[2] "Global Positioning System Standard Positioning Service Signal Specification (Second Edition)," June 2, 1995.

[3] B. Forssell. *Radionavigation Systems*. Prentice Hall, New York, 1991.

[4] B. Hofmann-Wellenhof, H. Lichtenegger, and J. Collins. *GPS Theory and Practice*. Springer-Verlag Wien, New York, 1994.

[5] K. Van Dyke. "Removal of SA: Benefits to GPS Integrity." *Proceedings of ION GPS-96*, Kansas City, MO, Sept. 1996, pp. 1657-1670.

[6] R. Hatch. "The Synergism of GPS Code and Carrier Measurements." *Proceedings of the Fourth International Geodetic Symposium on Satellite Positioning*, Las Cruces, New Mexico, 1982.

[7] A.J. Van Dierendonck, P. Fenton, and T. Ford. "Theory and Performance of Narrow Correlator Spacing in a GPS Receiver." *Proceedings of the ION National Technical Meeting*, Washington, DC, 1992, pp. 115-124.

[8] C. Kee. *Wide Area Differential GPS*. Ph.D. Dissertation, Stanford University, December 1993.

[9] P. Enge, T. Walter, S. Pullen, C. Kee, Y.C. Chao, and Y. Tsai. "Wide Area Augmentation of the Global Positioning System" *Proceedings of the IEEE*, Vol. 84, No. 8, August 1996, pp. 1063-1088.

[10] S.L. Frodge, et al. "Real-Time on-the-Fly Kinematic GPS System Results", *NAVIGATION*, Vol. 41, No. 2, Summer 1994, pp. 175-186.

[11] C. Cohen, B. Pervan, D. Lawrence, H.S. Cobb, J.D. Powell, and B. Parkinson. "Real-Time Flight Testing Using Integrity Beacons for GPS Category III Precision Landing", *Navigation*, Vol. 41, No. 2, Summer 1994, pp. 145-157.

[12] C. Cohen, et al. "Autolanding a 737 Using GPS Integrity Beacons", NAVIGATION, Vol. 42, No. 3, Fall 1995, pp. 467-486.

[13] P. Montgomery. *Carrier Differential GPS as a Sensor for Automatic Control*. Ph.D. Dissertation, Stanford University, June 1996.

[14] A. Conway. *Autonomous Control of a Model Helicopter Using Carrier Phase GPS.* Ph.D. Dissertation, Stanford University, February 1995.

[15] E.H. Teague, J.P. How, and B.W. Parkinson. "Carrier Differential GPS for Real-Time Control of Large Flexible Structures", *Proceedings of ION GPS-96*, Kansas City, MO, 1996, pp. 1355-1365.

[16] K.R. Zimmerman and R.H. Cannon Jr. "Experimental Demonstration of an Indoor GPS-Based Sensing System for Robotic Applications", NAVIGATION, Vol. 43, No. 4, Winter 1996-1997, pp. 375-395.

[17] S.C. Young, C.E. Johnson, and R.L. Schafer. "A Vehicle Guidance Controller", *Transactions of the American Society of Agricultural Engineers*, Vol. 26, No. 5, 1983, pp. 1340-1345.

[18] R.J. Palmer. "Test Results of a Precise, Short Range, RF Navigational/Positional System", *Proceedings of the First Vehicle Navigation and Information Systems Conference*, Toronto, Ontario, Canada, Sept. 1989, pp. 151-155.

[19] N.H. Brown, H.C. Wood, and J.N. Wilson. "Image Analysis for Vision-Based Agricultural Vehicle Guidance", *Optics in Agriculture*, Vol. 1379, 1990, pp. 54-68.

[20] J.R. Brandon and S.W. Searcy. "Vision Assisted Tractor Guidance for Agricultural Vehicles", *SAE Paper No. 921650*, International Off-Highway and Powerplant Congress and Exposition, Milwaukee, WI, Sept, 1992.

[21] A.A. Vetter. "Quantitative Evaluation of CDGPS Guidance for Ground-Based Agricultural Applications". *Applied Engineering in Agriculture*, Vol. 11, No. 3, 1995, pp. 459-464.

[22] S.C. Crow and F.L. Manning. "Differential GPS Control of Starcar 2", *Navigation*, Vol. 39, No. 4, Winter 1992, pp. 383-405.

[23] R.J. Palmer and S.K. Matheson. "Impact of Navigation on Farming", *ASAE Paper No. 88-1602*. International Winter Meeting of the American Society of Agricultural Engineers, Chicago, IL, Dec. 1988.

[24] G. Lachapelle, M.E. Cannon, H. Gehue, T. Goddard, and D. Penney. "GPS Systems Integration and Field Approaches in Precision Farming", *Navigation*, Vol. 41, No. 3, Fall 1994, pp. 323-335.

[25] J. Pointon and K. Babu. "LANDNAV: A Highly Accurate Land Navigation System for Agricultural Applications", *Proceedings of ION GPS-94*, Salt Lake City, UT, Sept. 1994, pp. 1077-1080.

[26] R. Clark and R. Lee. "A Comparison of Rapid GPS Techniques for Development of Topographic Maps for Precision Farming", *Proceedings of ION GPS-96*, Kansas City, MO, Sept. 1996, pp. 495-504.

[27] Williams, Robert C. *Fordson, Farmall, and Poppin' Johnny*. University of Illinois Press. Urbana, Illinois, 1987.

[28] H.D. Woodman. "Farming: The Nation's Small Big Business," in Carstensen, Rothstein, and Swanson eds., *Outstanding in His Field*. Iowa State University Press. Ames, Iowa, 1993.

[29] J. Tarrant. *Farming and Food*. Oxford University Press. New York, New York, 1991.

[30] M. Reisner. *Cadillac Desert*. Penguin Books, 1993.

[31] M. O'Connor, T. Bell, G. Elkaim, and B. Parkinson. "Real-Time CDGPS Initialization for Land Vehicles Using a Single Pseudolite", *Proceedings of ION National Technical Meeting*, Santa Monica, CA, January 1997, pp. 717-724.

[32] M. O'Connor, G. Elkaim, and B. Parkinson. "Carrier-Phase DGPS for Closed-Loop Control of Farm and Construction Vehicles", *Navigation*, Vol. 43, No. 2, Summer 1996, pp. 167-178.

[33] M. O'Connor, T. Bell, G. Elkaim, and B. Parkinson. "Automatic Steering of Farm Vehicles Using GPS", *Proceedings of the 3rd International Conference on Precision Agriculture*, Minneapolis, MN, June 1996, pp. 767-777.

[34] A.K. Barrows, P. Enge, B.W. Parkinson, and J.D. Powell. "Evaluation of a Perspective-View Cockpit Display for General Aviation Using GPS", *Navigation*, Vol. 43, No. 1, Spring 1996, pp. 55-69.

[35] Personal Interview with David Cox, Australian Farmer, June 25, 1996

[36] Personal Interview with Chuck Borba, Southwestern U.S. Farmer, February 1997

[37] Personal Interview with Steve Martori, Southwestern U.S. Farmer, March 17, 1997

[38] C.J. Chisholm, et al. "Safety, Health and Hygiene in Agriculture", *Safety Science*, Vol. 15, 1992, pp. 225-248.

[39] B. Pervan. *Navigation Integrity for Aircraft Precision Approach using the Global Positioning System*. Ph.D. Dissertation, Stanford University, SUDAAR 677, March 1996.

[40] D. Lawrence. *Aircraft Landing Using GPS*. Ph.D. Dissertation, Stanford University, September 1996.

[41] H.S. Cobb. *GPS Pseudolites: Theory, Design, and Applications*. Ph.D. Dissertation, Stanford University, SUDAAR 707, August 1997.

[42] B. Pervan, C. Cohen, and B. Parkinson. "Integrity Monitoring for Precision Approach Using Kinematic GPS and a Ground-Based Pseudolite", *Navigation*, Vol. 41, No. 2, Summer 1994, pp. 159-174.

[43] C. Bartone. "Advanced Pseudolite for Dual-Use Precision Approach Applications", *Proceedings of ION GPS-96*, Kansas City, MO, Sept. 1996, pp. 95-105.

[44] D. Lawrence, H.S. Cobb, C. Cohen, J. Christie, J.D. Powell, and B. Parkinson. "Maintaining GPS Positioning in Steep Turns Using Two Antennas", *Proceedings of ION GPS-95*, Palm Springs, CA, Sept. 1995, pp. 1451-1459.

[45] M. El-Gindy and J.Y. Wong. “A Comparison of Various Computer Simulation Models for Predicting the Directional Responses of Articulated Vehicles”, *Vehicle System Dynamics*, Vol. 16, 1987, pp. 249-268.

[46] R.G. Kallenbach. “Identification Methods for Vehicle System Dynamics”, *Vehicle System Dynamics*, Vol. 16, 1987, pp. 107-127.

[47] J.Y. Wong. *Theory of Ground Vehicles*. Wiley, New York, 1978.

[48] J.R. Ellis. *Vehicle Dynamics*. London Business Books Ltd., 1969.

[49] G.M. Owen. “A Tractor Handling Study”, *Vehicle System Dynamics*, Vol. 11, 1982, pp. 215-240.

[50] R.H. Owen. “Directional Dynamics of a Tractor-Loader-Backhoe”, *Vehicle System Dynamics*, Vol. 11, 1982, pp. 251-265.

[51] D.A. Crolla and H.B. Spencer. “Tractor Handling during Control Loss on Sloping Ground”, *Vehicle System Dynamics*, Vol. 13, 1984, pp. 1-17.

[52] K. Noh and D. Erback. “Self-Tuning Controller for Farm Tractor Guidance”, *ASAE Paper No. 911861*.

[53] A. Modjtahedzadeh and R.A. Hess. “A Model of Driver Steering Control Behavior for Use in Assessing Vehicle Handling Qualities”, *Transactions of the ASME*, Vol. 115, Sept. 1993, pp. 456-464.

[54] S. Boyd. “Lecture Notes for EE363: Introduction to Linear System Theory”, Autumn Quarter, 1994.

[55] Bryson A.E. and Ho Y.C., *Applied Optimal Estimation*, Hemisphere Publishing Corp., 1975.

[56] N. Wiener. *Extrapolation, Interpolation and Smoothing of Stationary Time Series, with Engineering Applications*. Wiley, New York, 1949.

[57] B. Widrow and S. Stearns. *Adaptive Signal Processing*. Prentice-Hall, Inc., New Jersey, 1985.

[58] J.P. Norton. *An Introduction to Identification*. Academic Press, 1986.

[59] M. Idan. *An Identification Algorithm Based on Smoothing*. Ph.D. Dissertation, Stanford University, July 1990.

[60] A.B. Cox and A.E. Bryson. “Identification by a Combined Smoothing Nonlinear Programming Algorithm.” *Automatica*, Vol. 16, 1980, pp. 689-694.

[61] A. Bryson. “Lecture Notes for AA278: Dynamic Optimization”, Winter Quarter, 1994.

[62] B.S. Keller. *On-Line Physical Parameter Identification and Adaptive Control of a Launch Vehicle*. Ph.D. Dissertation, Stanford University, 1993.

[63] A. Gelb. *Applied Optimal Estimation*. Analytic Sciences Corp., 1989.

[64] Franklin, Powell, and Workman. *Digital Control of Dynamic Systems*. Addison-Wesley Publishing Company, Inc. Reading, Massachusetts, 1990.

[65] E. Abbott. *Land-Vehicle Navigation Systems: an Examination of the Influence of Individual Navigation Aids on System Performance*. Ph.D. Dissertation, Stanford University, March 1997.